FORMATION AND GROWTH MECHANISMS OF A HIGH TEMPERATURE INTERFACIAL LAYER BETWEEN Al AND TiO_2

Jairaj J. Payyapilly

Dissertation submitted to the faculty of the Virginia Polytechnic Institute and State University in partial fulfillment of the requirements for the degree of

Doctor of Philosophy
in
Materials Science and Engineering

Dr. Kathryn V. Logan, Committee Chair
Dr. David E. Clark
Dr. William T. Reynolds, Jr.
Dr. Michael J. Kelley

19th November 2008
Blacksburg, Virginia.

Keywords: interface reaction, liquid aluminum, titanium dioxide, titanium aluminide, oxidation-reduction, growth mechanism

FORMATION AND GROWTH MECHANISM OF A HIGH TEMPERATURE INTERFACIAL LAYER BETWEEN Al AND TiO_2

JAIRAJ PAYYAPILLY

ABSTRACT

The product of interaction between Al and TiO_2 at elevated temperature has a wide range of applications in refractory, structural and electronics industries (refractory tiles, tank armor, fuel cells, and microelectronic devices). This research attempts to understand the extent of interaction between Al and TiO_2 when the reactant surfaces are in contact at elevated temperature and normal atmospheric pressure. The interfacial region between the reactant compounds is examined using analytical techniques; and the formation of TiAl as the interfacial compound is described. The thermodynamics of the Al – Ti – O system is explained as it relates to the particular conditions for the Al – TiO_2 reaction research. Thermodynamic principles have been used to demonstrate that the formation of TiAl is favored instead of other Ti_xAl_y compounds for the set of conditions outlined in this thesis. A study of the mechanism of interactions in the interfacial region can help towards being able to determine the reaction kinetics that lead to the control of microstructure and thus an improvement in the material performance. An appropriate model that describes the formation of TiAl at the interface is described in this study. The formation of TiAl at the interface is a result of the reduction reaction between TiO_2 and Al. The O released during the reduction of TiO_2 has been investigated and demonstrated to partly remain dissolved in TiAl at the interfacial region. Some O reacts with Al as well to form crystalline Al_2O_3 in the interfacial layer.

ACKNOWLEDGEMENTS

The author wishes to thank his advisor, Dr. Kathryn Logan for the encouragement, and belief in his ability as a researcher. He would also like to extend his gratitude to Dr. William Reynolds Jr., Dr. David Clark, and Dr. Michael Kelley for their participation in this study and serving as committee members of the author's dissertation. The author would also like to thank Dr. William Reynolds Jr. for the lengthy discussions in the evenings. The author gained enormously from his thoughts and suggestions. The author would also like to acknowledge the help from Dr. Reynolds and Dr. Claudia Rawn (Oak Ridge National Laboratory) in several characterization techniques during this study. The author wishes to extend his acknowledgement to Dr. Stephen Kampe and Dr. Kelley for their critiques that have helped to improve certain aspects of the thesis.

Special thanks to the National Institute of Aerospace, Hampton, for funding this project and also for sheltering the author's office during his stint at Hampton. The author would like to thank Dr. Nagraj Kulkarni for his constant encouragement throughout the course of this work. The author extends many thanks to the MMRG group for the constant encouragement and constructive criticism towards this project.

The author thanks his wife for her patience and understanding during the course of this work. Finally, the author would like to acknowledge the support and encouragement from his parents, siblings, and friends.

TABLE OF CONTENTS

LIST OF FIGURES

CHAPTER 2

CHAPTER 3

CHAPTER 4

LIST OF TABLES

1.0 INTRODUCTION

The current chapter describes the importance of and explains the common route to synthesize a TiAl – Al_2O_3 composite. The chapter outlines the motivation for the topic of research and the main research objectives.

1.1 Reaction Synthesis of Intermetallic – Ceramic Composites

TiAl based intermetallics have useful properties like low density (3.7 – 3.9 gm/cm^3 as compared with superalloys having 8.3 gm/cm^3)[1]; high oxidation limit of 900°C (as compared to 650°C for Ti_3Al based alloys); high strength value of 400 – 650 MPa; and adequate creep resistance at temperatures to 1000°C (compared with Ti_3Al (760°C). Mechanical properties of γ-TiAl alloys are sensitive to microstructure. The microstructure of γ-TiAl alloys has been reported to vary appreciably with small changes in alloy composition and processing parameters.[2,3]

Toughness of TiAl based intermetallic alloys at ambient temperatures could be improved by the introduction of matrix based composites (TiAl-matrix reinforced with SiC, Al_2O_3 or TiB_2 particles or fibers).[4,5] Al_2O_3 has been identified as a thermodynamically stable reinforcement phase for a γ-TiAl matrix.[6,7] Intermetallic – oxide interpenetrating phase composites have been proposed for better mechanical properties for structural applications. Several processing techniques have been suggested by various authors for the synthesis of a TiAl – Al_2O_3 composite.

One of the most common ways used for synthesis of such interpenetrating phase composites is by infiltrating liquid metal into a porous ceramic preform.[8] The liquid metal infiltration method is however limited to the manufacturing of Al – containing

composites whose high temperature applications are limited by the low melting point of Al. An *in-situ* process is needed[9] to counter such problems. Matrices and reinforcements that could be formed by *in-situ* reactions of completely different starting materials was suggested by Subramanian *et al.*[9] Subramanian *et al.*[9] demonstrated the formation of an iron aluminide matrix composite reinforced with alumina particles that was synthesized by an *in-situ* displacement reaction between Fe-Al powder and Fe_2O_3 powder. A similar *in-situ* displacement reaction to synthesize TiAl-Al_2O_3 composite was performed by Horvitz *et al.*[6] Horvitz *et al.*[6] blended a 70:30 molar ratio of Al and TiO_2 powders. The powders were compacted by cold pressing. A compacted powder sample was placed between preheated (800 – 1000°C) rams of an Instron test machine. When the temperature of the sample was sufficiently high, the powder mixture reacted by a thermal explosion. Horvitz *et al.*[6] explained that the thermal explosion is the result of the moderately exothermic $3TiO_2 + 7Al \rightarrow 2Al_2O_3 + 3TiAl$ self-propagating high temperature synthesis (SHS) reaction. Other researchers have reported the use of such SHS reaction technique for the synthesis of intermetallic – ceramic composites.

1.2 Justification of Research

The $10Al + 3TiO_2 + 3B_2O_3 \rightarrow 5Al_2O_3 + 3TiB_2$ SHS reaction at standard atmospheric pressure was shown by Logan[10] to produce a composite $5Al_2O_3 + 3TiB_2$ as the reaction product. After the SHS reaction involving the reactant powder mixture was initiated, the reaction front propagated with a speed ranging from 2.4 mm/sec to 7.5 mm/sec depending on the nature of powder packing.[10] The temperature change during the SHS reaction was recorded to be 50°C/min. A unique microstructure with

high aspect ratio grains was obtained by *Logan*[11] at 10°C/min. Neither the mechanism, nor the factors responsible for the unique microstructure have been explained in the literature.

An effective way to affect the rate of change in temperature during the SHS reaction could be by the self-formation of an interfacial compound between the reacting species that would act as a barrier.[12,13,14]

Knowledge of the interaction between individual reactant components would be necessary to determine whether a barrier could be made to form between the reactant pairs. The SHS interaction between Al and B_2O_3 has been studied previously and reported by McLemore.[15] McLemore[15] reported that the interaction between Al and B_2O_3 yielded $2Al_2O_3.B_2O_3$ at 870°C in some cases, and $9Al_2O_3.2B_2O_3$ in others. Al_2O_3 was reported to have formed at 1035°C for every experiment reported by McLemore.[15] The reaction between Al and TiO_2 at elevated temperatures is documented as a common route to synthesize a TiAl – Al_2O_3 composite.[7] Knowledge of the mechanism of reaction component interactions causing the composite formation can provide a basis for prediction and control of product characteristics.

1.3 Objective of Research

The objective of my research is to understand the interactions and mechanisms that lead to a possible interface between Al and TiO_2 when the two components are in contact with each other at 700ºC isothermal condition and standard atmospheric pressure. Advanced analytical techniques and thermodynamics will be used to understand the growth mechanism of the resultant interface.

2.0 BACKGROUND AND LITERATURE REVIEW

The current chapter explains the necessary concepts and relevant findings from the literature pertaining to the current research. In particular, thermodynamics of the Ti-Al-O system that is reported in literature is explained.

2.1 SHS Reaction

An SHS reaction involving aluminum, anatase and anhydrous boron oxide powders forms a composite of alumina and titanium diboride as given by Equation (2.1).[16] Information about formation of product phases other than the stoichiometric reaction product as given by Equation (2.1), has not been generally reported.

$$3TiO_2 + 3B_2O_3 + 10Al \rightarrow 3TiB_2 + 5Al_2O_3 \qquad (2.1)$$

Logan[11] has observed that compounds and phases that form at the SHS reaction heating rate (~50°C/min) are different from products that form during the lower reaction heating rates (~10°C/min) involving the same reactants. Some compounds and phases that form at a lower heating rate have a high-aspect ratio morphology compared with products that form at a higher heating rate, as shown in *Figure 2.1*.[11] Materials with high aspect ratio morphology could potentially be used for structural applications with improved properties such as toughness[17,18] and strength[17].

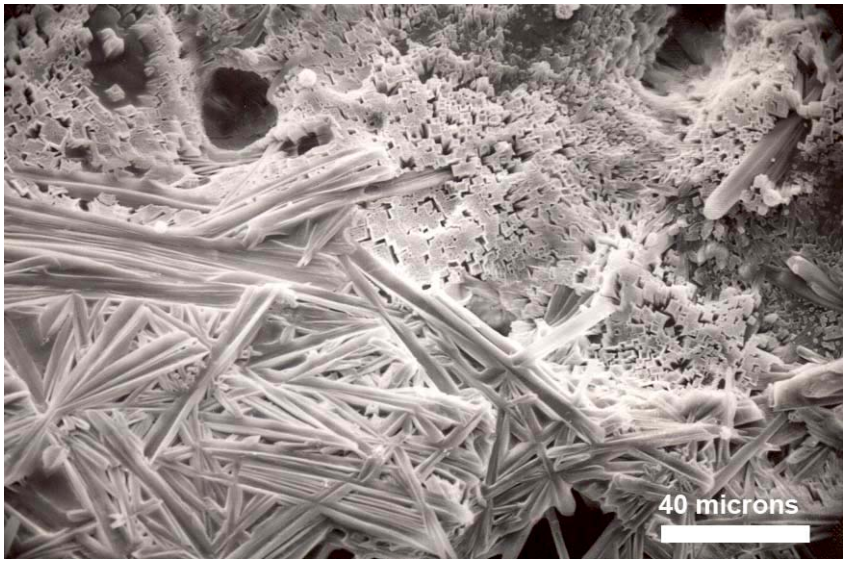

Figure 2.1: Microstructure of the reaction product having high aspect ratio crystals formed at a lower heating rate as observed by *Logan*.[11] (printed with permission)

A brief outline of events that take place during an SHS reaction that produce the Al_2O_3-TiB_2 composite product follows:[16]

- A stoichiometric proportion [as shown in Eq. (2.1)] of Al, TiO_2 and B_2O_3 powders are mixed to form a reactant mixture.
- The reactant mixture is placed in a refractory crucible and heat is supplied from an external source to initiate the reaction.[10]
- The B_2O_3 powder begins to melt as the temperature of the powder mixture reaches 450°C.
- The melted B_2O_3 coats the small particles of TiO_2 as it spreads into the interior of the sample by capillary action and also coats the Al particles.[19]
- The Al and TiO_2 particles are isolated from the atmospheric oxygen as a consequence of the molten B_2O_3 coating.
- Al reduces the oxides of Ti and B to elemental metals[19] and in the process forms Al_2O_3. Oxygen required for the oxidation of Al is obtained from the

reduction of the oxide reactants and a small amount from the ambient air. The exothermic nature of the reaction causes an increase in temperature of the reactants.[19] As the heat evolved from the reaction increases, Al expands because of its higher coefficient of thermal expansion, while Al_2O_3 does not expand to the same extend due to its relatively low coefficient of thermal expansion. The difference in thermal expansion coefficients causes the surface oxide layer to crack and continuously expose fresh elemental Al.

- When the temperature reaches 660°C, Al melts and begins to flow out of the oxide shell. Al is directly exposed to B_2O_3 and TiO_2.

At about 1060°C the two oxide components and Al react to form titanium diboride (TiB_2) and negligible amounts of $Al_{18}B_4O_{33}$.[20] Near stoichiometric amounts of Al_2O_3 and TiB_2 are the final products of the SHS reaction as shown in Eq. (2.1).[10]

2.2 SHS Reactant Components

Depending on the SHS reaction conditions, some stable and metastable compounds could form between the reacting compounds. The final SHS reaction product is a mixture of $Al_2O_3 – TiB_2$. Binary or ternary reactant systems comprising a combination of Al, Al_2O_3, TiO_2, and B_2O_3 react among themselves until equilibrium is attained to form the final stoichiometric compound.

A list of the potential reactant pairs involved in the $Al_2O_3 – TiB_2$ SHS reaction system (Equation 2.1) are:

i. $Al – TiO_2$

ii. $Al – B_2O_3$

iii. $TiO_2 – Al_2O_3$

iv. $TiO_2 – B_2O_3$

v. $Al_2O_3 – B_2O_3$

A passive layer of Al_2O_3 forms on the surface of Al. Interaction of Al with either oxygen or an oxygen-containing compound forms a stable Al_2O_3.[21] Al – Al_2O_3 is not considered a reactant pair since Al_2O_3 is a stable compound formed by oxidation of Al; although some interaction is possible.

Particle – particle interaction between the individual components was studied and reported by Logan *et al.*[22,10] Logan *et al.*[10] investigated particle size and powder compaction effects on the initiation temperature for the following powder mixtures: (i) $4Al + 3TiO_2$, and (ii) $2Al + B_2O_3$ in order to study the SHS produced $Al_2O_3 – TiB_2$ product.

Logan *et al.*[10] found that the reaction between an Al and TiO_2 loose powder mixture ignited from room temperature proceeded in a slow and controlled manner at about 0.4 mm/sec. It was reported that the Al – TiO_2 SHS reaction would not initiate when pressed pellets of the Al and TiO_2 powder mixture were used. α–Al_2O_3 and TiN were the major products and small amounts of TiO_2 were detected.

It was interesting to note that only pressed pellets of the Al – B_2O_3 powder mixture would initiate.[10] It was further noted that the pellets containing coarse Al and coarse B_2O_3 powders initiated but would not self – propagate.[10] The combustion front of the Al – B_2O_3 SHS reaction propagated in a spiral oscillation from the top to the bottom at about 1.0 mm/second. The product of the reaction was reported to be largely α–Al_2O_3 and small amounts of Al, B_2O_3 and a solid solution of $9Al_2O_3.2B_2O_3$.[10] McLemore[15] determined the activation energy for the formation of

$2Al_2O_3.B_2O_3$ from the reaction between Al and B_2O_3 to be between 120 and 165 kcal/mol. The activation energy for the formation of Al_2O_3 from the same reactants was determined to be between 210 and 235 kcal/mol.

The remaining three reactant pairs $TiO_2 - Al_2O_3$, $TiO_2 - B_2O_3$ and $Al_2O_3 - B_2O_3$ are nonreactive and therefore are not relevant to this investigation.

2.3 Al – TiO_2 System and Applications

Al interaction with TiO_2 could be a rate determining factor that would be useful in the control of the $Al+TiO_2+B_2O_3$ SHS reaction kinetics. Diffusivity of a species into a compound could have significantly different values depending on the phase of the compound encountered by the diffusing species.[23] A study of the individual reactant components would help to determine the rate limiting step. Such a study that involves the examination of the interface between the reactants would be difficult using small spherical particles (powder samples); since the interface between the two particles would be difficult to examine using an area specific characterization technique like the SEM or the TEM. The interface between the two components would also be difficult to study if one of the reactants is in the liquid state at the temperature of interest. A diffusion couple study is a conventional route to study the interface between two reactants.[24] A film-substrate structure would ensure easy accessibility to examine the interface. The compound having the lower melting point could be chosen to be deposited as the film over a substrate (compound with the higher melting point). Heating a film-substrate ($Al - TiO_2$) structure could result in the formation of an interfacial compound(s) for the Al-Ti system. It is possible that oxygen would diffuse from the oxide (TiO_2) to form Al_2O_3 and Al would diffuse from the Al film to form

either an Al - Ti intermetallic or Al_2O_3 or both. Intermetallic compound phases have been identified for the Al-Ti system having different structures: $Ti_3Al(\alpha_2)$, $TiAl(\gamma)$, Al_2Ti ($HfGa_2$ type tetragonal), Al_3Ti (simple tetragonal) and other possible metastable phases.[25,6]

Titanium aluminides form having high melting temperature, good oxidation resistance and low density suitable for high temperature applications when Al and TiO_2 react. Al_2O_3 has been reported as a second phase formed within the titanium aluminides. Techniques like gas-pressure infiltration,[26,27] liquid metal infiltration into porous preforms,[8] reactive melt infiltration,[28,29] directed metal oxidation,[30,31] and hot isostatic pressing have been used to synthesize the combination of intermetallic-ceramic composites. The aluminide – alumina mixture has been used as reinforcement for *in-situ* Al based alloy metal matrix composites.[32,33,34] Titanium aluminide composites are used as binders along with carbides or Al_2O_3 for structural applications, even when the aluminide is the minor component of the composite.[35] The combination of TiAl or Ti_3Al, and Al_2O_3 are used for the production of *in-situ* aluminide – alumina composites for various applications.[36,37,38] The Al-TiO_2 system has been used for producing *in-situ* metal matrix composites by vortex casting[33,39] and *in-situ* intermetallic matrix composites by squeeze casting[40,41,42]. Feng *et al.*[34] have indicated that there are often intermediate steps between the starting compounds and the final product after a reaction occurs in such systems. Insufficient knowledge of the intermediate steps hinders the optimization of properties of the composite products formed by such reactions. The advantage of such an intermetallic system is that the thermo-mechanical properties, such as wear resistance, environmental

stability and high temperature strength, are dominated by Al_2O_3 while the intermetallic phase significantly improves the toughness of the component through a crack-bridging mechanism. The TiAl phase is usually the preferred intermetallic reinforcement due to a combination of properties like low density, high melting temperature and excellent oxidation resistance.[6]

2.4 Interaction between Al and TiO_2

The interaction between Al and TiO_2 has been studied previously under various conditions of temperature and pressure[43,44,45,46] yielding a composite $TiAl_3$ and Al_2O_3 as the final product. The experiments have all involved some form of pressurization of the reactant mixture at some point in time. Example experiments that involve interaction between Al and TiO_2 as reported in the literature are explained below.

Feng *et al.*[34] used an Al - TiO_2 powder mixture with a weight percentage mixture of 88.33:16.67 Al:TiO_2 that was initially milled, then uniaxially cold-pressed to form green compact pellets. The samples were heated to 1100ºC at 10ºC per minute, and then cooled to room temperature at 10ºC per minute. $TiAl_3$ and α-Al_2O_3 were reported to have been the final product. Intermediate γ-Al_2O_3 and TiO phases were also reported to have formed during heating that were not present when the reaction was cooled to room temperature. The authors have hypothesized three steps during the reaction that lead to the formation of the final product mixture. The first step involved the formation of TiO and γ-Al_2O_3 intermediate phases. The second and third steps involved formation of α-Al_2O_3 and $TiAl_3$. Evidence of the presence of $TiAl_3$ and TiO has been derived from X-ray diffraction analysis. γ-Al_2O_3 has also been reported to have formed as determined by X-ray diffraction analysis. Pan *et al.*[47] reported the

presence of γ-Al_2O_3 using high resolution TEM. Both authors have reported that γ-Al_2O_3 forms as an intermediate phase that either transforms to the more stable α-Al_2O_3; or the γ-Al_2O_3 reacts with another compound to form a ternary compound. For example γ-Al_2O_3 reacts with Mg to form $MgAl_2O_4$. The presence of $TiAl_3$ has also been reported from the X-ray diffraction analysis.

The interaction between TiO_2 and Al have been reported by Gheorghe *et al.*[46] during pressure infiltration; and by Pan *et al.*[47] during squeeze casting processes of a TiO_2 pre-form with Al. $TiAl_3$ and α-Al_2O_3 were reported as the final product. $TiAl_3$, TiAl or Ti_3Al could form as part of the final product during the reaction between Al and TiO_2, depending on the volume of the reactants consumed during the reaction as stated by Pan *et al.*[47]. Criteria for the formation of each of the three compounds were unclear from the explanation in the report. In other words, the ratio of Al:TiO_2 consumed during the reaction was not reported, possibly since it was not known. The report also suggested that the pores at the reaction interface were due to the volume shrinkage between the reactant and product compounds. Gheorghe *et al.*[46] and Pan *et al.*[47] also hypothesized a three step product-formation process that was derived from results from the experiments.

Run-hua Fan *et al.*[7] have recently reported the formation of γ-TiAl and Al_2O_3 when reacting Al with TiO_2 during a non-isothermal reaction. The work demonstrated that two modes of reaction stages were possible depending on the rate of heating of the reactant components for the reaction $3TiO_2 + 7Al \rightarrow 3TiAl + 2Al_2O_3$. A mole fraction ratio of 7:3 Al:TiO_2 powder mixture was mixed in a planetary mill and then cold pressed into 10 mm diameter pellets under a uniaxial pressure of 100 MPa. The

pellet samples were heated at different heating rates and held for a specific soaking period to study the characteristics of the synthesis reaction. γ-TiAl and Al_2O_3 were found as products after the reaction at higher heating rates (15 K/minute). During the interaction, *fcc*-TiAl was reported to have formed initially which later transformed to the more stable γ-TiAl by ordering.

Horvitz *et al.*[6] reported the formation of TiAl and Al_2O_3 as the outcome of the interaction between Al and TiO_2 under various conditions of temperature and pressure. The authors reported TiAl and Al_2O_3 as the main products and small amounts of Ti_3Al after the SHS reaction of the reacting components. The product of reaction after thermal explosion was reported to be similar in composition to the TiAl – Al_2O_3 SHS reaction. The reaction between Al and TiO_2 could be controlled since an interfacial layer of Al_2O_3 formed between the two reactants, thereby slowing the reaction.[6]

A reaction was not observed between Al and TiO_2 when the reactant component mixture was held at 800ºC between press-rams. X-ray diffraction of the resultant mixture showed only the reactants. However, when the reactant component mixture was held at 800 ºC for about 20 minutes, a mixture of $TiAl_3$ and Al_2O_3 was formed and small amounts of TiO and Ti_2O_3 were observed. When the samples were held at 875 ºC and 950 ºC between the press-rams, thermal explosions occurred and the final reaction mixture contained TiAl, Ti_3Al and Al_2O_3. When samples were constrained under the press-rams to 50 MPa at 950 ºC, TiAl and Al_2O_3 were formed with small amounts of Ti_3Al. When the reactant component mixture was reactive hot pressed (RHP) at 950 ºC for one hour, a complete reaction was not observed. The end

products did not reveal remains of reactants after the reaction: but large amounts of intermediate compounds, like TiO, Ti_2O and $TiAl_2$ were observed besides the usual TiAl, Ti_3Al and Al_2O_3.

The outcome of the interaction between Al and TiO_2 is dependent on conditions like temperature, pressure and composition as reported by Feng *et al.,*[34] Pan *et al.,*[47] Gheorghe *et al.,*[46] Run-hua Fan *et al.,*[7] and Horvitz *et al.*[6]. The outcomes of interaction between Al and TiO_2 at the temperature range of 660°C (melting point of Al) to 850°C (a reported thermite reaction to form $TiAl_3$[46]) has not been reported in the literature.

2.5 Ti – Al – O Thermodynamics

The Ti-Al-O system has been partially studied from the point of view of the thermodynamics of the ternary system. Attempts to calculate the Ti-Al-O phase diagram at temperatures of significance for applications of interest are listed below.

2.5.1 Binary Systems

The binary systems of interest here are Al – O, Ti – O and Ti – Al.

2.5.1.1 Al – O

Equilibrium phases in the Al-O binary phase diagram are (i) liquid Al at the high temperature Al-rich end, (ii) liquid Al_2O_3 near the high temperature O-rich end, (iii) solid *fcc*-Al at low temperature with very small solubility of O, (iv) hexagonal Al_2O_3 (α-Al_2O_3 or corundum) that is commonly believed to have small but unknown deviation from the stoichiometry, and (v) the gas phase.[48] *Figure 2.2*

shows the Al-rich side of the Al-O phase diagram. It is noted that the solubility of O in pure Al is shown to be low at the temperature range of 700ºC.

Besides the thermodynamically stable α-Al_2O_3, Al_2O_3 has several polymorphs that are metastable. The thermodynamically metastable Al_2O_3 polymorphs are divided into two broad categories: (i) *fcc* and (ii) *hcp*, based on location of the oxygen anions.[49] The γ, η (cubic), θ (monoclinic), and δ (either tetragonal or orthorhombic) polymorphs are based on the *fcc* structure.

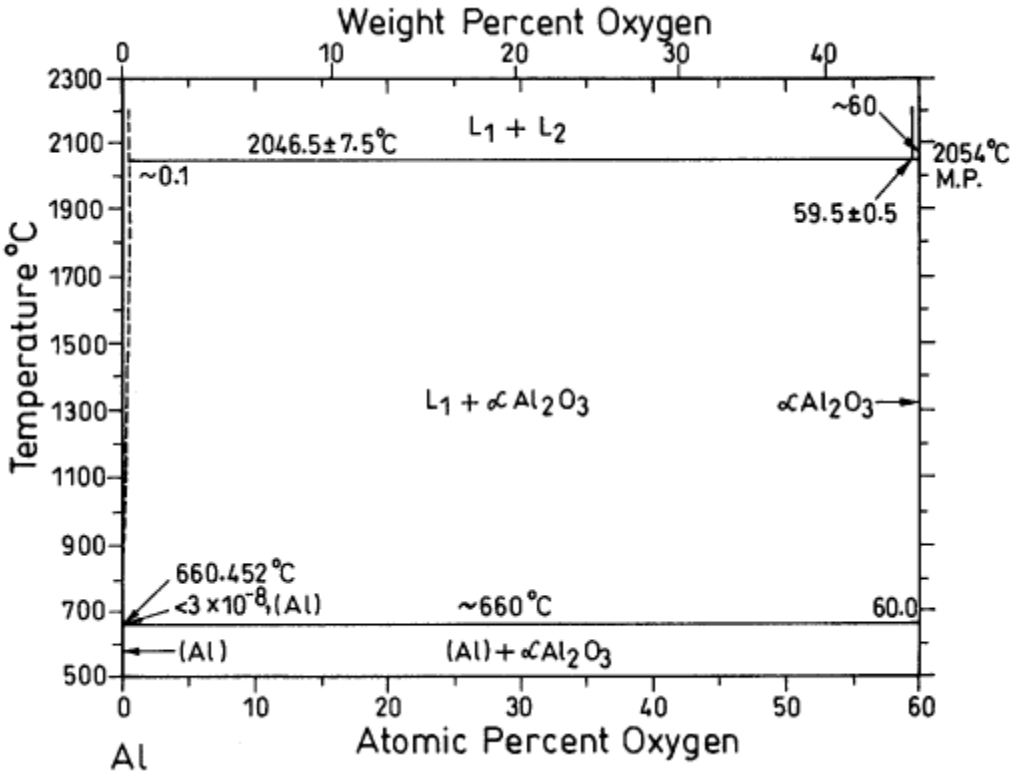

Figure 2.2: Al-O binary phase diagram[48]

The α (trigonal), κ (orthorhombic), and χ (hexagonal) phases are based on the hexagonal closed packed (*hcp*) structure. New monoclinic phases have been identified by Levin *et al.*[50]

Some researchers have reported the presence of metastable Al_2O_3 phases, during the interaction between Al and TiO_2 as a transition phase before the more stable α-Al_2O_3 is formed; while others have obtained the stable phase directly.[51,51,46,47,53,54,55]

The discrepancy revolving around the rate of oxidation of Al to form alumina is worthy of mention. Doremus[56,57] reported that the oxidation of alloys containing Al to form an Al_2O_3 - scale is much faster than the calculated values of the diffusivities of Al and O. The activation energy measured for the oxidation is less than that for diffusion. Doremus[56] thus claims that Wagner's theory of oxidation does not hold true for oxidation of Al. An alternative model suggested by Doremus involves diffusion of uncharged 'AlO molecules'. The author further claims that it is possible to find reasonable diffusivity values for AlO molecules that correspond to the measured oxidation rates. However, neither a direct measurement of the concentration of the diffusing species has been made nor has the transport of AlO molecules been verified.[56]

Pint *et al.*[58] is of the opinion that formation of alumina scales satisfied Wagner's theory of oxidation. Pint *et al.*[58] reported that extrapolated grain-boundary diffusivity relations are consistent with the oxidation rates. Pint *et al.*[58] further refute the mechanism of transport by AlO molecules using the argument that reported experimental results were inconsistent with the growth of alumina scales by uncharged species. Also, the growth rate of such scales can be altered by an applied current.[58]

The above explanation is part of the reason why the current research does not include the study of the interaction between Al and Al_2O_3. The explanation about the solubility of O in Al at 700ºC is relevant to the discussion about oxygen released during the Al – TiO_2 reaction. When Al alloys were oxidized in air, web-like structures were observed by *Nychka and Clarke,*[59] on the surface of the Al particles. *Nychka and Clarke,*[59] have explained the formation of such structures by the diffusion of Al towards the oxide shell occurring more rapidly at the Al_2O_3 grain boundaries compared to within the grains. Al that is diffused outward is oxidized at the surface to form Al_2O_3 which appears as a web-like structure over the surface of grains.

2.5.1.2 Ti – O

Figure 2.3 shows the Ti – O phase diagram that was reported by Massalski.[48]

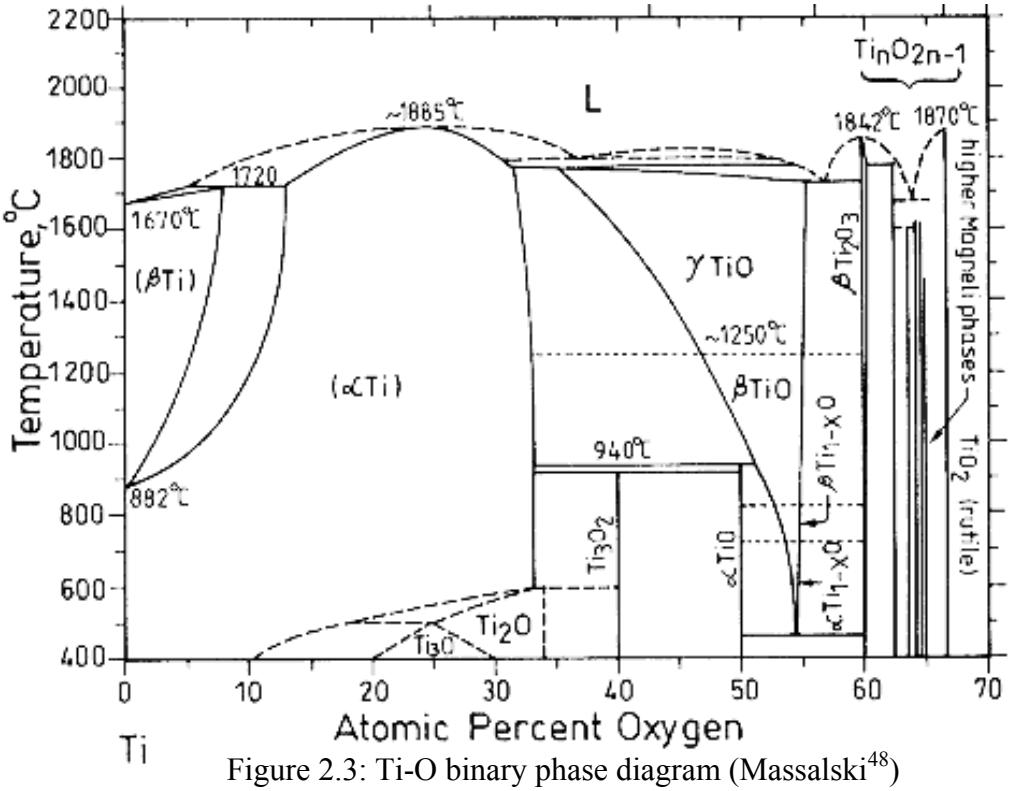

Figure 2.3: Ti-O binary phase diagram (Massalski[48])

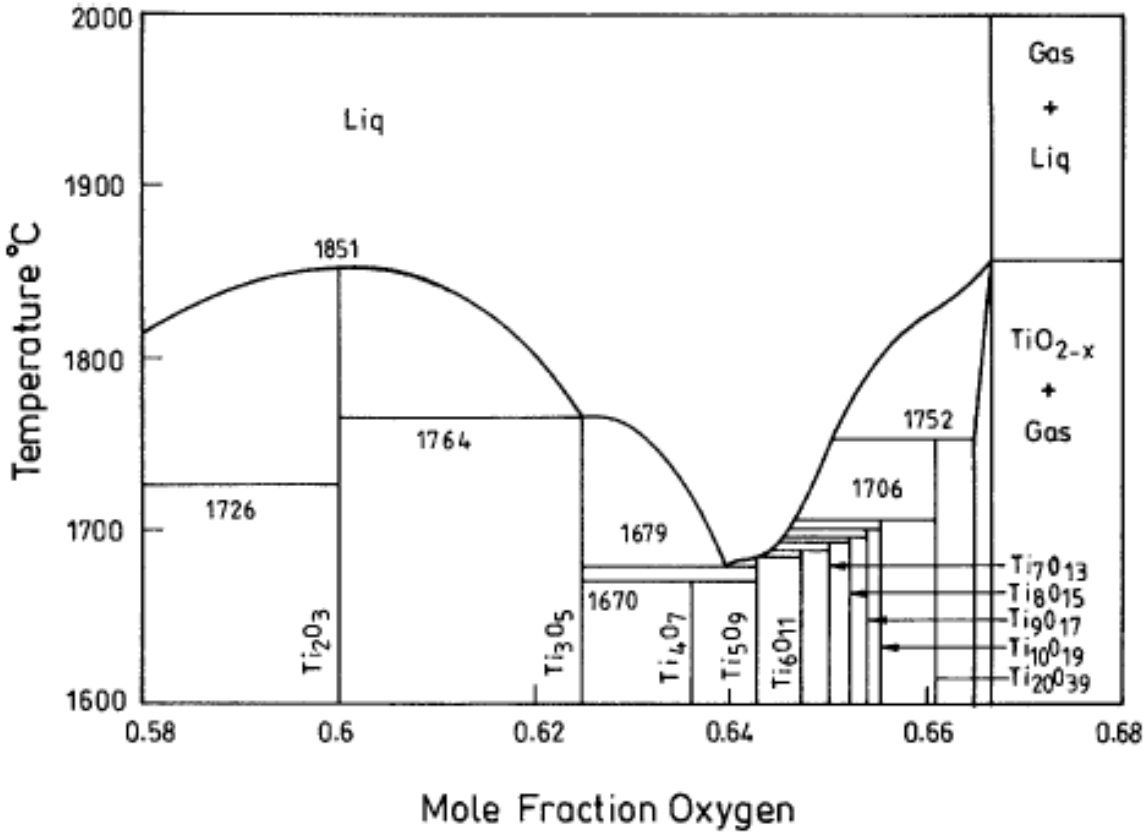

Figure 2.4: Ti-O binary phase diagram showing the Magnelli phases (Waldner *et al.*[60])

At low temperatures, as shown in *Figure 2.3*[48], the α-Ti (hexagonal close packed structure) shows a high solubility of oxygen. Dissolved oxygen is probably responsible for stabilization of the high temperature β-Ti (fcc). The *hcp* phases Ti_2O and Ti_3O are reported at low temperatures.[61] Peritectoid reactions α-Ti + Ti_2O_3 → Ti_2O at ~600ºC and α-Ti + Ti_2O → Ti_3O at ~500ºC are responsible for the formation of Ti_2O and Ti_3O respectively.[61] For both reactions the components α-Ti, Ti_3O_2, Ti_2O and Ti_3O are seen to have a high solubility of oxygen (~17 to 40 atomic percent oxygen). A peritectic reaction L + α-Ti ↔ γ-TiO at 1770ºC forms γ-TiO that has 34.5 atomic percent of oxygen. γ-TiO transforms to β-TiO at ~1250ºC. α-TiO forms by a peritectoid reaction at 940ºC

where the oxygen content in α-TiO is 50 atomic percentage. At the higher oxygen content side of the Ti-O phase diagram, β-Ti_3O_5, β-Ti_2O_3 and TiO_2 form by a peritectic and two different congruent reactions. The congruent reactions to form β-Ti_2O_3 and TiO_2 occur at 1842ºC and 1870ºC respectively. Waldner *et al.*[60] have shown the occurrence of the Magnelli phases (Ti_nO_{2n-1}) also at the higher oxygen side of the calculated phase diagram as shown in *Figure 2.4*.

2.5.1.3 Ti – Al

Equilibrium phases in the Ti-Al system are as follows:[62]

(i) liquid

(ii) disordered solution phases

(iii) *hcp*-(αTi) – maximum solubility of Al is ~45%

(iv) *bcc*-(βTi) – maximum solubility of Al is ~48%

(v) *fcc*-Al – maximum solubility of Ti is ~0.7%[1]

(vi) ordered intermetallic compounds [Ti_3Al (ordered hcp structure), γ-TiAl and $TiAl_3$ (both have ordered *fcc* superstructure), $TiAl_2$ and δ- phases both having bcc structure].

Figure 2.5 shows the calculated Ti-Al phase diagram compiled by Massalski.[48] Discrepancies still appear to be present between some phases in the Ti-Al system[63] which indicate that the system is not well calculated and optimized. Kaufman was first to investigate the Ti-Al system.[64,65,66] Early attempts by Kaufman to calculate the Gibb's free energy of formation of the ordered compounds Ti_3Al, TiAl and $TiAl_3$ were carried out by assuming that the compounds were line compounds.[66]

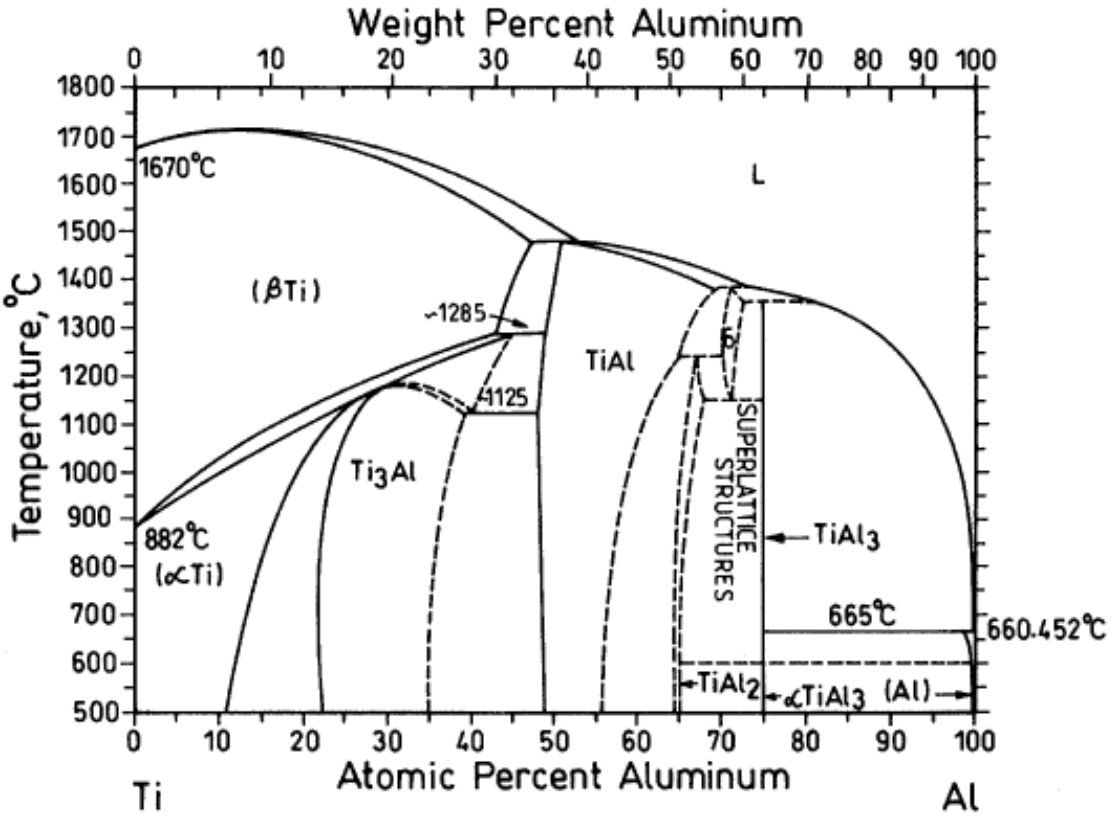

Figure 2.5: Ti-Al binary phase diagram by Massalski[48].

The phase diagram calculated by Murray[67] took into consideration the homogeneity range of Ti_3Al and TiAl. The model that was used by Murray[65] combined the description of the sublattices of the compounds and used the Bragg-Williams approximation. Li *et al.*[68] calculated Gibb's free energy of the Ti-Al system using Ti_3Al data generated by Murray[67] and also included the thermodynamic data for the phases: α- Ti(Al), β-Ti(Al) solid solutions and $TiAl_2$. Li *et al.*[68] used a polynomial expansion for the excess free energy of the Ti_3Al and TiAl in the known homogeneity range[68]. Parameters of the polynomial expression for Gibb's free energy were calculated by using lattice stability of Ti and Al

established by Dew-Hugues and Kaufman[66]. The resultant free energy diagram at 1100°C K is shown in *Figure* 2.6.

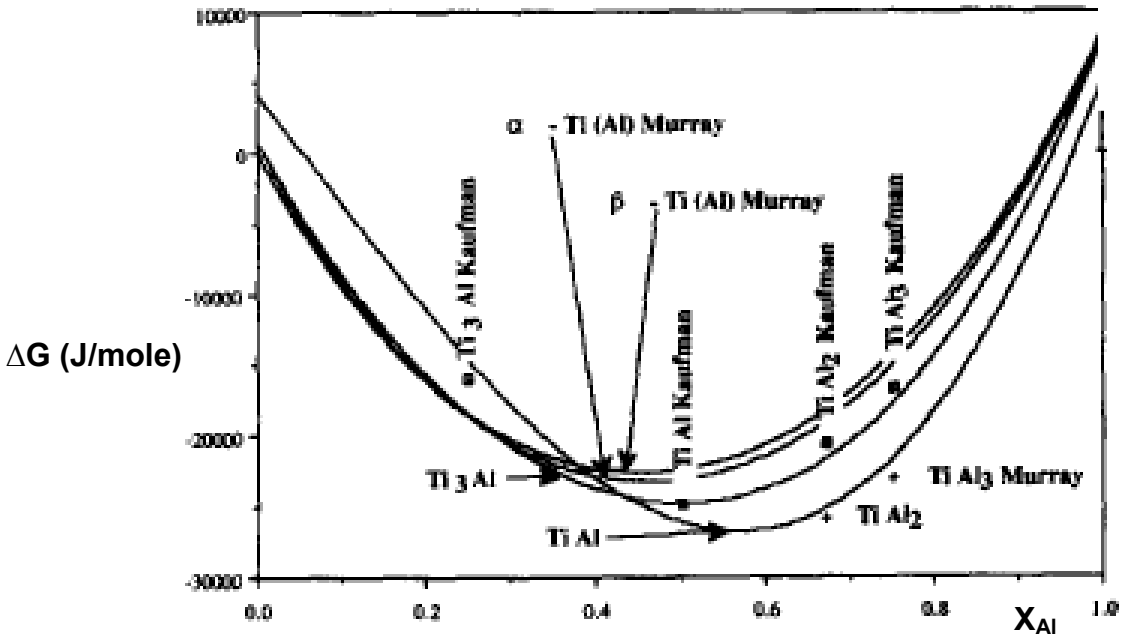

Figure 2.6: Ti-Al Gibb's free energy diagram calculated at 1100°C by Li *et. al.*[68] Calculated values by Murray and Dew-Hughes are used for comparison.

Work by Li *et al.*[68] shows that the TiAl phase has a lower Gibb's free energy than Ti_3Al and $TiAl_3$ at atmospheric pressure and 1100°C. *Section 2.5* explains the reports that describe the interaction between Al and TiO_2 under various conditions of pressure and temperature. The interaction yields $TiAl_3$ as part of the product. Work by Li *et al.*[68] indicates that at 1100°C, the Gibb's free energy of TiAl is lower than $TiAl_3$.

Kattner *et al.*[62] used experimental data from Murray[69] and Mishurda and Perepezko[70] for optimization of the thermodynamic quantities for the Ti-Al system. The sections of interest in the current research are the ordered

intermetallic compounds Ti_3Al, TiAl and $TiAl_3$. Kattner *et al.*[62] used random mixing of Ti and Al atoms on each sublattice to derive the analytical Equation 2.5.1.

$$
\begin{aligned}
G = {} & x_{Ti} * G_{Ti}^{\circ} + x_{Al} * G_{Al}^{\circ} \\
& + R * T * \left\{ n_{Ti}^{1} * \ln\left(n_{Ti}^{1}\right) + n_{Al}^{1} * \ln\left(n_{Al}^{1}\right) + n_{Ti}^{2} * \ln\left(n_{Ti}^{2}\right) + n_{Al}^{2} * \ln\left(n_{Al}^{2}\right) - N^{1} * \ln N^{1} - N^{2} * \ln N^{2} \right\} \\
& + \Delta G^{f} + n_{Ti}^{2} * G_{Ti}^{2} + n_{Al}^{1} * G_{Al}^{1} + n_{Ti}^{1} * n_{Al}^{1} * \left\{ G_{0}^{1} + (n_{Ti}^{1} - n_{Al}^{1}) * G_{1}^{1} \right\} \\
& + n_{Ti}^{2} * n_{Al}^{2} * \left\{ G_{0}^{2} + (n_{Al}^{2} - n_{Ti}^{2}) * G_{1}^{2} \right\} + n_{Ti}^{2} * n_{Al}^{1} * G^{12}
\end{aligned}
\qquad (2.5.1)
$$

where $x_{Ti} = n_{Ti}^{1} + n_{Ti}^{2}$ $\qquad$ $x_{Al} = n_{Al}^{1} + n_{Al}^{2}$

$N^{1} = n_{Ti}^{1} + n_{Al}^{1}$ $\qquad$ $N^{2} = n_{Ti}^{2} + n_{Al}^{2}$

n_{Ti}^{1}, n_{Al}^{1}, n_{Ti}^{2}, and n_{Al}^{2} are the mole fractions of Ti and Al atoms on Ti (1) and Al (2) sublattices. N^{1} and N^{2} are the site fractions of Ti and Al sublattices respectively. G_{Ti}° and G_{Al}° are the Gibb's free energy at the reference state for Ti and Al respectively. ΔG^{f} represents the Gibbs free energy per mole of the perfectly ordered phase at the stoichiometric composition. G_{Ti}^{2} and G_{Al}^{1} are the Gibbs free energy of formation of one mole of substitutional Ti and Al atoms on the Al and Ti sublattices. G_{0}^{1}, G_{1}^{1}, G_{0}^{2} and G_{1}^{2} are coefficients of polynomial interaction terms between atoms on the same sublattice. G^{12} represents the term for the coefficient of interaction between the substitutional atoms on the different sublattices.

2.5.2 Ternary Phases

Free energy equations, solubility limits of the components, and other thermodynamic information of the ternary phases in the Ti-Al-O are not well documented in the literature compared to the other phases (unary and binary). The literature shows only three ternary phases that are recorded, the *X*-phase, Al_2TiO_5, and $Al_6Ti_2O_{13}$.[61,71]

High temperature applications involving titanium aluminides depend on the oxidation resistance of the γ-TiAl phase. Al_2O_3 forms a continuous layer on the γ-TiAl surface depleting the sub-surface layer of Al. A stoichiometric ternary phase known as the *X*-phase forms as a result.[61] Kussmaul *et al.*[72] has summarized details of results from the work on the X-phase as shown in *Table 2.1*.[73,74,75]

Table 2.1: Available Literature on X-Phase

Ti:Al:O (at. %)	Symmetry	Lattice Parameters	Oxidation of γ-TiAl
50:30:20	Cubic	a = 0.69 nm	900ºC, Ar + 20% O_2
37.5:25:37.5 ±10 at. % O	Cubic	a = 0.69 nm	1000ºC, O_2
37.5:25:37.5 ±5 at. % O	Cubic	a = 0.69 nm	900ºC, air

Seifert and Aldinger[76] reported decomposition of Al_2TiO_5 to form TiO_2 and Al_2O_3 at a temperature below 1300ºC; while there are others who reported the decomposition to take place at temperatures between 1200ºC and 1280ºC.[58] Seifert and Aldinger[76] suggest that Al_2TiO_5 is a stoichiometric phase at high oxygen partial pressure; but as oxygen partial pressure decreases, stoichiometric Al_2TiO_5

decomposes to form a reduced form of the Al_2TiO_5, Al_2O_3 and O_2 is liberated. A further decrease in O pressure leads to decomposition of the reduced Al_2TiO_5 phase to form Al_2O_3 and Ti_2O_3.[76] Thermodynamic information for $Al_6Ti_2O_{13}$ is not reported since the compound has been recently discovered.[71]

Thermodynamics of the Ti-Al-O ternary system have been calculated at isothermal conditions for various elevated temperatures; but very little experimental data are available to complete the ternary phase diagram. A detailed literature search has revealed that attempts have been made to calculate the ternary Ti-Al-O phase diagram at 500ºC, 700ºC, 800ºC, 871ºC, 900ºC, 945ºC and 1100ºC.

Not much information is available for the Ti-Al-O ternary at 500ºC and 700ºC as is seen in *Figure 2.7*. Lee *et al.*[77] have calculated the phase diagram of the ternary system at 500ºC and 700ºC. The difference in the slope of the curve seems to be different at both temperatures which indicate the higher solubility of Al in Ti with an increase in oxygen at 700ºC. Luthra[78] calculated the ternary phase diagram at the isothermal 800ºC section as is shown in *Figure 2.8*. Luthra[78] did not consider Ti_3O (a metastable phase) for equilibrium diagram calculations. It is noted that Ti_3O is not expected to form at temperatures above 500ºC as per the binary phase diagrams.

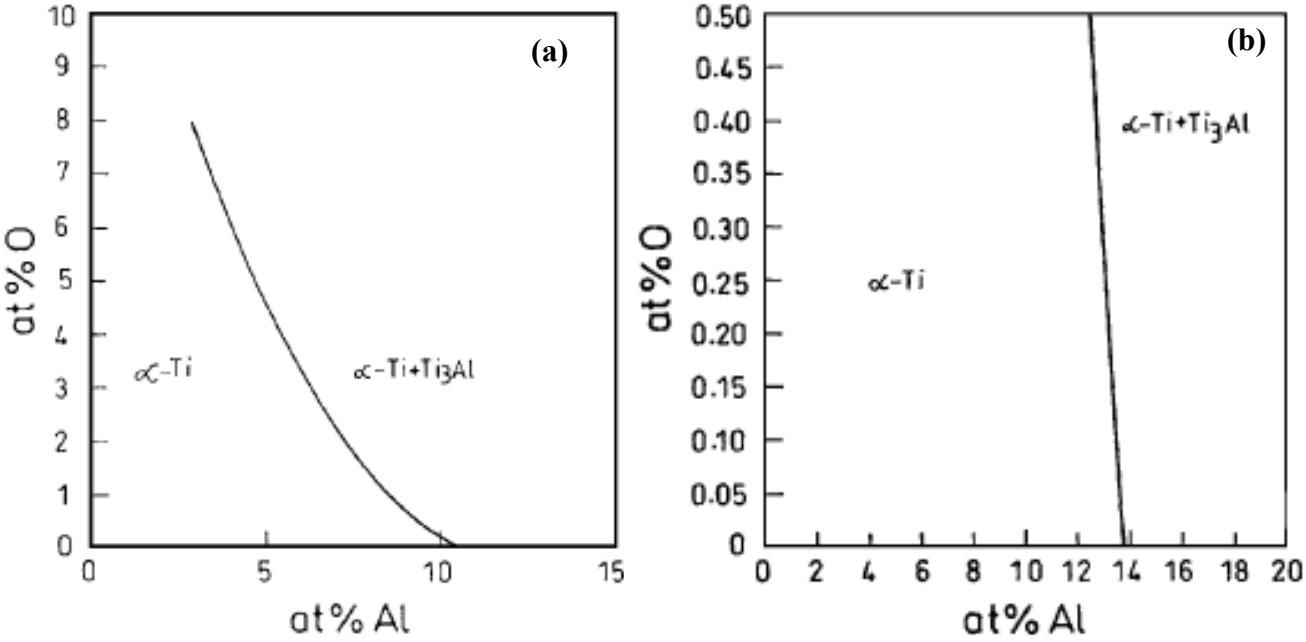

Figure 2.7: Calculated isothermal section (at Ti-rich regions) of the Ti-Al-O ternary phase diagram at (a) 500ºC and (b) 700ºC (Lee *at al.*[77])

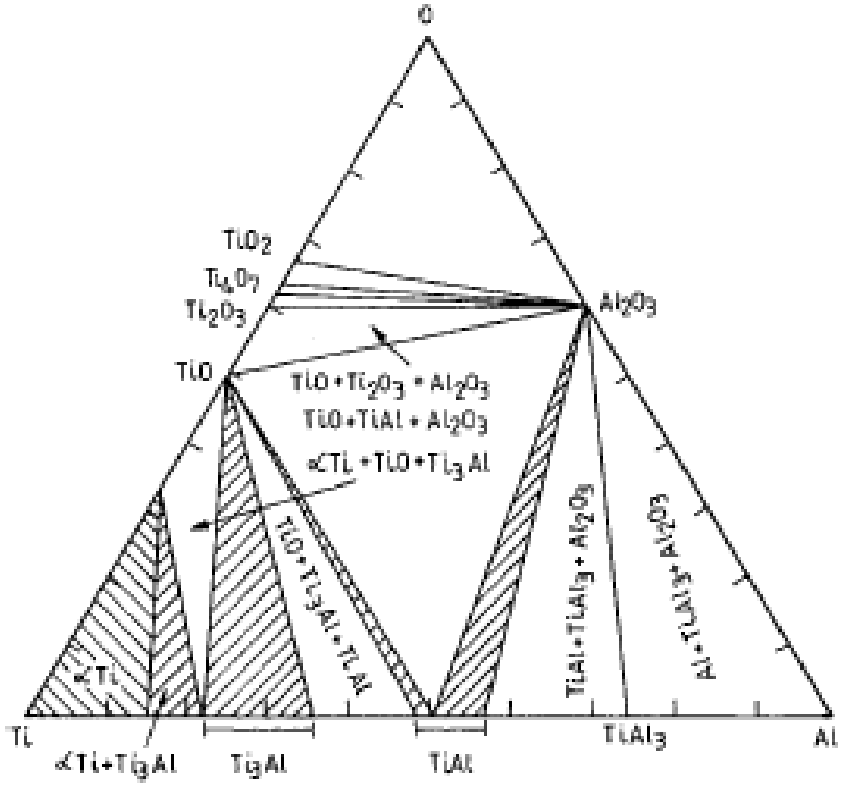

Figure 2.8. A calculated isothermal section of Ti-Al-O phase diagram at 800ºC (Luthra[78])

Tressler *et al.*[79] made one of the earliest evaluations of the Ti-Al-O ternary system at 871ºC. Tressler *et al.*[79] proposed two possible sections of the ternary as shown in *Figure 2.9*. The two sections are almost identical except that there are differences in the equilibrium between TiAl, TiO, and Ti_2O_3 in one case, and between Ti_3Al, TiO, and Ti_2O_3 in the other. It is of interest to note that the authors were investigating the reaction path between Ti and Al_2O_3 at 871ºC. The reaction path was determined to be $Al_2O_3 \rightarrow TiO \rightarrow Ti_3Al \rightarrow \alpha$-Ti as the layers of compounds from Al_2O_3 to α-Ti.

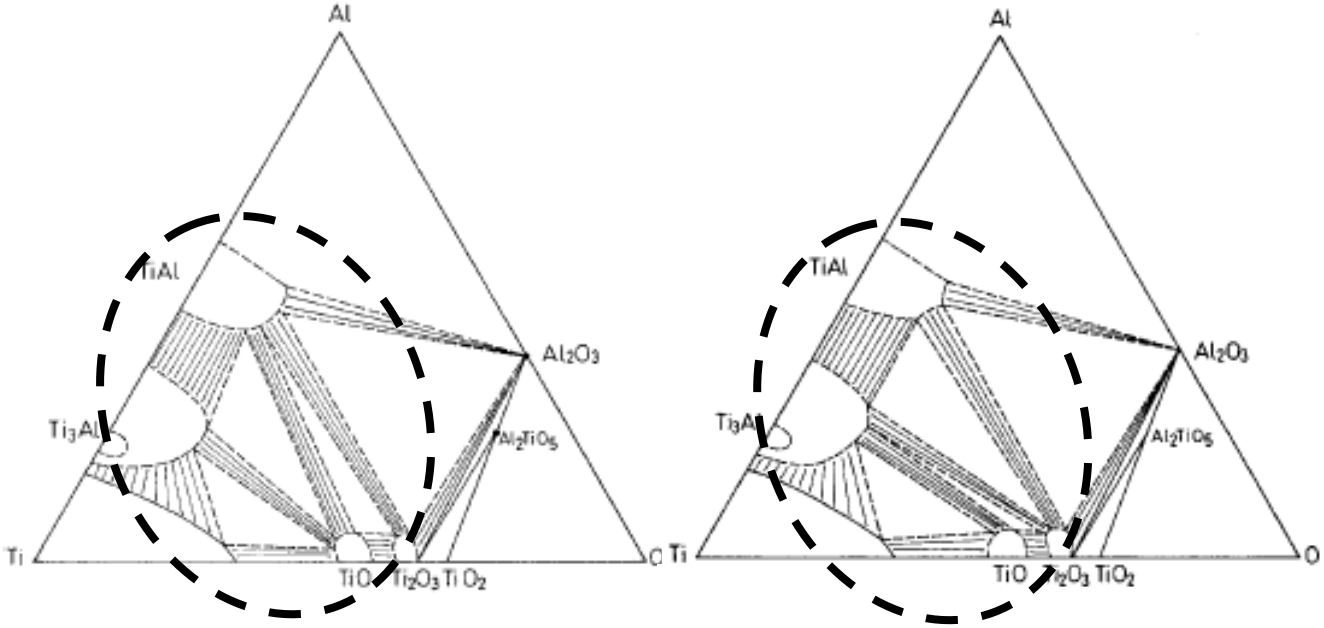

Figure 2.9: Two possible isothermal sections of the Ti-Al-O ternary system calculated by Tressler *et al.*[79]

The reaction sequence was verified by preparing diffusion couples and heating the couples for extended periods of time at 871ºC. The TiO phase was not detected by the X-ray diffraction technique, but was claimed to be present by the reflection electron diffraction technique. Later it was suggested by Choi et al.[80], Li *et al.*[68] and Zhang *et al.*[81] that the TiO phase was incorrectly identified and could instead be the TiAl

phase. Zhang *et al.*[81] stated that the sequence with TiO as represented above is not thermodynamically possible since Al would have to diffuse from a higher activity in Al_2O_3, to a low value in TiO, and again to a high value in Ti_3Al.

At 900ºC, Rahmel *et al.*[82] calculated the Ti-Al-O phase diagram considering Ti_3Al, TiAl and $TiAl_3$ as line compounds (shown in *Figure 2.10*). Rahmel *et al.*[82] assumed that the compounds had no solubility for any species in order to simplify calculations.

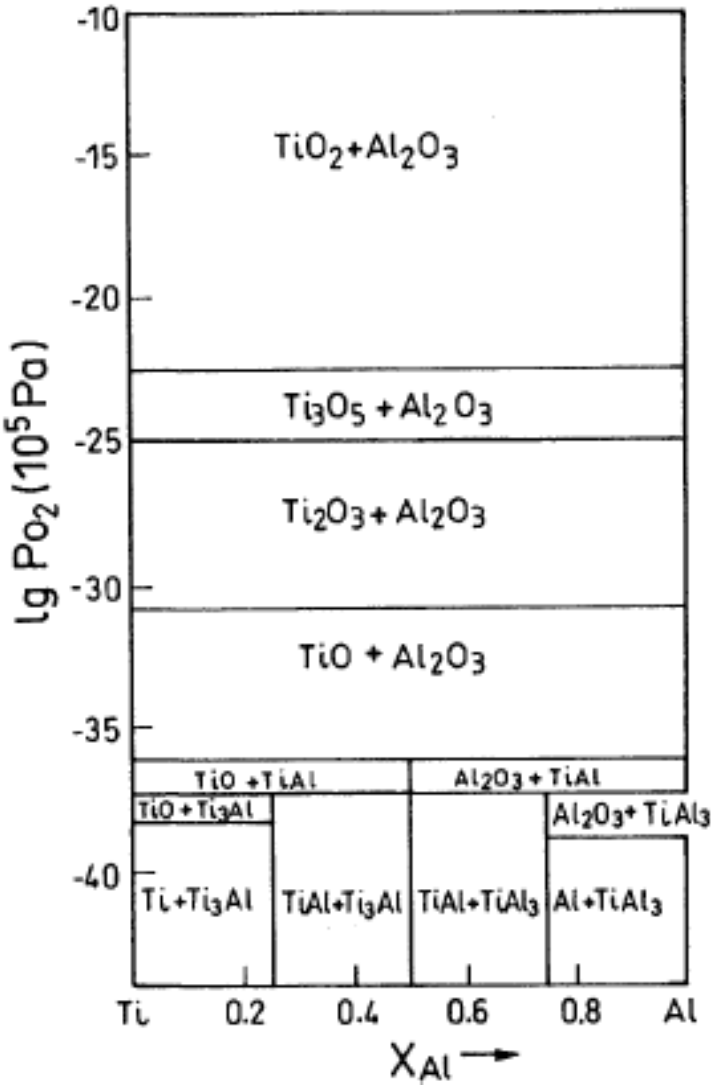

Figure 2.10: Isothermal section of the Ti-Al-O ternary system at 900ºC calculated by Rahmel *et al.*[82]

Kelkar *et al.*[83] assessed parts of the Ti-Al-O ternary system. *Figure 2.11* shows the 945ºC isothermal section of the ternary system calculated by Kelkar *et al.*[83] based on the boundary conditions evaluated by Murray *et al.*[84], Kattner *et al.*[62] and Wriedt *et al.*[85] for the Ti-O, Ti-Al, and Al-O systems respectively. Regions in the phase diagram having a three phase field are represented with filled circles, and the two phase fields with open circles. Tie-lines established by Kelkar *et al.*[83] are represented by solid lines; and the ones previously established are represented by dashed lines. Single phase regions are represented as shaded areas and the three-phase regions are marked with Roman numerals. The tie-lines with alternating long and short dashed lines are based on diffusion couple experiments with two phase samples. The phase diagram also shows a single phase field representing the ternary phase Al_2TiO_5.

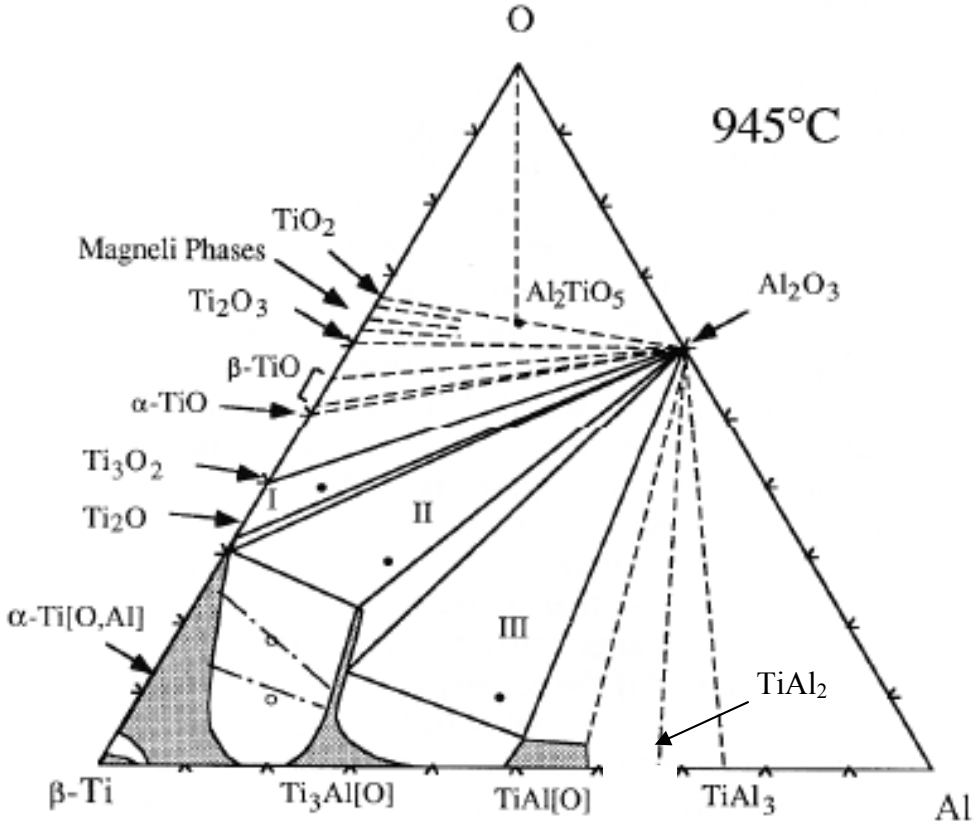

Figure 2.11: 945ºC isothermal section of the Ti-Al-O ternary system based on experimental evaluations on the base diagram calculated by Murray *et al.*[84], Kattner *et al.*[62] and Wriedt *et al.*[85]

Figures 2.12 and *2.13* show isothermal sections of the Ti-Al-O phase equilibrium at 1100ºC as calculated by Li *et al.*[68] and Lee *et al.*[77] respectively. It is noted that the TiAl phase region on both phase diagrams (*Figures 2.12 and 2.13*) have very little solubility of oxygen at 1100ºC.

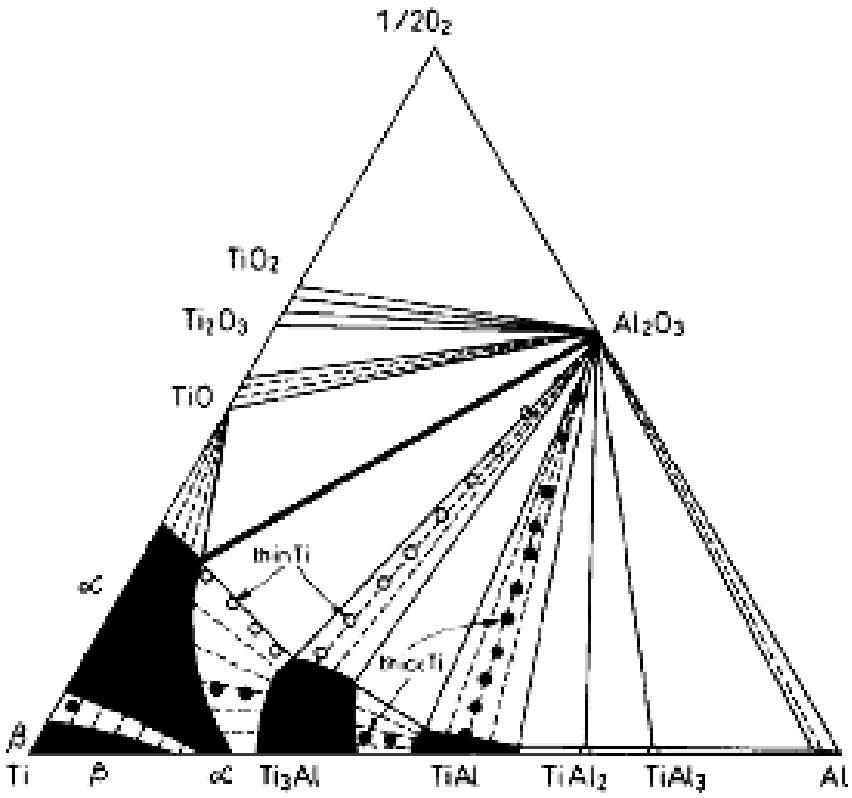

Figure 2.12: Isothermal section of the Ti-Al-O as calculated by Li *et al.* [68] with Ti-Al_2O_3 diffusion paths superimposed.

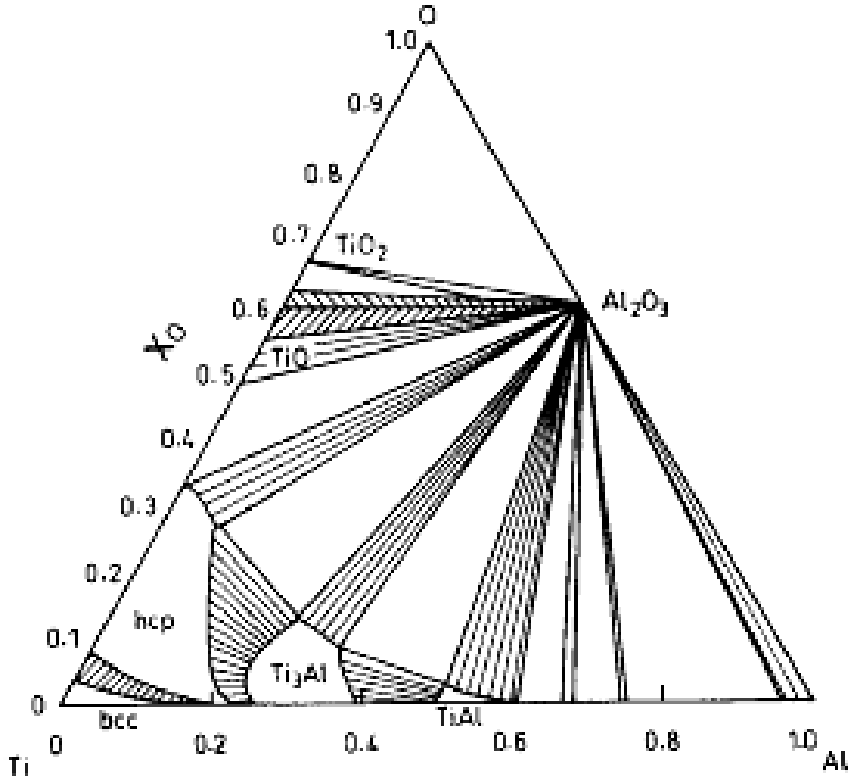

Figure 2.13. Isothermal section of the Ti-Al-O as calculated by Lee *et al.*[77].

2.6 An Explanation for the Oxygen Released During the Al – TiO_2 Reduction Reaction

Al is expected to reduce TiO_2 at elevated temperatures to form titanium aluminides. Reduction of TiO_2 results in the liberation of oxygen. There are discrepancies about what happens to the liberated oxygen as explained below. Some reports revealed that Al_2O_3 was formed as dense crystalline particles by the oxidation of Al that reduced TiO_2.[34,36,46,47,55] Some reports suggested that oxygen was trapped in the intermediate layer since the mobility of oxygen and other diffusing species was low and hence formation of Al_2O_3 did not take place.[44]

It has been suggested by Zhang *et al.*[44] that O^{2-} liberated during the reduction of TiO_2 stayed in the $TiAl_3$ grains as a supersaturated solid solution. Zhang *et al.*[44] suggested that O^{2-} ions do not have mobility at the temperature range around 800ºC to be able to combine with Al^{3+} ions formed by the oxidation reaction to form any polymorph of Al_2O_3. The O^{2-} and Al^{3+} ions required a period of time (incubation time) to nucleate to stable compounds. The incubation time was significantly reduced at 1000 ºC so that α-Al_2O_3 nucleated and grew at the elevated temperature.[44]

Zhang *et al.*[44] reported that the reaction:

$$3TiO_2 + 13Al \rightarrow 3TiAl_3 + 2Al_2O_3 \qquad (2.6)$$

was possibly responsible for the formation of the aluminide when the reactants interacted at elevated temperature. Based on *Equation 2.6*, 33% of the volume of the product would be Al_2O_3 assuming that all the oxygen produced by the reduction of TiO_2 was converted to Al_2O_3. An explanation for the significant amount of oxygen has not been reported. Lefebvre *et al.*[86] developed a theoretical model that showed that the equilibrium solubility of oxygen in titanium aluminide phases was not much, and that the solubility decreased significantly with an increase in Al content in the phases. The model suggested that the decrease in solubility of oxygen was primarily due to the decrease in number of suitable interstitial sites in the crystal when the Al content was increased. According to the model[86], the solubility of oxygen in the γ-TiAl phase that contains 50 at% Al, was about zero. The $TiAl_3$ phase had a higher Al content than TiAl; therefore, the solubility of oxygen was lower. The report stated that if the O^{2-} ions exist, they were in a highly metastable state in the $TiAl_3$ phase. Zhang *et al.*[42] suggested that Al^{3+} and O^{2-} ions that were present in the titanium

aluminide grains as a metastable solution could precipitate as fine Al_2O_3 particles in the aluminide phase by low temperature aging. Further research would be needed to study and prove it.

Oxygen could possibly be present in the Al layer. As observed in the Al-O phase diagram in *Figure 2.2* in *Section 2.5.1.1*, Al does not have much solubility (close to zero) for oxygen at the temperature range of 700ºC. Levis and Kaplan[87] and Das *et al.*[61] have also shown that the solubility of oxygen in Al was very low. It has also been reported by Kubaschewski and Hopkins[88] that oxygen has very small solubility (close to zero) in Al at 700ºC and above. One of the reasons for the limited solubility could be that the equilibrium partial pressure of oxygen for the oxidation reaction of Al is tens of orders of magnitude lower than the partial pressure of oxygen found in most experimental and industrial applications.[89] Due to such conditions, Al tended to oxidize to form an oxide rather than form a solid solution of oxygen in Al.

3.0 EXPERIMENTAL APPROACH

Determination of the interface between Al and TiO_2 was approached experimentally and the mechanism of formation and growth of the interface was determined by use of theoretical calculations and analytical tools.

3.1 Theoretical Determination of Possible Interfacial Compound(s)

Table 3.1: Possible compounds expected to form in the Ti-Al-O system.

Compound	Molecular Structure	Crystallographic Structure
Aluminum	Al	Face centered cubic
Titanium	Ti	Hexagonal closed pack
Oxygen	O_2	--
Aluminum oxides	α-Al_2O_3	Hexagonal closed pack
	γ-Al_2O_3	Face centered cubic
Titanium aluminides	$TiAl_3$	Tetragonal
	γ-TiAl	Tetragonal
	Ti_3Al	Hexagonal closed pack
Titanium dioxide	TiO_2 (rutile)	Tetragonal
	TiO_2 (anatase)	Tetragonal
Magnelli phase	Ti_2O_3	Hexagonal closed pack

Possible compounds and phases in the Al-Ti-O system that could form by the interaction between Al and TiO_2 are listed in Table 3.1. Formation of an interfacial compound was assessed using thermodynamic principles. Standard thermodynamic principles were used with appropriate assumptions to determine the lowest energy

state of the existing system by calculating free energy states of possible compounds in association with the interacting components of Al and TiO_2. The compounds resulting in the lowest energy state were the ones that were expected to form during the reaction. Elements and compounds of interest during the interaction between Al and TiO_2 are listed in Table 3.1.

Thermochemical data of the relevant compounds of interest at specific temperatures and other thermodynamic parameters are not available. Gibb's free energy equations listed by *FactSage*^{TM} were checked for validity by using the equations at specific temperature values. The free energy values were compared with those from the JANAF-Thermochemcial Tables (the more widely accepted thermo-chemical data). Calculations that show the verification of thermochemical data from *FactSage*^{TM} with that from the JANAF-Thermochemical Tables are presented in *Appendix I*. It was shown that the values obtained by using the equations in *FactSage*^{TM} compared well with the values reported in the JANAF-Thermochemical Tables and were thus used for calculations.

The experiments performed were largely classified into two categories:

- The first set of samples was the powder samples used for preliminary X-ray diffraction analysis.
- The second set of samples was the film-substrate samples that were treated to specific conditions.

The treated samples were further characterized to explain the results obtained using suitable analytical tools.

3.2 Experimental Reaction Model Parameters

The region of interest in the current research was exclusively the interface between Al and TiO_2 as is shown in *Figure 3.1*. The isothermal temperature chosen for the current study was 700ºC due to the reason stated in *Section 2.6*. Samples that were treated to elevated temperature were soaked for an extended period of time so that the interaction between film and substrate could generate a sufficiently wide interfacial region to allow investigation.

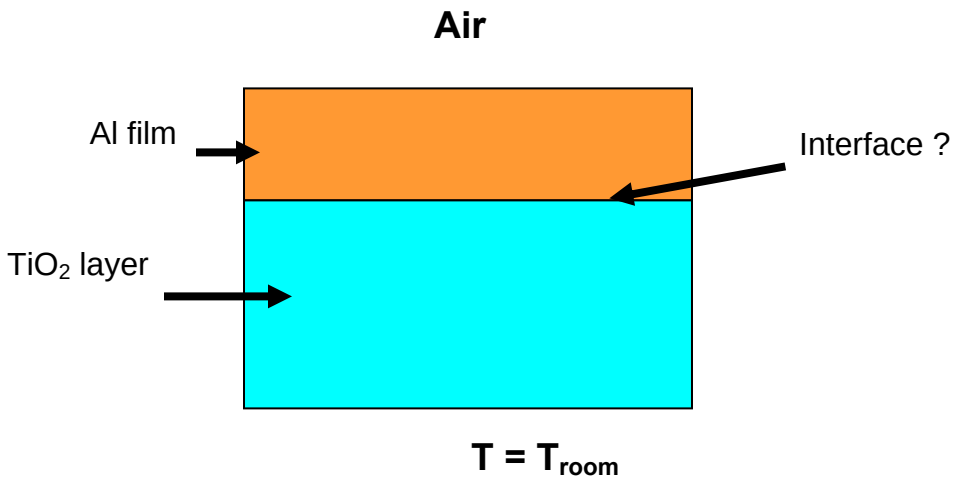

Figure 3.1: Schematic of the interfacial region as the area of interest for the study.

3.3 Diffusion Couple Substrate Structure

The experiments were designed to study the extent of interaction between Al and TiO_2 particles. A diffusion couple experiment is the conventional way to study particle – particle interaction; therefore, a simple system consisting of a flat interface between the starting materials in the form of a diffusion couple was chosen. Vacuum deposition grade TiO_2 (99.9 % pure/ *CERAC Inc.)* was used as a 10 - 12 mm diameter

x 4 - 5 mm thick substrate. An aluminum (99.9% pure, *CERAC Inc*.) film about 4-5 μm thick was sputter deposited (Innovative Coatings LLC.) on the rutile substrate. Surface roughness of the substrates was less than one *μm* as was determined using AFM. The surface texture allowed adequate adherence of the film to the substrate after deposition. It is noted here that grains of TiO_2 usually have stacking faults present at the surface of the grains that run into the interior of the grains;[91,92] and the stacking faults usually terminate within the grains.

Figure 3.2 shows a schematic of Al deposition on a TiO_2 substrate. The film thickness of 4-5 *μm* was chosen so that the area of interaction of the X-ray beams would include the interface between Al and TiO_2.

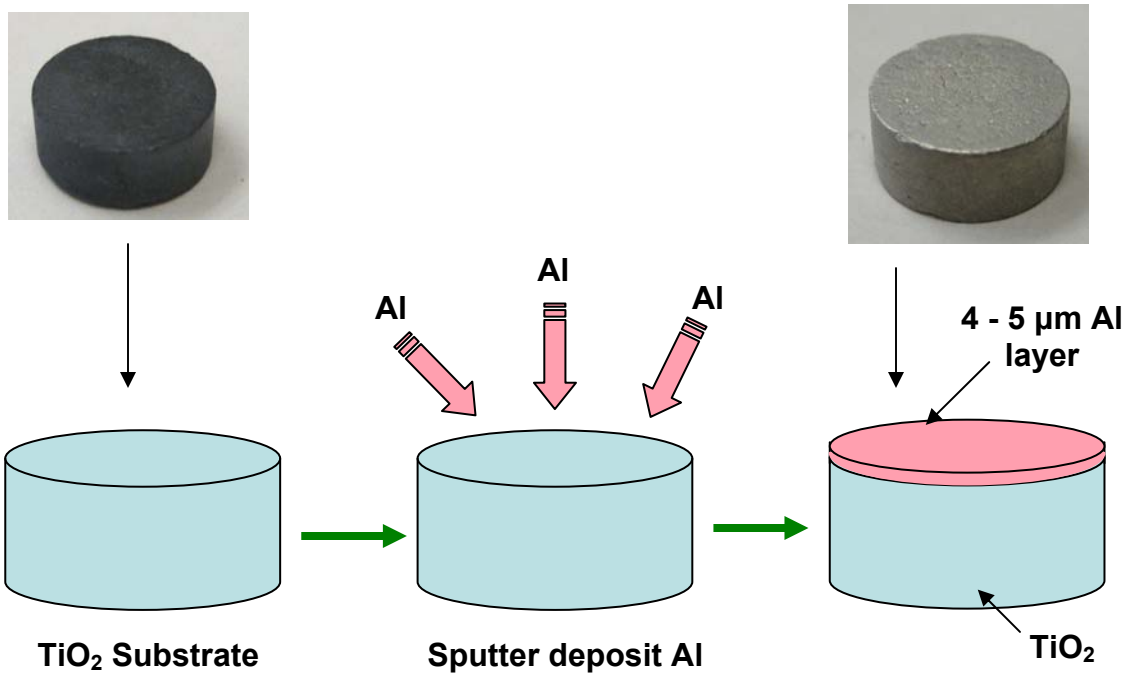

Figure 3.2. Schematic of 4-5 μ Al film sputter deposited on TiO_2 substrate sample.

The film-substrate samples were treated at elevated temperatures for extended periods (9 and 36 hrs) of time. The diffusivity of O at 700˚C into Al_2O_3 ($1.8x10^{-23}$ m^2/second) was used to calculate the depth of diffusion for either of the diffusing species by using the well known equation:

$$l = \sqrt{Dt} \qquad (3.3)$$

where l is the depth of diffusion for the diffusing species, D is the diffusivity of the diffusing species into substrate and t is the time required for diffusion. It was calculated that the diffusing species (oxygen) would travel a depth of about 50 nm, and 100 nm by exposing the sample to 700˚C for 9 hours, and 36 hours respectively.

3.4 Identification of Interfacial Compound(s) Using XRD

Samples of powdered Al (atomized *325 ALCOA*) were mixed thoroughly with TiO_2 (anatase) powder (*Fisher Scientific Inc.*) in a 4:3 molar ratio of Al:TiO_2. The 4:3 molar ratio of Al:TiO_2 was used so that there would be sufficient Al to reduce TiO_2 completely in the event that the oxidation-reduction reaction would go to completion as shown by *Equation 3.4*. Batches 15 mg in size were prepared by mixing 4.65 mg of Al powder with 10.34 mg of TiO_2 powder. The powder sample mixture was then loaded in a furnace maintained at 700ºC in air. The powder sample was held at 700ºC in the furnace for 9 hours to allow the TiO_2 to interact with the Al.

$$4Al + 3TiO_2 \rightarrow 2Al_2O_3 + 3Ti \qquad (3.4)$$

The powder mixture was loaded into the sample tray of the Philips X'Pert Pro MPD X-ray diffractometer for analysis. Powder diffraction was conducted in triplicate on different samples to check for repeatability. Diffraction scans ranged

between 2θ values 20º and 90º. The step size was 0.0167º; the time per step was 100.33 seconds; and the scan speed was 0.012° per second. The total time of scan per sample was 56 minutes and 53 seconds. Slow scans were performed between 2θ values 36º and 40º to resolve closely spaced peaks. The film-substrate [Al-TiO_2 (rutile)] samples were analyzed using X-ray diffraction to determine the presence of new phases or compounds; either at the surface, or at the interface of the film-substrate samples. It was observed earlier that when the film-substrate samples were heated at elevated temperatures (700°C) the melted Al rolled off the surface resulting in a large loss of Al. Two film-substrate samples were then sandwiched together (see Figure 3.3) before heat treatment. The sandwiched samples were heated in a furnace preheated to 700ºC and held at 700ºC for 9, or 36 hours. The samples were cooled to room temperature by furnace cooling. The samples were gently detached from the sandwich arrangement, and the Al sides of the samples were used for X-ray diffraction analysis.

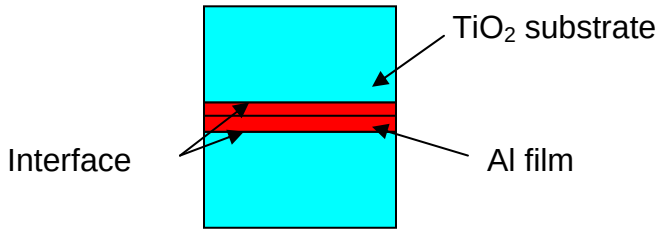

Figure 3.3. Schematic of two film-substrate Al-TiO_2 (rutile) samples sandwiched one on top of the other.

An unheated film-substrate sample was heated *in-situ* in an X-ray diffractometer and scanned by the X-ray diffractometer at regular intervals of temperature (400°C,

600°C, 650°C and 700°C). An *in-situ* scan experiment while heating samples in the X-ray diffractometer was performed to detect possible interactions between the film and substrate that could potentially result in the formation of a new metastable compound. The new compounds could later transform to a more stable state at equilibrium when cooled to room temperature. A Philips X'Pert Pro MPD X-ray diffractometer was used with an Anton PAAR XRK-900 high temperature stage to continuously monitor the film-interface-substrate at various elevated temperatures in air at near isothermal conditions. The objective of the experiment was to determine the temperature at which another phase could originate. Data about possible transformation of new phases and their transformation to more stable phases could be obtained. The continuous scan mode using a Cu K_α radiation with a step interval of 0.02° (2θ) and a count time of one second/step was used to collect the data. The experiments were carried out in air. The PANanalytical X-Pert Plus software was used to evaluate the peaks obtained from the diffraction spectra.

The Al – TiO_2 samples were loaded onto the high temperature stage of the Philips X'Pert Pro MPD X-ray diffractometer. The high temperature stage used a muffle furnace that heated the small sample space to a maximum of 900°C. The thermocouple used to measure the temperature of the sample was situated close to the surface of the sample. Also, the heating chamber had a relatively small volume that ensured the temperature measurement would be as close to accurate as possible.

3.5 Morphological Understanding of the Interface

3.5.1 Diffusion Couple Samples: Al – TiO_2 Film – Substrate Structure

A LEO model 1550 Field Emission Scanning Electron Microscope at 5 kV was used to investigate the two types of samples (film-substrate and powder samples).

The surface of the Al – TiO_2 (film – substrate) sample that was held at 700°C for 9 hours was compared to the surface of the unheated Al – TiO_2 (film – substrate) sample using the SEM. The morphology of the substrate-interface-film regions was compared before and after the samples were heated to an elevated temperature.

3.5.2 Powder Mixture Samples

The second set of samples was a mixture of Al powder and either Al_2O_3 powder, or TiO_2 powder. Al/Al_2O_3 and Al/TiO_2 powder mixture samples were heated to 1200°C in either air (oxidizing environment), or He (non-oxidizing environment) (99.999% purity). The Al – Al_2O_3 powder interfaces were investigated using the SEM. The Al/A_2O_3 powder samples were studied using the

SEM to check whether the Al_2O_3 shell outside the Al particles would break to allow liquid Al to interact with the particles outside of the shell.

3.6 High Resolution Identification of the Interfacial Phase(s) and Compound(s)

The interface of the film-substrate samples was investigated using the TEM to compare morphology before and after heating to an elevated temperature for different periods of time. Cross-sectional slices were prepared from both heated and unheated samples, then Focused Ion Beam (FIB) was used to mill thin sections at the sample interface. The sample preparation procedure is explained below in this section.

Attempts were made to prepare samples for TEM studies by the traditional route (dimpling followed by ion milling); but a significant amount of copper re-deposited onto the dimpled surface. The deposited copper interfered with the existing material; so it was decided to use the FIB to prepare the samples for the TEM study. The procedure for TEM sample preparation using FIB is explained below.

Figure 3.4. The FIB – SEM position of sample relative to the two beams.

The FEI HELIOS NANOLAB 600 dual beam focused ion beam was used here to mill small slices at the interface of the sample treated to elevated temperature. *Figure 3.4* shows the sample with two beams in the FIB system: one beam is used to mill material from the surface of the sample; while the other is used like an SEM to scan the working surface.

A suitable spot on the sample containing the interface was selected. The platinum FIB probe was then inserted and the required amount of platinum was deposited on the surface of the sample (see *Figure 3.5*). An Ar-ion beam was used to mill material on both sides of the platinum strip as shown in *Figure 3.6*. The sideways-cut that was employed to mill material from both sides of the platinum strip is called a "staircase cut" (see *Figure 3.6).* A "cleaning cut" was then used to clean the edges on both sides of the platinum strip and remove most of the re-deposited material from the area of interest.

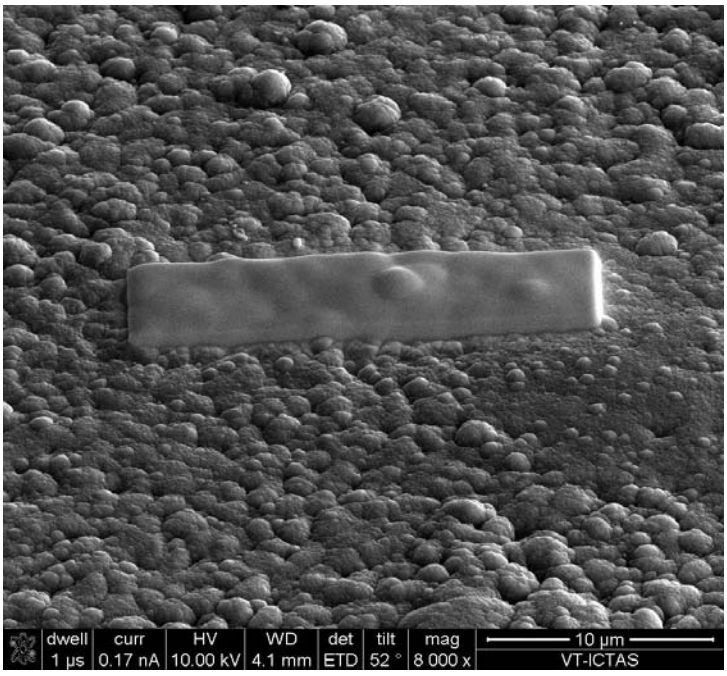

Figure 3.5. Platinum strip deposited on the surface of the sample to be FIBed.

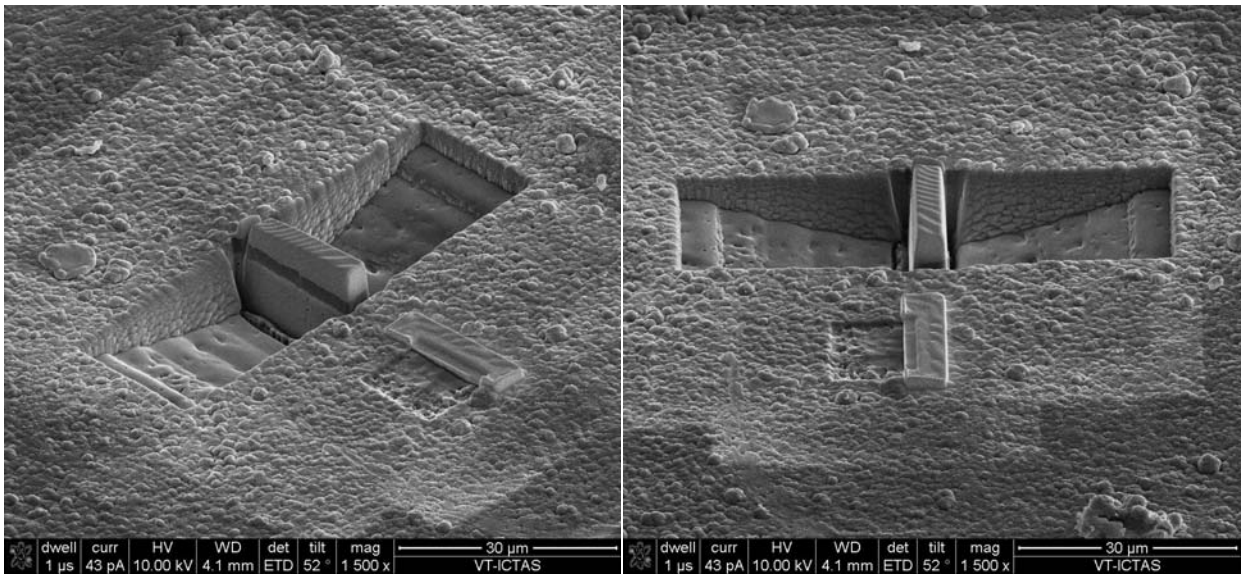

Figure 3.6. Material milled away from both the sides of the platinum strip using the FIB.

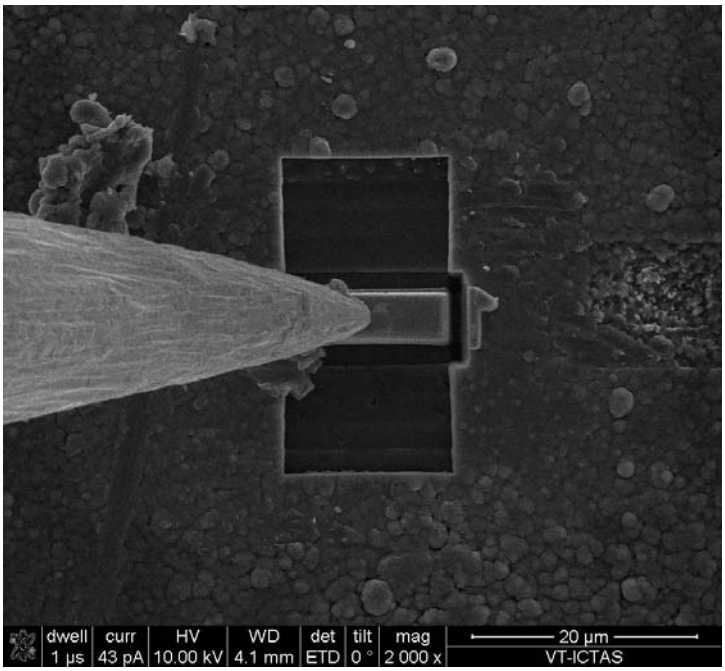

Figure 3.7. OmniProbe® is attached to the area of interest after which the sides are cut.

The bottom of the strip was detached from the bulk sample using the "undercut" beam. The sample strip of interest was attached to the bulk only at the sides. *Figure 3.7* shows an OmniProbe® attached to the area of interest after the sides of the strip were milled with the ion beam. The strip of interest was supported only by the OmniProbe® and was entirely detached from the bulk sample. The sample was next attached to a grid using platinum as shown in *Figure 3.8* and was then ready to be thinned as required for TEM applications [regular Bright Field (BF) and Dark Field (DF) imaging, lattice imaging, STEM etc.]

Material was removed from either side of the sample slice to make it thinner. A lower current ion beam was employed for this purpose so as to avoid excessive erosion that could damage, or even destroy, the sample beyond use for TEM investigation. *Figure 3.9* shows the side view of a thinned sample and *Figure 3.10* shows the top view. The sample was thinned to about 150 nanometers to make it suitably electron transparent to be probed with the TEM, and was then ready to be studied.

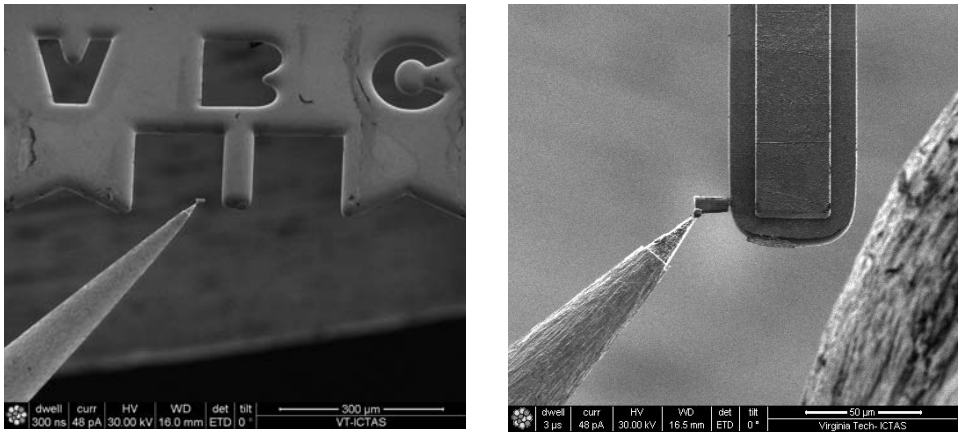

Figure 3.10. Stages of attachment of the sample strip onto grid using the OmniProbe® and platinum using the FIB.

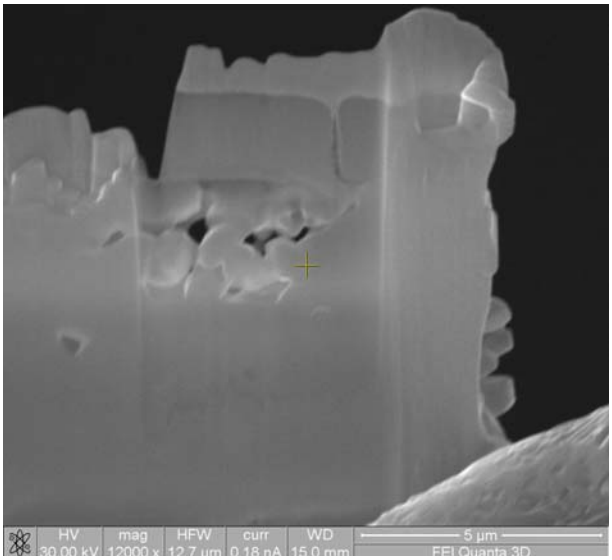

Figure 3.9. Side view of thinned sample showing the platinum layer, the thin film layer, the interface and the substrate attached to the grid.

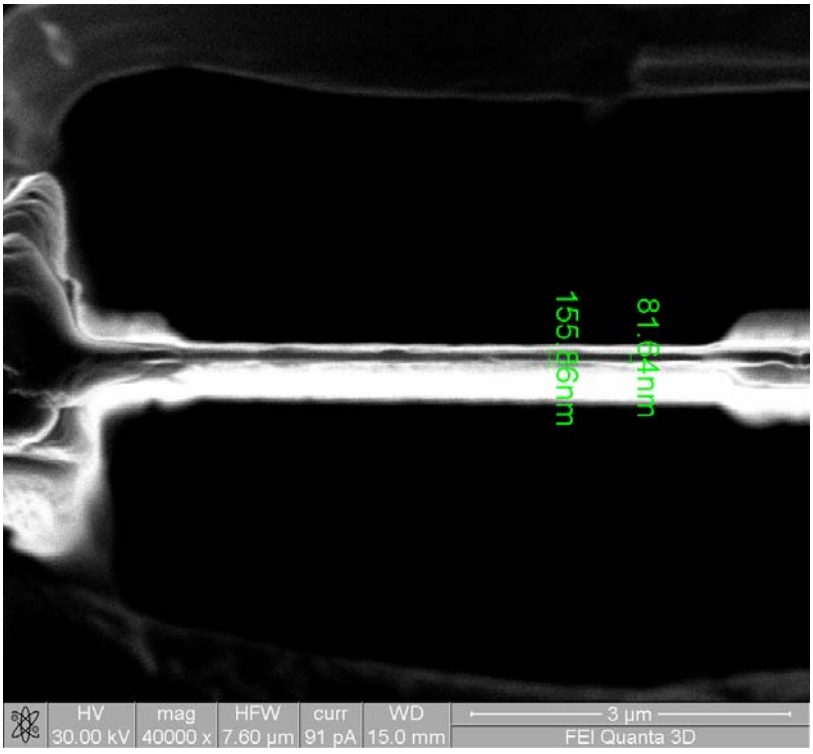

Figure 3.10. Top view of sample thinned to about 150 nanometers.

4.0 RESULTS AND DISCUSSION

Al is usually covered with a thin passive layer of Al_2O_3 due to oxidation. The current chapter explains the results obtained from experiments when Al_2O_3 in contact with Al was heated to elevated temperatures (1000ºC to 1300ºC). Film-substrate and Al powder samples covered with Al_2O_3 were studied and results at elevated temperature are explained here.

This chapter also describes the results obtained during the high temperature experiments when Al and TiO_2 interacted for extended periods of time. Formation of the interfacial region and identification of the interfacial compound(s) are explained. A theoretical model for the formation and growth of the interfacial compound is postulated and proof of various elements of the model are explained in this chapter using thermodynamics and analytical tools like the SEM, FIB and TEM.

4.1 Effect of Temperature on the Al_2O_3 Shell around Al

The surfaces of alumina substrates coated with Al were compared before and after heating to elevated temperatures. The surfaces appeared to be different after being heated to 700°C. The surface of the sample before it was heated to 700°C was uniformly covered with aluminum as shown in *Figure 4.1 (a)*. After the sample was heated to an elevated temperature, the surface of the sample was observed to have some regions that were not evenly covered with Al as shown in Figure *4.1 (b)*. At about 660°C, aluminum melts. It was observed that the Al apparently melted and formed into spheres of different sizes on the Al_2O_3 substrate surface as seen in *Figure 4.1 (b)*. During cooling to room temperature there was no means to observe morphological changes on the substrate and interface.

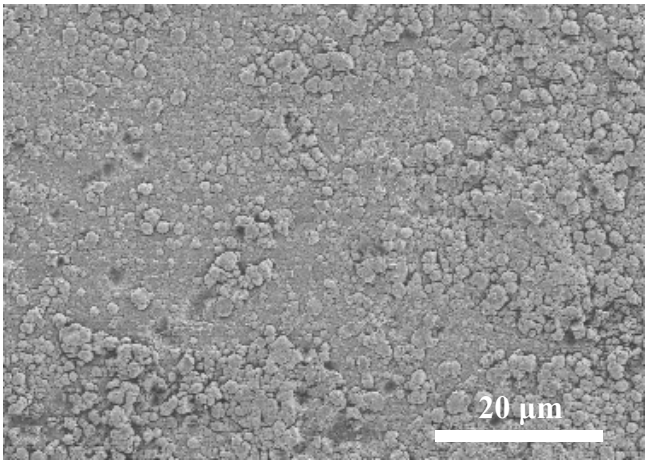

4.1 (a)

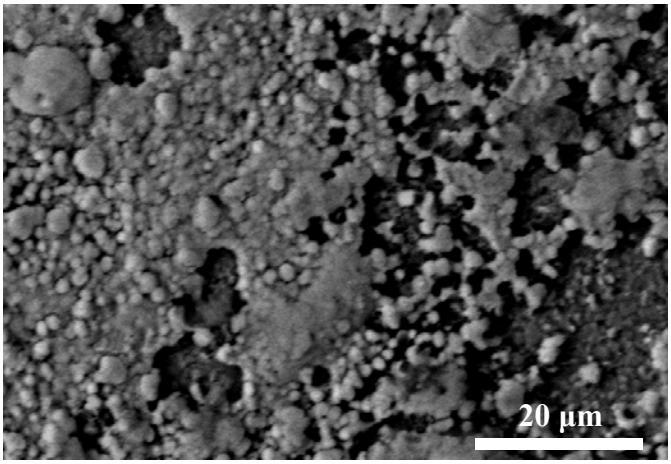

4.1 (b)

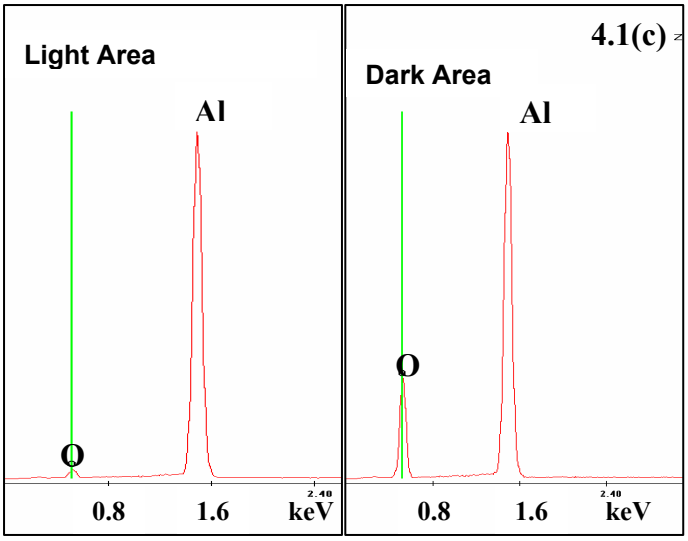

Figure 4.1. (a) Alumina substrate surface evenly covered with aluminum before heating; (b) Exposed alumina substrate surface after heating to 700°C; (c) EDS spectra at the dark and bright regions from b.

Figure 4.1 (c) shows the EDS spectra from the dark and bright areas in *Figure 4.1 (b)* of the Al_2O_3 (substrate) – Al (film) samples. The EDS spectra showed that the dark area contained significantly more oxygen than the bright areas indicating that the dark areas (substrate) were not entirely covered with Al (metal) after the sample was heated to 700°C. The interface between the Al_2O_3 substrate and the Al film was identified from a fractured sample (*Figure 4.2*) after the sample was heated and cooled. The region between the substrate and the interface in one case, and the film

and the interface in the other, were not easy to observe using the SEM. The thickness of the film was observed to be reduced from 4 – 5 μm to about 2 - 3 μm after heat treating and cooling as measured by SEM.

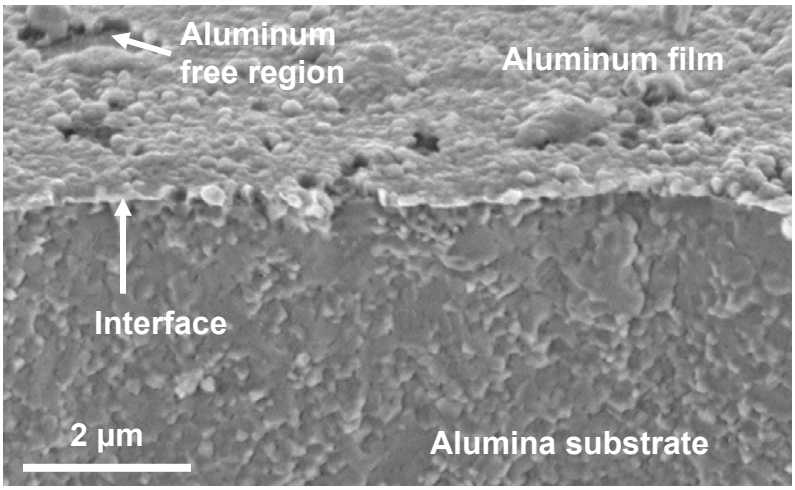

Figure 4.2. Interface between substrate and film identified for a fractured sample.

Al powder samples having an average particle size of 50 μm diameter were heated in air. *Figure 4.3 (a)* and *(b)* are microstructures of the surface of an Al particle after the sample was heated to 1300°C at a heating rate of 10°C per minute. The surface showed several web-like structures. The web-like structure on the surface of the Al powder sample seemed much like the ones observed by *Nychka and Clarke* as described in *Section 2.5.1.1* .

The oxide shell was apparently broken (*Figure 4.3*) due to the difference in the coefficient of thermal expansion between Al and Al_2O_3. The Al_2O_3 layer on Al would not have expanded at the same rate as Al. The coefficient of thermal expansion of Al and Al_2O_3 are 24×10^{-6} /ºC and 8×10^{-6} /ºC respectively at room temperature. Hence Al would have expanded more rapidly than Al_2O_3 at elevated temperature. It was

interesting to observe the texture on the surface of the Al_2O_3 shell [*Figure 4.3 (b)*] around the Al particle which is indicative of the direction of growth of the oxide on the metal surface. *Figure 4.4* shows an Al particle after it was heated to 1300ºC and cooled to room temperature. The Al_2O_3 outer shell was observed to be ruptured and only the hollow remains of the shell was observed. After the Al_2O_3 shell ruptured, it would be possible for the liquid Al to flow out of the shell at the elevated temperature and interact with the components outside the shell.

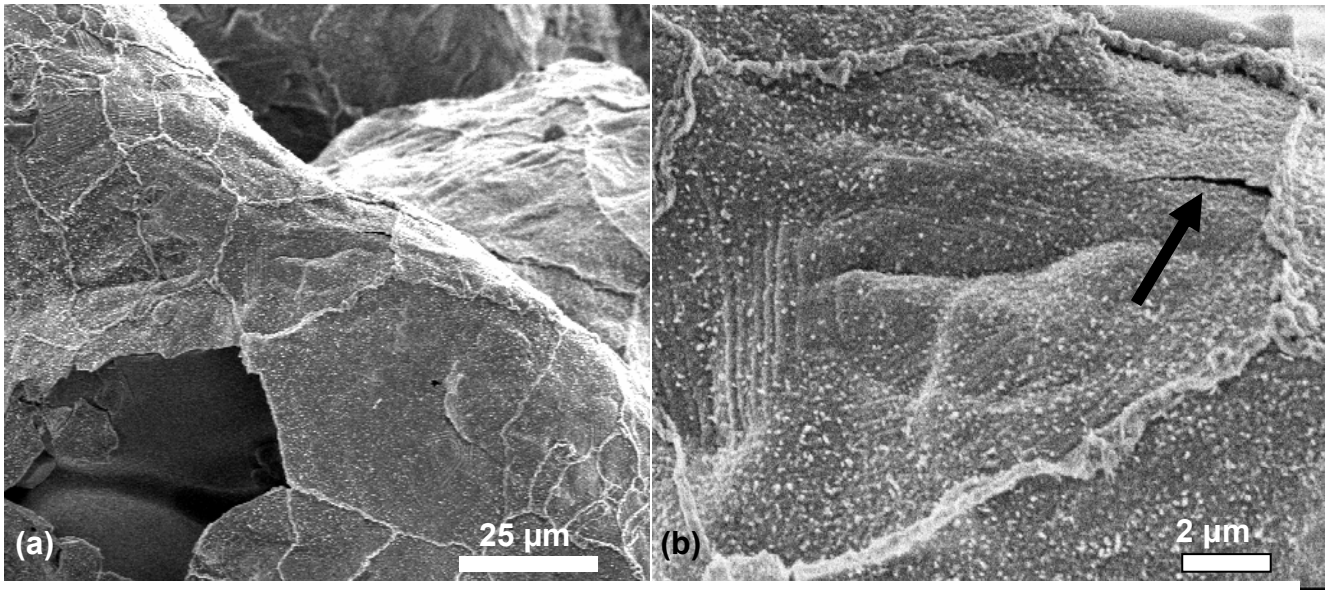

Figure 4.3: Features on the surface of Al particle after heating to 1300°C.

The Al that is usually covered with a layer of Al_2O_3 would then be in contact with the compounds that are not encompassed by the Al_2O_3 passivating shell and could thus interact at elevated temperature.

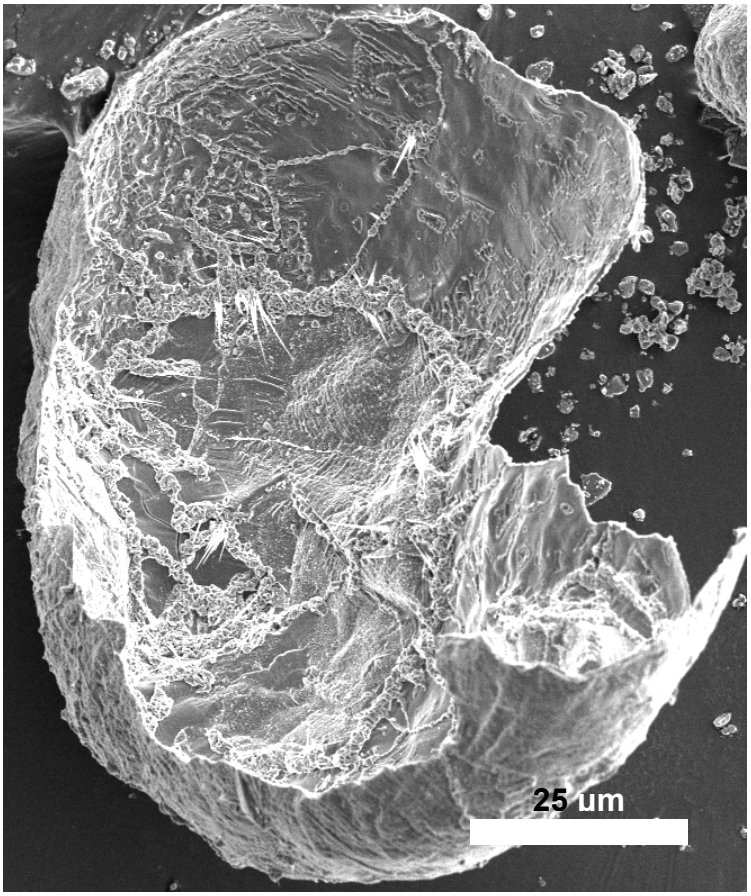

Figure 4.4: Hollow Al_2O_3 shell that contained Al particle before heating to elevated temperature.

4.2 High Temperature Interaction between Al and TiO_2

4.2.1 Identification of Interfacial Compound(s) Using XRD: Powder Samples

Figure 4.5 shows the X-ray diffraction pattern of a powder mixture (4:3 mole ratio of Al:TiO_2) soaked for 9 hours at 700°C and cooled to room temperature by furnace cooling. The spectrum in *Figure 4.5* shows peaks corresponding only to the reactants Al and TiO_2. There was no indication of any other phases in this spectrum.

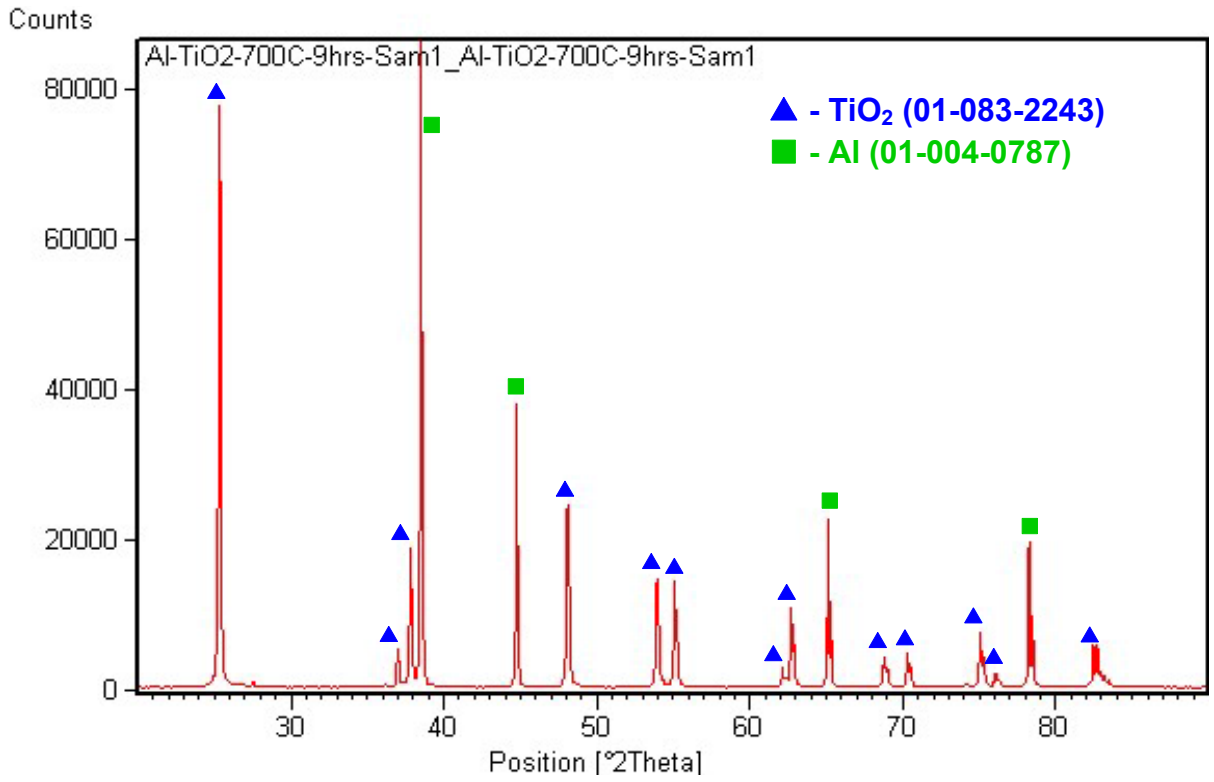

Figure 4.5. X-ray diffraction spectrum for 4:3 molar ratio of Al:TiO_2 powder heated to 700ºC for 9 hours.

A slow scan X-ray diffraction was performed between 2-θ values 25º and 50º in an attempt to resolve peaks that were either close to one another or those that were superimposed on another. *Figure 4.6 (a)* shows the slow scan X-ray spectrum. Additionally, an ultra slow scan [*Figure 4.6 (b)*] was performed to resolve the peak at 38.5º. Both slow scan attempts failed to reveal any other phase or compound other than the reactants Al and TiO_2.

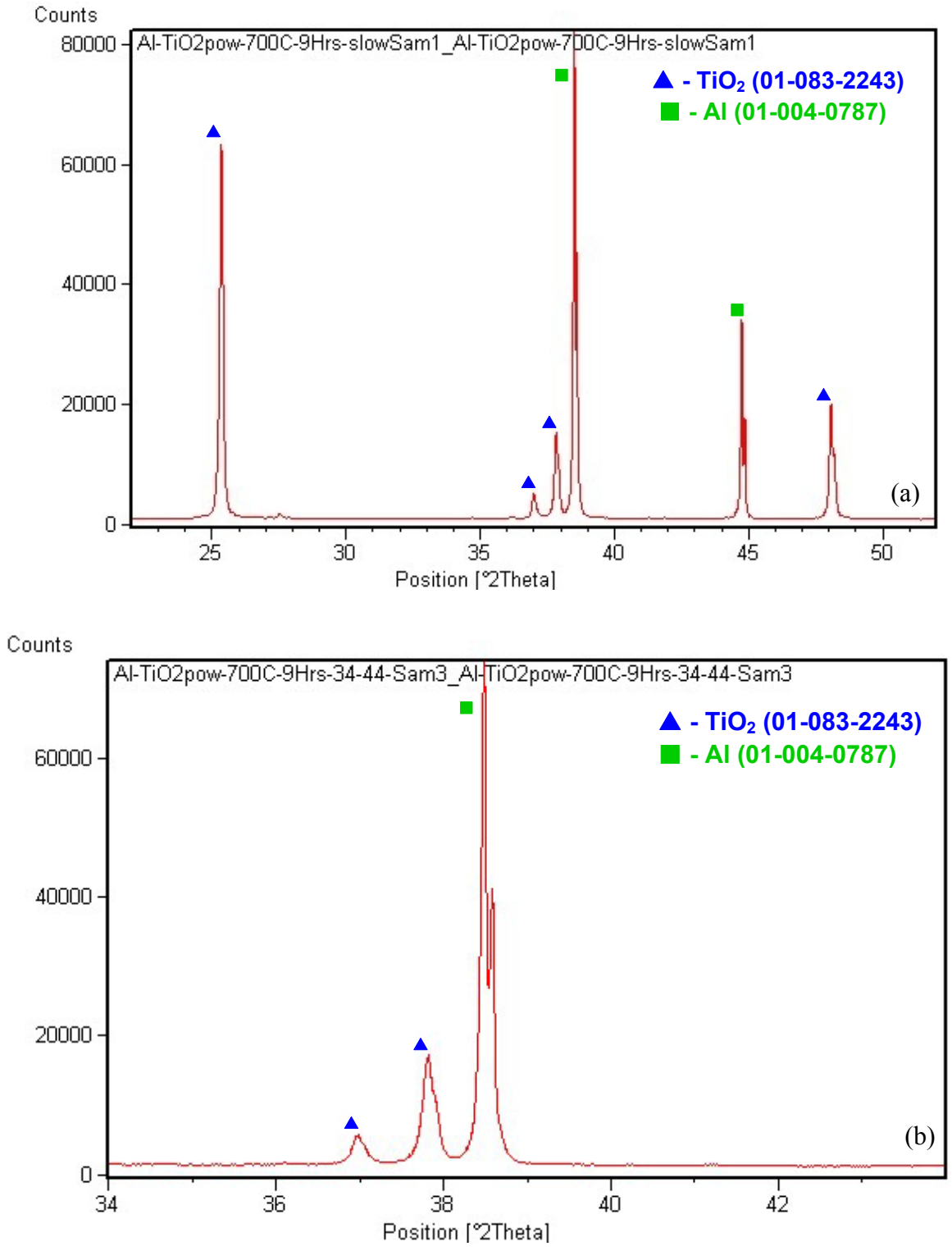

Figure 4.6 (a) Slow and (b) ultra slow X-ray diffraction spectra respectively of Al and TiO_2 powder heated to 700ºC for 9 hours.

4.2.2 Identification of Interfacial Compound(s) Using XRD: Film – Substrate Samples

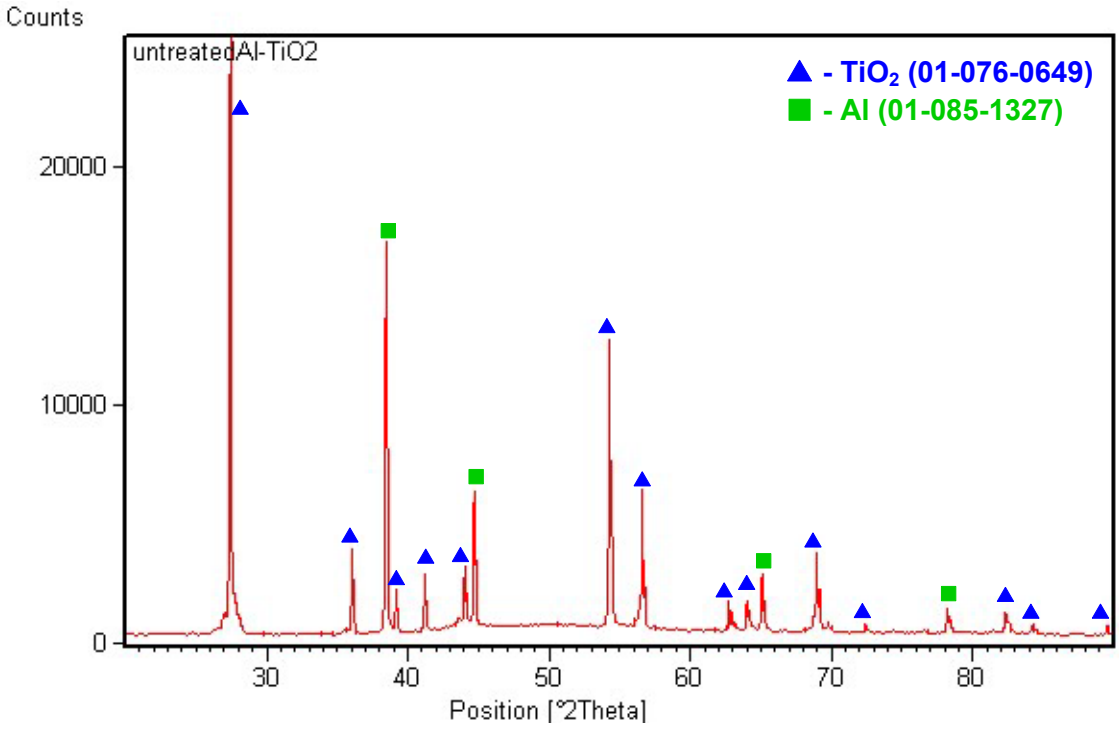

Figure 4.7. X-ray diffraction spectrum of an unheated Al-TiO_2 film-substrate sample.

The XRD spectrum of the unheated film-substrate sample is shown in *Figure 4.7*. The spectrum shows only Al and TiO_2 peaks as was expected. The film-substrate sample was heated to 700°C, soaked for 9 hours and cooled to room temperature by furnace cooling. The sample surface was then scanned using the X-ray diffractometer.

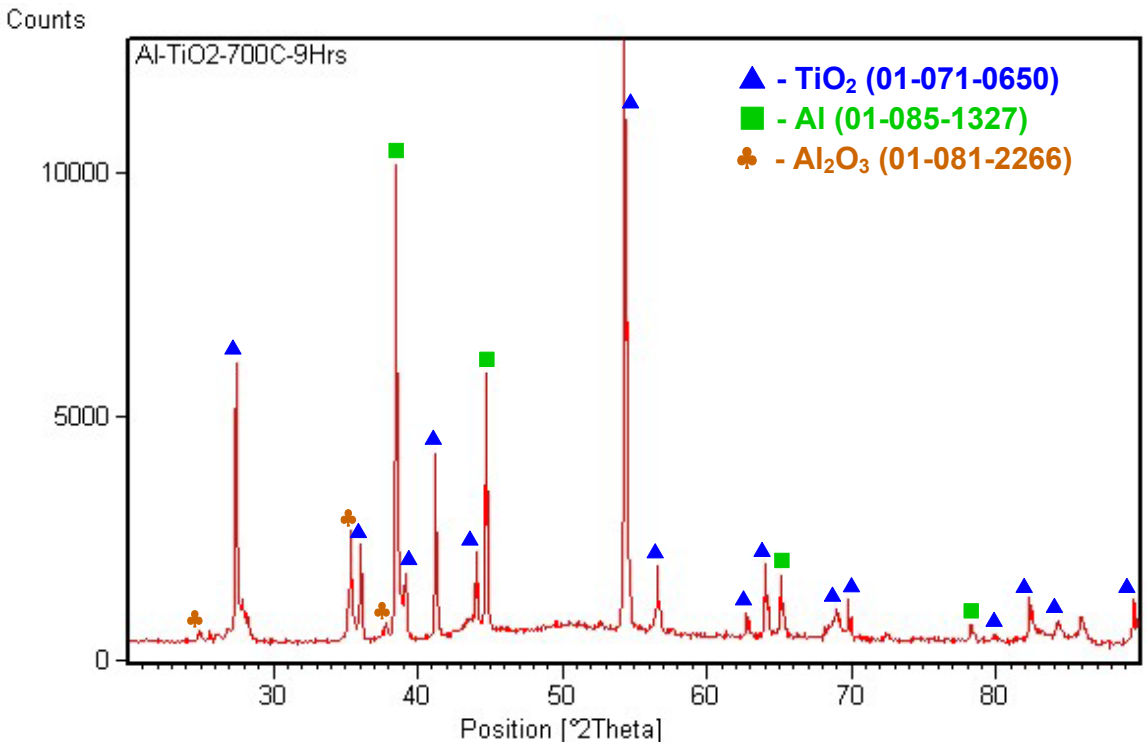

Figure 4.8. X-ray diffraction spectrum of Al-TiO_2 film-substrate sample heated to 700ºC, soaked for 9 hours showing peaks of Al_2O_3.

Figure 4.8 shows the diffraction pattern of the heated sample. α-Al_2O_3 peaks were observed in the spectrum along with the Al and TiO_2 peaks.

The volume of interaction of the X-ray beam incorporates the surface of the film, the interface between the film and the substrate, and a part of the substrate. α-Al_2O_3 could have formed on the surface of the sample (Al-side) that is exposed to air or it could form at the interface between Al and TiO_2 during the oxidation - reduction reaction between the reactants at elevated temperature. XRD data is not sufficient to determine the details about the formation of the observed α-Al_2O_3. X-ray diffraction is not an appropriate technique to determine the location of oxide formation.

Figure 4.9 shows the X-ray diffraction spectra of a sample that was scanned at several temperature intervals while heating to 700ºC. It was observed that Al peaks disappeared from the scans at 650ºC and above. Since Al melts at about 660°C and is no longer in the crystalline state, the peaks representing certain planes of Al atoms disappeared beyond the melting point of Al. There was no indication of new phases or transition phases forming as the Al peaks disappeared.

A possible explanation for the absence of a new phase can be explained by a small amount of interfacial compound (if it exists) constituting the thin interfacial region. The interfacial region can occupy only a fraction of the volume of interaction between the X-ray beam and sample volume. The X-ray detector receives the majority of the diffracted beam signal from the film or substrate region. The small fraction of the diffracted beam would not be significant compared to the diffracted beams from the other areas. Therefore, a bulk characterization technique like X-ray diffraction is not a suitable characterization technique to analyze the interface for determination of the existence of an interfacial compound. A more location specific analytical tool is required to examine the interface and determine the interfacial compound.

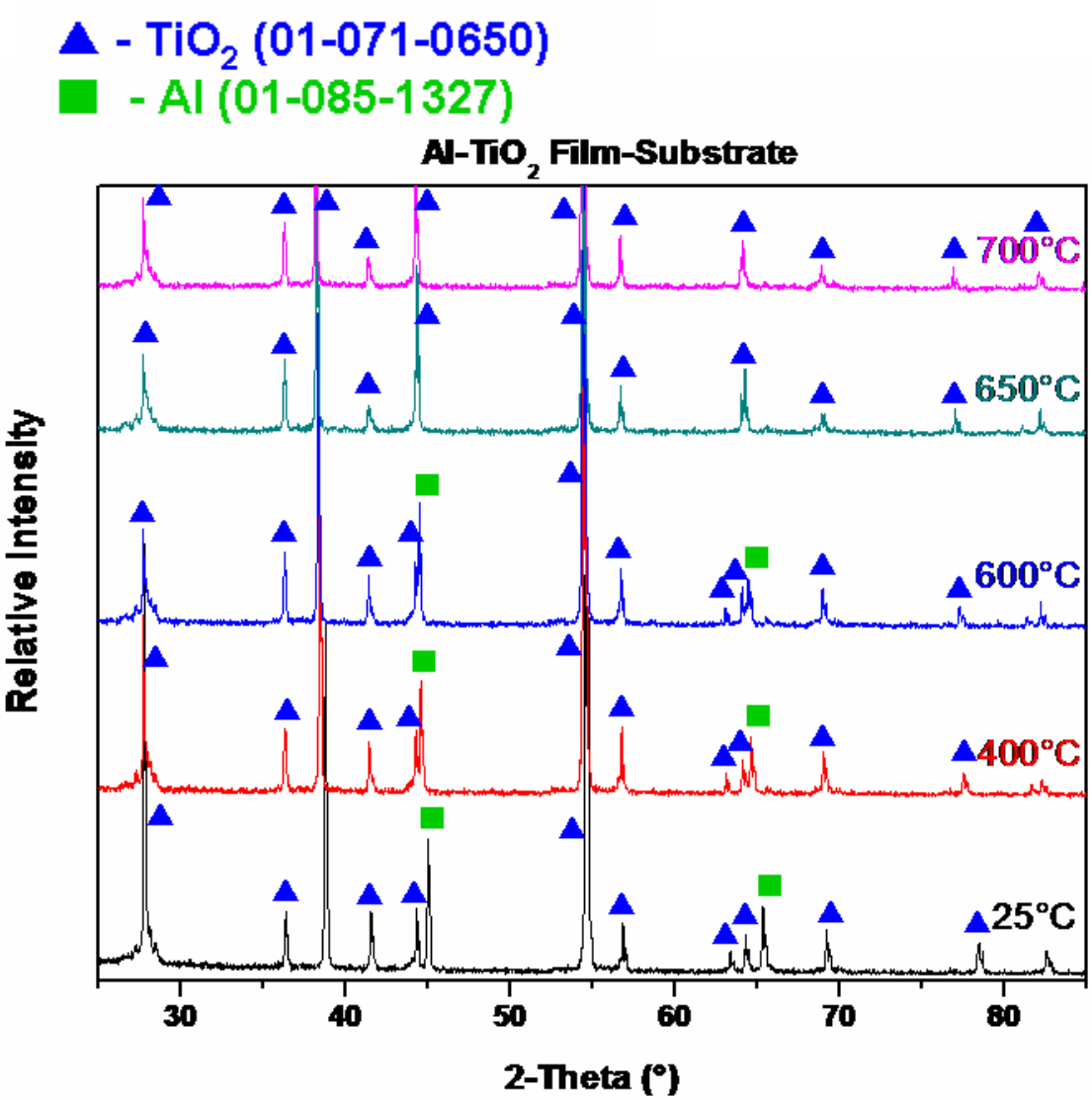

Figure 4.9. X-ray diffraction spectra of Al-TiO_2 sample heated from room temperature to 700ºC *in-situ*.

4.3 Morphological Understanding of the Interfaces

4.3.1 Diffusion Couple Film – Substrate Structure

The unheated film-substrate Al-TiO_2 sample was fractured and the cross section was studied (*Figure 4.10*) using SEM to compare nature and morphology of the interface with a sample that was heated to 700ºC and soaked for 9 hours.

The demarcation at the interfacial region, shown in *Figure 4.10*, which separates the film from the substrate in an unheated sample, is well defined. The Al deposited on the substrate is in the form of a columnar structure.

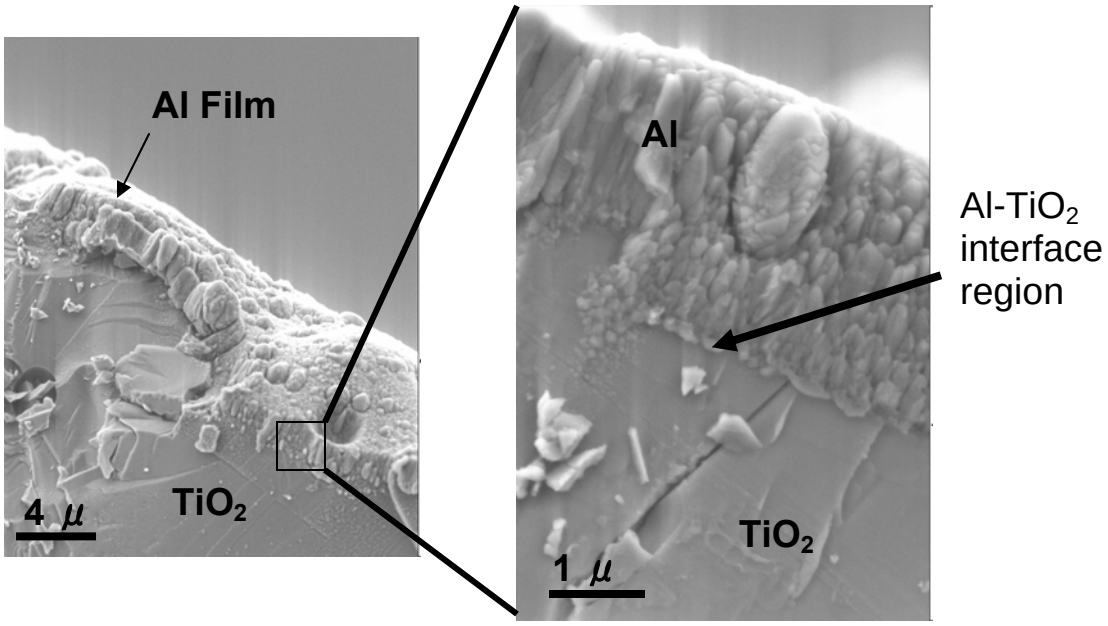

Figure 4.10. Interface of an unheated Al-TiO_2 sample.

Figure 4.11 shows the fractured surface of a film-substrate Al-TiO_2 sample that was heated to 700ºC and soaked for 9 hours. The interface between the film and the substrate was clearly visible. The thickness of the film was reduced after the sample was soaked for 9 hours at 700ºC as observed in the micrograph in *Figures 4.12* and *4.13*. Electron dispersive spectroscopic (EDS) analysis at the substrate, interface and film semi-quantitatively revealed the atomic composition at the respective locations after the sample was heated at 700°C for 9 hours. EDS data confirmed that the film had Al and little Ti while the substrate side had Ti. The interface contained a significant amount of both Al and Ti.

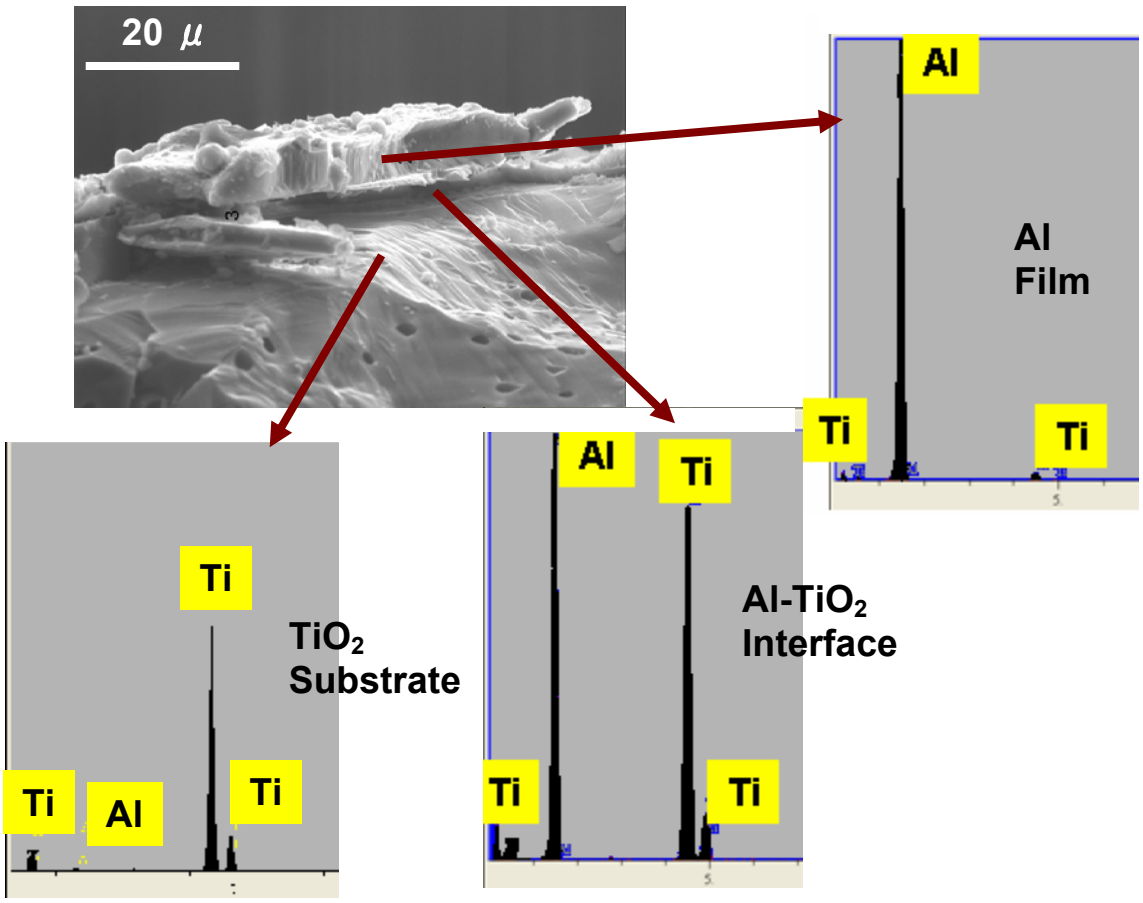

Figure 4.11.Cross section of fractured Al-TiO_2 film-substrate sample heated to 700°C for 9 hrs and electron dispersive spectra (EDS) of the corresponding regions.

The sandwich structures for the unheated and the heated samples were prepared as shown in *Figures 4.12* and *4.13*. The thickness of the film was measured before and after soaking at 700ºC. It was observed that the thickness of Al on the surface of the TiO_2 substrate was reduced after the sample was heated to 700ºC and cooled to room temperature.

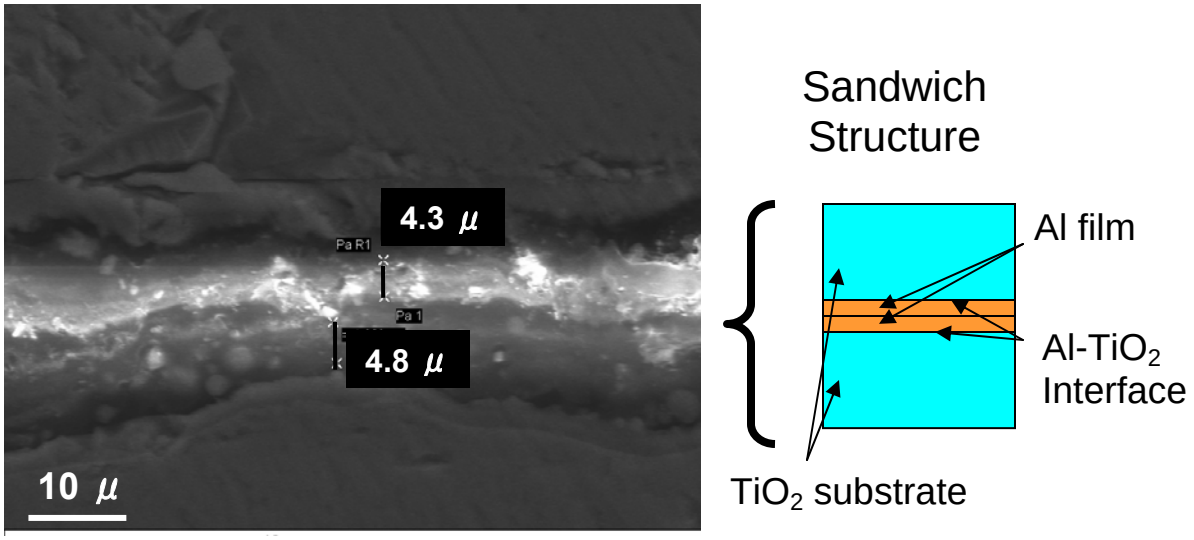

Figure 4.12. Two unheated film-substrate samples in sandwich structure to measure the Al-film thickness.

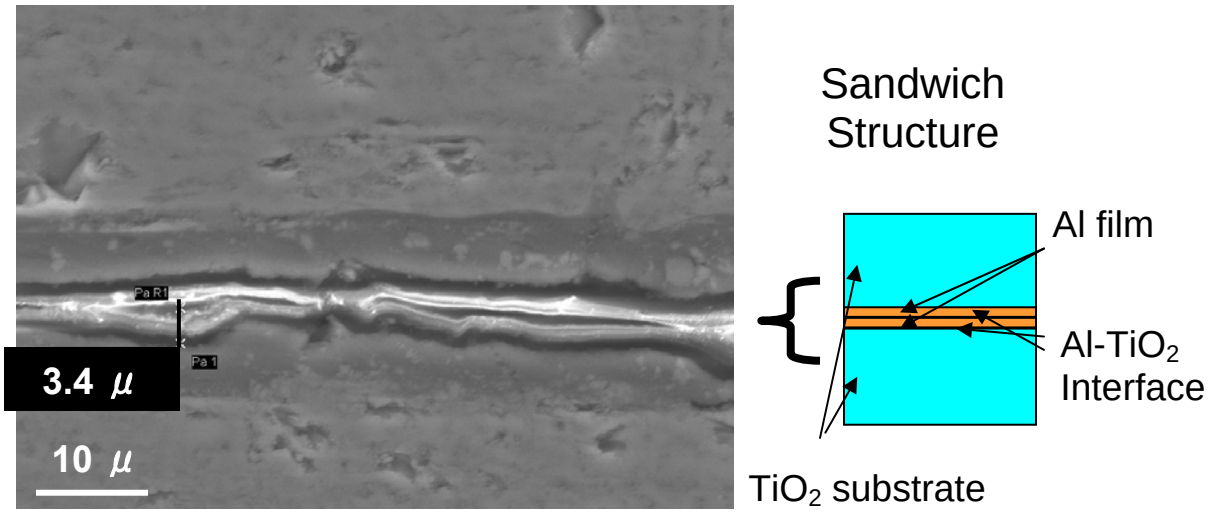

Figure 4.13. Two heated film-substrate samples in sandwich structure to measure the Al-film thickness.

The interface between the Al film and TiO_2 substrate is clearly identified in both unheated and heated samples. The interface appears to be a defined demarcation at the resolution offered by the SEM.

4.3.2 Surface and Interfacial Morphology for Powder Mixture Sample

An Al and TiO_2 powder mixture was heated under oxidizing (air) and non-oxidizing conditions (flowing He). It was observed that the Al film was not entirely reacted for the formation of the oxide even when the sample was heated in air; proof of which is also shown in *Section 4.4*.

The surfaces of Al powder particles that were heated in air were compared with those heated in He at 10ºC per minute to an elevated temperature (shown in *Figure 4.14)*. *Figure 4.15* shows the surfaces of two similar samples heated to a temperature range between 700ºC and 1000ºC at 40ºC per minute in both air and He. The small TiO_2 particles were observed on the surface of the large Al particles in all cases after the powder mixture was heated to the elevated temperature and cooled to room temperature. The surfaces of all four samples had web-like structures. The lines (of web-like structures) were thicker on the samples heated in air than on the ones heated in He (*Figure 4.14*) possibly due to greater oxidation occurring along the grain boundaries (represented by web) when heated in air. Another observation is that more TiO_2 particles seemed to be adhered to the Al particles heated at the faster heating rate when heated in air. Not much difference in surface morphology was observed for samples heated at a slow or fast heating rate when in a He environment.

(a) heated in air (b) heated in He

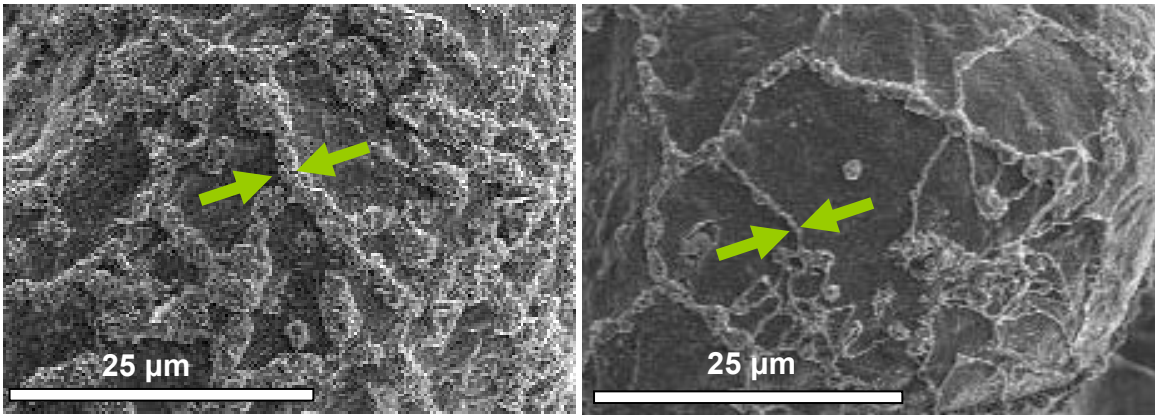

Figure 4.14. Surfaces of Al particles that were heated with TiO_2 powder in (a) air and (b) He at a low heating rate 10ºC per minute.

(a) heated in air (b) heated in He

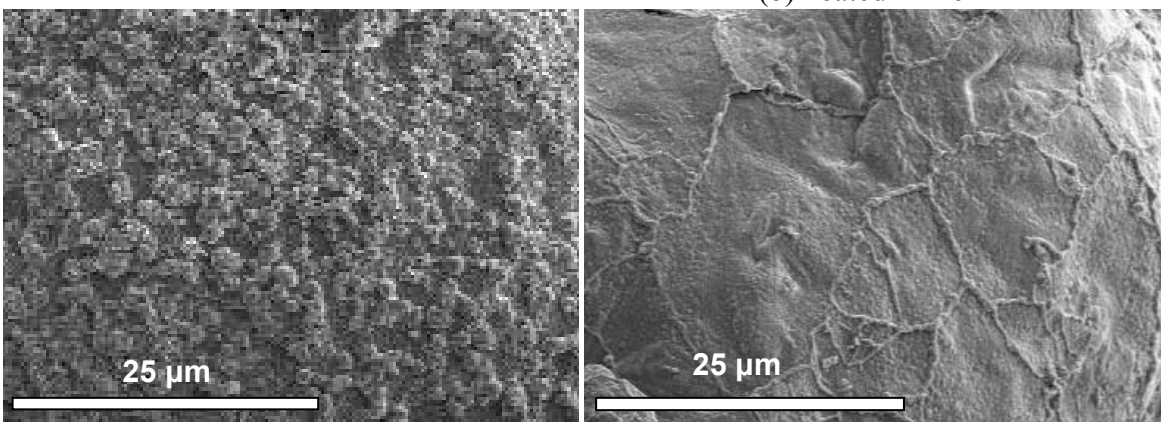

Figure 4.15. Surfaces of Al particles that were heated with TiO_2 powder in (a) air and (b) He at a more rapid heating rate 40ºC per minute.

It is thus observed that experiments performed in air and He are similar as far as interaction between Al and TiO_2 are concerned; except that the extent of interaction appeared greater in air as compared to a He environment. *Figure 4.16* shows micrographs of the cross sections of an Al particle that was heated with TiO_2 powder and FIBed from the surface towards the interior of the sample.

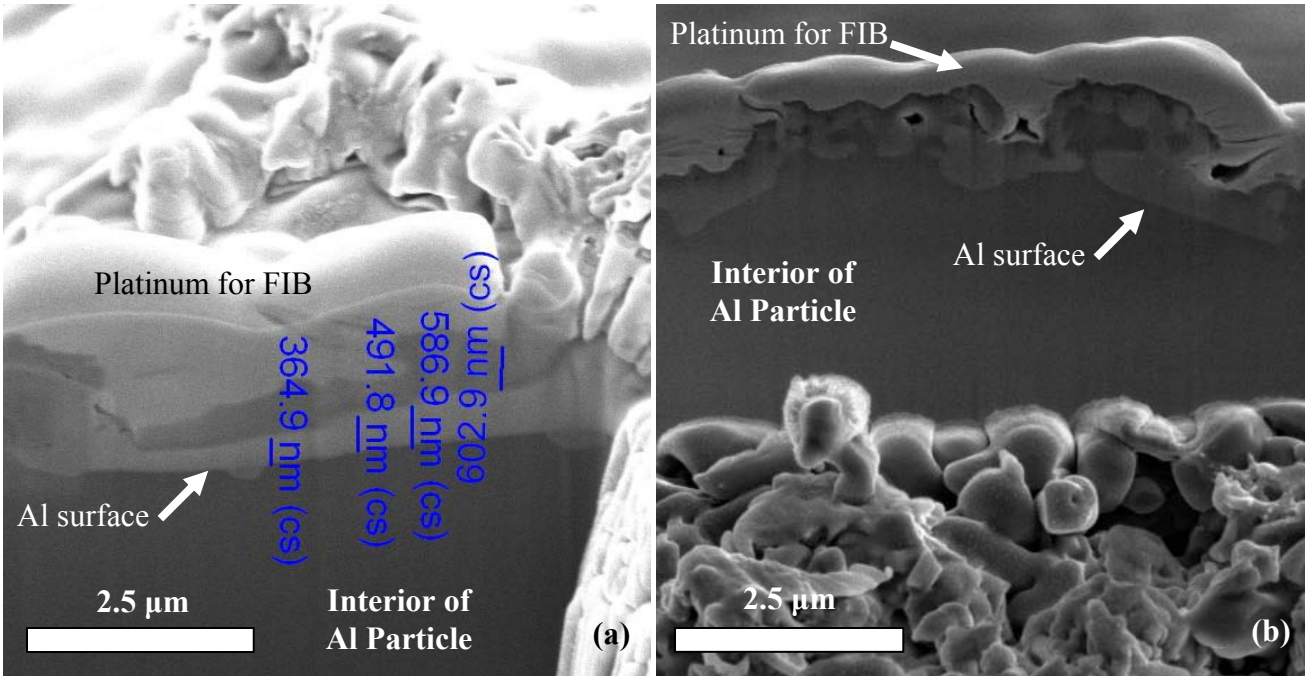

Figure 4.16. Cross section of the Al particle milled from the surface towards the interior for sample heated at (a) 10ºC/minute and (b) 40ºC/minute.

The surface of Al is observed to be flatter for the sample heated at 10ºC/minute (lower heating rate) than the surface of Al for the sample heated at 40ºC/minute (faster heating rate). The interface region was observed to be too thin to allow determination of the composition using EDS with either SEM or FIB. The interface between the Al film and TiO_2 substrate was identified for both the unheated sample and heated sample, using SEM and FIB. It was concluded that the interface appeared to be a 'line' at the resolution limit offered by the SEM. It was also concluded that area specific techniques with better resolution was needed to further study the interface to identify the compound at the interface and also determine the nature of the interface.

An analytical technique like transmission electron microscopy (TEM), was required to determine the compound formed at the interface and to explain the mechanisms involved in the formation of the interfacial compound. The selective area electron diffraction (SAED) analysis capability that is area specific was an added advantage to the high resolution imaging on the TEM.

4.4 High Resolution Identification of the Interfacial Phase(s) and Compound(s)

Details about the nature of the interface, particularly the morphology, continuity of the interfacial region, shape of the edges on both sides of the interfacial region, and the compound(s) that form the interfacial region was studied using the TEM.

4.4.1 Interface Comparison

The interface of an unheated Al-TiO_2 film-substrate sample was considered the basis of comparison with a similar sample treated to 700ºC for 9 hours. A small section of the interface between the film and the substrate (that contains the interface and parts of the film and the substrate) was milled using a focused ion beam; and the interface was examined to study the morphology of the interface using TEM. *Figure 4.17* shows the TEM micrograph of the unheated sample milled at the interface.

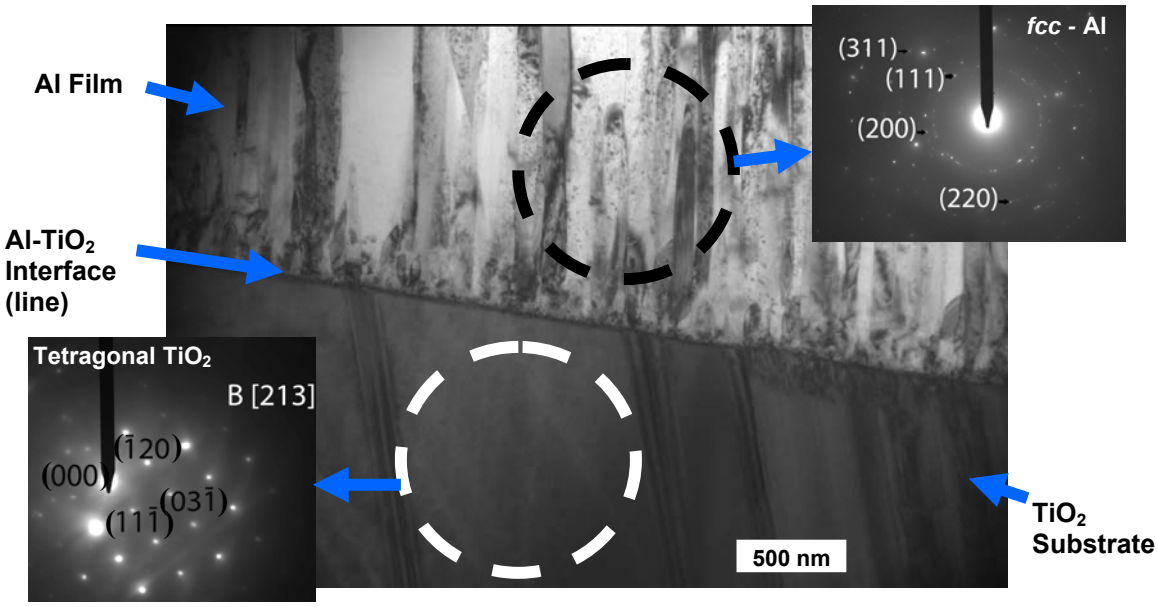

Figure 4.17: TEM micrograph of the interface of an unheated Al-TiO_2 film-substrate sample.

The film (having columnar grains of Al) above the boundary of the interface, was confirmed to be *fcc*-Al by electron diffraction of a selected area on the film within the dark dotted circle shown in *Figure 4.17*. Bright rings (shown in the upper right inset in *Figure 4.17*) resulted from electron diffraction of several grains of *fcc*-Al with different orientations. An area on the other side of the interfacial boundary was selected, as shown by the white dotted circle in *Figure 4.17* for electron diffraction. The diffraction pattern showed a dot pattern (lower left corner inset in *Figure 4.17*) that was indexed to the [213] zone of the *tetragonal* TiO_2 rutile structure. The indexed diffraction patterns from the regions separated by the boundary of the interface (as shown in *Figure 4.17*) on the micrograph confirmed that the two regions were the film and substrate

respectively for the unheated sample. The interface was a clear thin boundary that separated the film from the substrate.

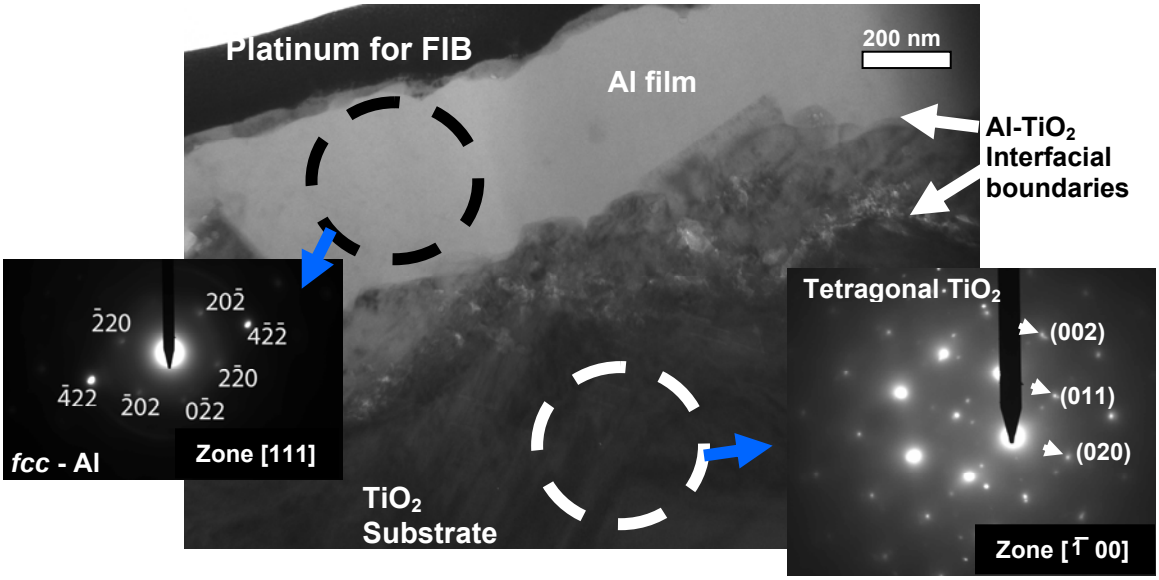

Figure 4.18: TEM micrograph of the interface of the Al-TiO_2 film-substrate sample heated for 9 hours at 700ºC.

The interface for the Al-TiO_2 film-substrate sample that was soaked for 9 hours at an isothermal condition of 700ºC is shown in *Figure 4.18*. The top dark region in the micrograph is the platinum that was deposited to facilitate milling of the material for the TEM sample preparation using a FIB. The dark dotted circle indicates the area that was selected for electron diffraction using a suitable aperture on the TEM. The dot pattern shown in the inset (bottom left corner) was the indexed diffraction pattern representing *fcc*-Al. A similar region (Al-film) for the unheated sample, as shown in *Figure 4.17,* showed a ring pattern of various *fcc* planes of Al. Al would have melted on the substrate when the sample was heated to a temperatures beyond 660ºC and on cooling it would have re-solidified as large grains. The area selected for diffraction on the upper side of the interface

was perhaps a single large grain and not several grains as in the unheated sample (*Figure 4.17*). This explains why a dot pattern was obtained in the heated sample while a ring pattern was obtained for an unheated sample. Similarly, the diffraction pattern of a selected area (shown by the white dashed circle) from an area below the interface was indexed to the *tetragonal*-TiO_2 structure as shown in *Figure 4.18*.

The film and the substrate regions were clearly identified for the treated sample. The difference in the nature of the interface between the unheated and the heated sample as observed in the microstructures (in *Figure 4.19*) was that the interface in the unheated sample was a clear line of demarcation while that for the heated sample was an area with a finite width.

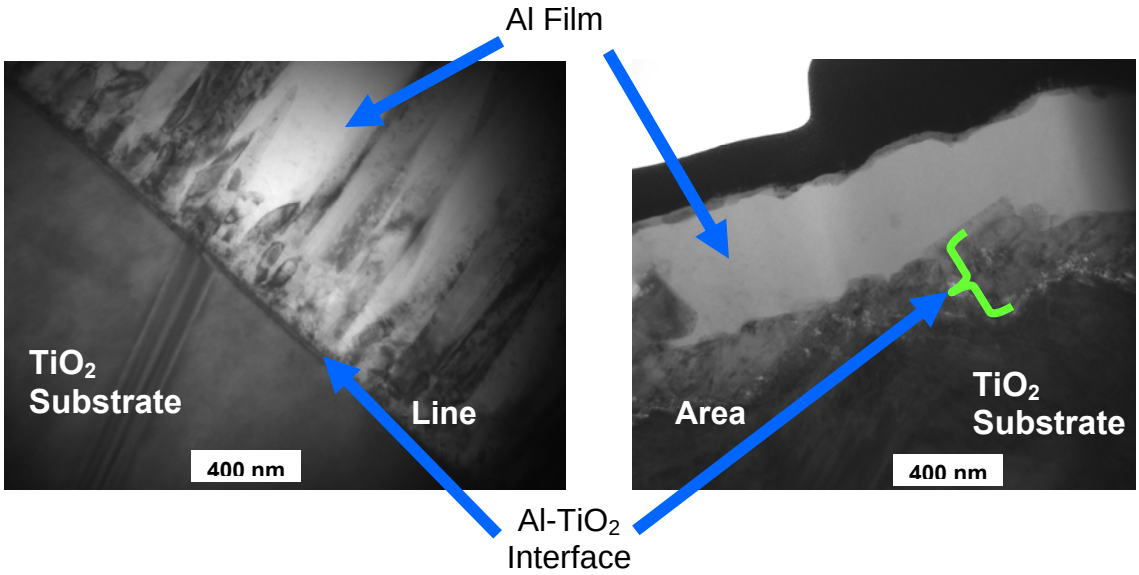

Figure 4.19: Comparison of interface regions between the unheated and heated Al-TiO_2 film-substrate samples.

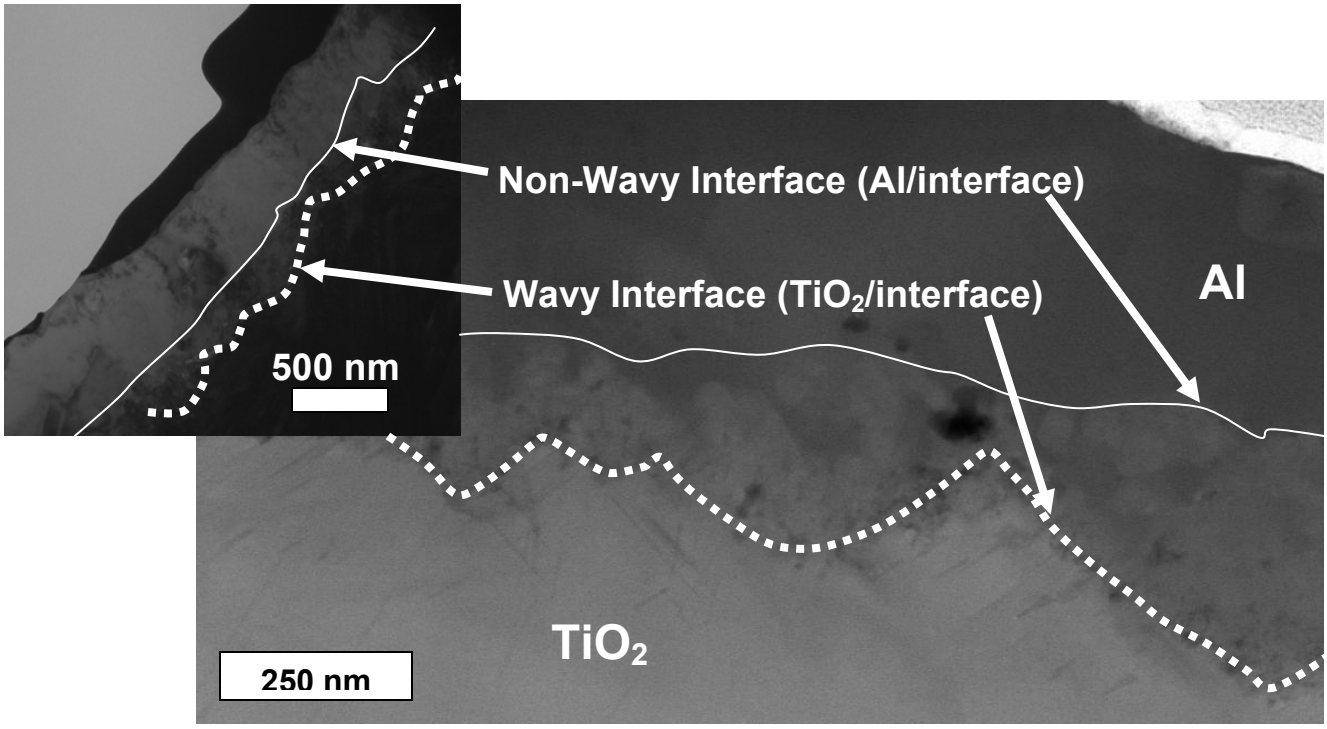

Figure 4.20: STEM micrograph of the interface on the FEI TITAN. The inset is the image at the same location on 420 Philips TEM both showing the wavy interface on one side and almost straight on the other.

Figure 4.20 represents a Scanning Transmission Electron Microscopy (STEM) micrograph (obtained on FEI TITAN TEM) of the interface of the Al-TiO_2 film-substrate sample that was soaked for 9 hours at 700ºC. The inset shows the same interfacial region using an objective lens in a 420 Philips TEM. The white dotted lines in both micrographs indicate the boundary between the interfacial region and the TiO_2 substrate. The boundary between the interfacial region and the TiO_2 substrate was distinctly wavy in shape; while the boundary between the interfacial region and the Al film (indicated by solid line) was more or less straight, except for the small rugged edges that protruded from the

interfacial region into the Al side. The nature and occurrence of the upper boundary is explained in the latter part of this chapter. The interfacial region was continuous at the interface between the film and substrate. Certain regions in the interface were observed to be thin while other regions appeared to be thick as shown in *Figure 4.21*. The sites where the interfacial region rise to the highest point (blue arrows) were the thinnest regions at the interface; while the sites where the wavy region dipped to form a concave curve (green arrows) were thick regions as shown in *Figure 4.21*. Although the interface seemed smooth with one straight boundary and one wavy boundary as shown in the side view (*Figure 4.21*), it was observed that the interface was not as smooth throughout as was observed at a different location at the interfacial region (*Figure 4.20*).

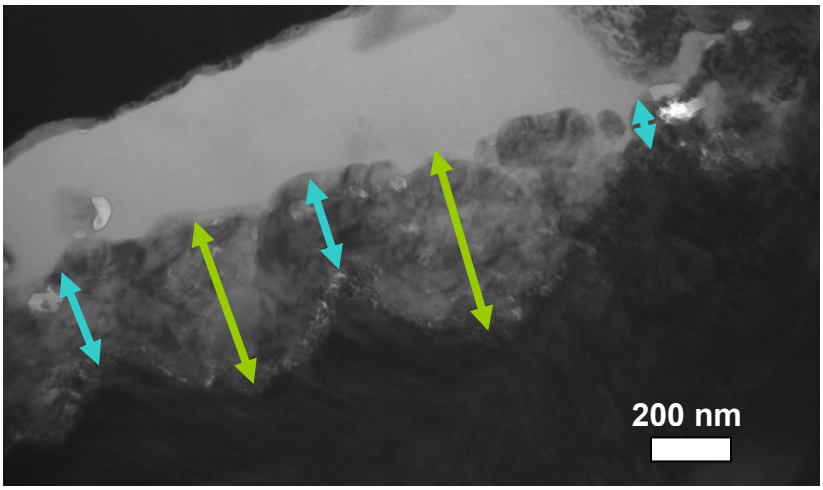

Figure 4.21: TEM micrograph showing the thinner and thicker regions of interface.

4.4.2 Interface Compound Identification

The interfacial region was clearly located as explained in the previous section and information about the nature of interface was described in *Section 4.4.1*. The

current section describes the identification of the compound present in the interfacial region.

Figure 4.22 shows a specific site of the interfacial region where the interfacial compound(s) protruded into the Al film above the interfacial layer.

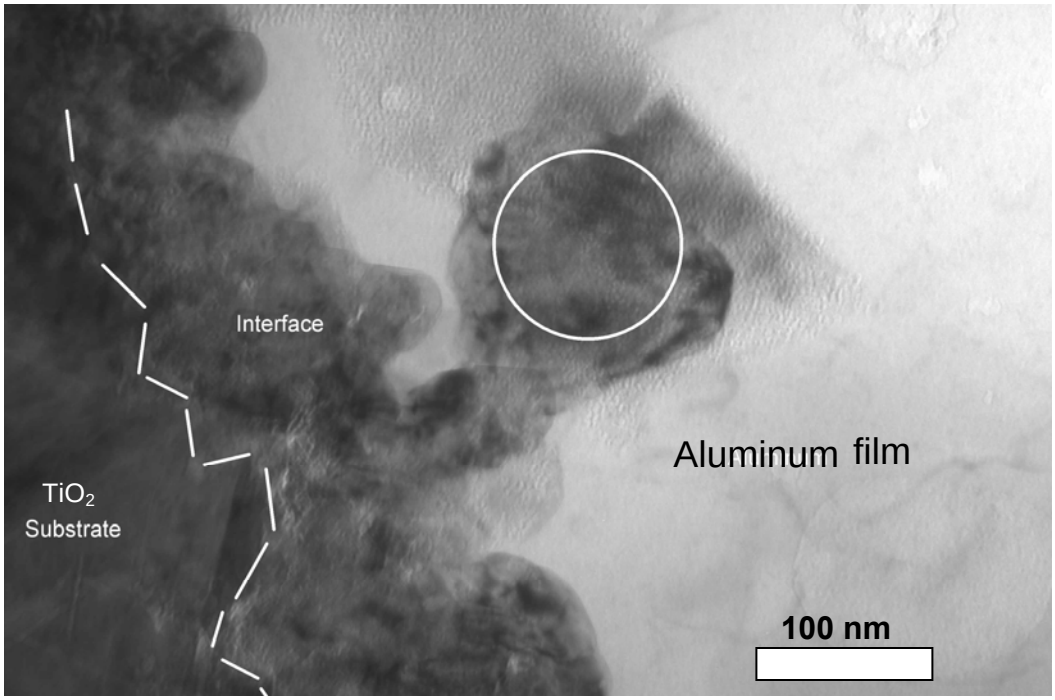

Figure 4.22: Part of the interfacial region protruded into the Al layer. The circle marks the region where the aperture was placed for electron diffraction.

Figure 4.23 (a) shows an electron diffraction pattern of the circular area marked on *Figure 4.22*. The pattern was indexed to the [213] zone of a tetragonal TiAl compound, commonly known as the TiAl phase. The McTempas® software was used to generate an electron diffraction pattern that matched within reasonable limits with the one shown in *Figure 4.23 (a)*. Parameters used for generation of the pattern were obtained from the JCPDS file number 00-005-0678. The lattice parameters were: $a = b = 3.976$ *Å*, $c = 4.0490$ *Å*; $\alpha = \beta = \gamma =$

90°. The calculated d-spacing for generated planes, as shown in *Figure 4.23 (a)*, were $d(\bar{1}\bar{1}1) = \boldsymbol{d}(1\,1\bar{1}) = 2.31$ *Å*, $d(1\bar{2}0) = 1.78$ *Å*, $d(2\bar{1}\bar{1}) = 1.63$ *Å*. *Figure 4.23 (b)* represents translation of the $(1\,1\bar{1})$ plane (encircled white dot) to the center for dark field imaging.

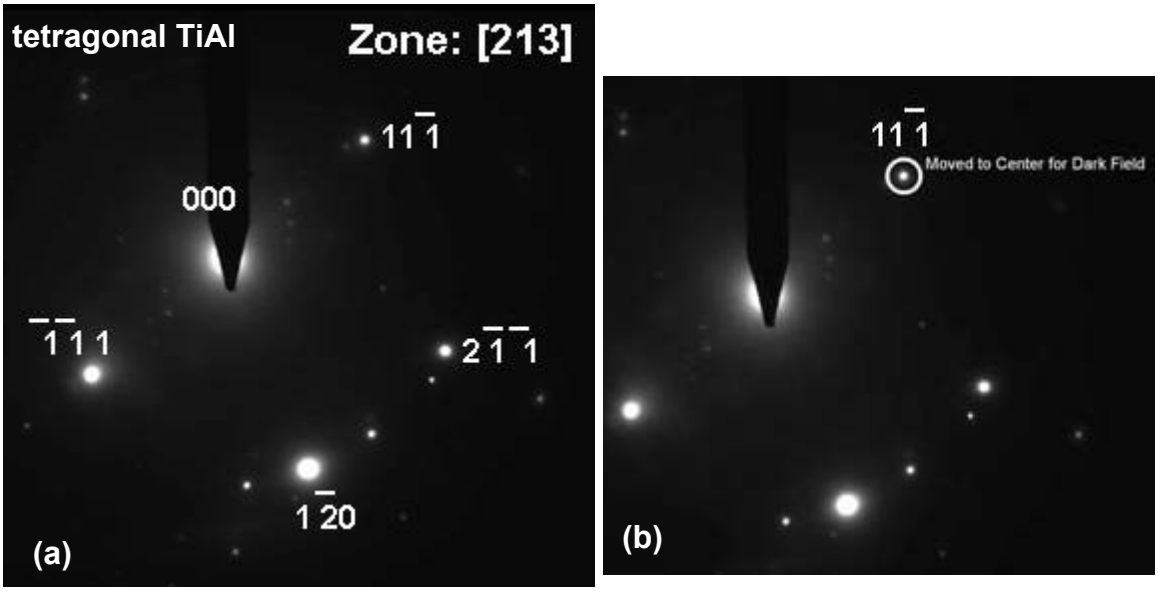

Figure 4.23. (a) Indexed electron diffraction pattern of the circled region on Figure 4.22; (b) (11-1) plane displaced to the center for dark field imaging on the 420 Philips TEM.

Figure 4.24 (a) represents a dark-field image of the $(1\,1\bar{1})$ plane marked on *Figure 4.23 (b)*. All the grains that were oriented in the $(1\,1\bar{1})$ direction are highlighted in the micrograph. Thus it was concluded that the grain in *Figure 4.22* that protruded out of the interfacial region was the TiAl grain having a $(1\,1\bar{1})$ orientation. It was important to know whether the presence of the TiAl phase was an isolated occurrence or whether more regions of the interface contained the TiAl phase. In order to verify the presence of additional TiAl along the interface,

the low magnification dark-field TEM micrograph of the same plane [$(1\,1\bar{1})$ plane] was observed to check whether more regions along the interface were highlighted. *Figure 4.24 (a)* is the dark-field high magnification TEM micrograph of the protruded grain shown in *Figure 4.22*. *Figure 4.24 (b)* represents the low magnification dark-field TEM micrograph $(1\,1\bar{1})$ at the interface. It was interesting to note that regions all along the interface were highlighted. It was also noted that there were certain areas [as shown in *Figure 4.26 (b)*] within the TiAl interfacial region that were dark. It is possible that the dark regions could be one of the two:

(i) dark regions were the TiAl compound with an orientation other than $(1\,1\bar{1})$.

(ii) a different compound formed at the interface other than the TiAl, eg. Al_2O_3 that was also expected to form due to the release of oxygen during the reduction of TiO_2 by Al.

The presence of the dispersed dark regions in the TiAl interface is explained later in this chapter.

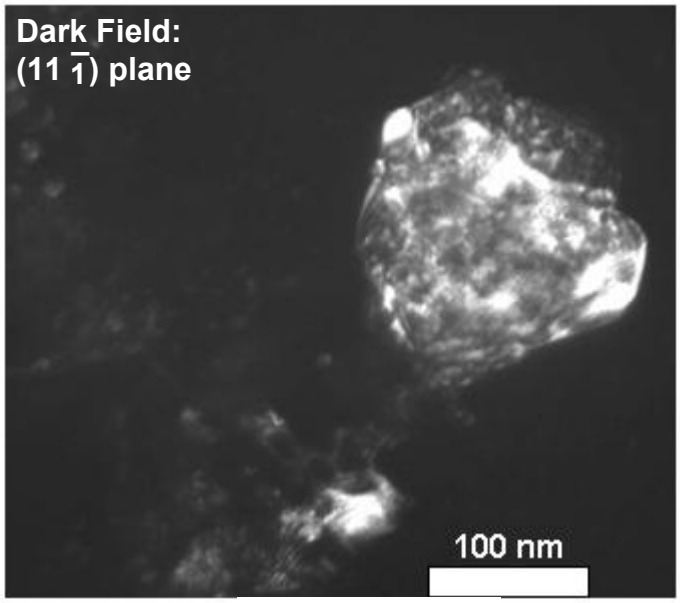

Figure 4.24 (a)

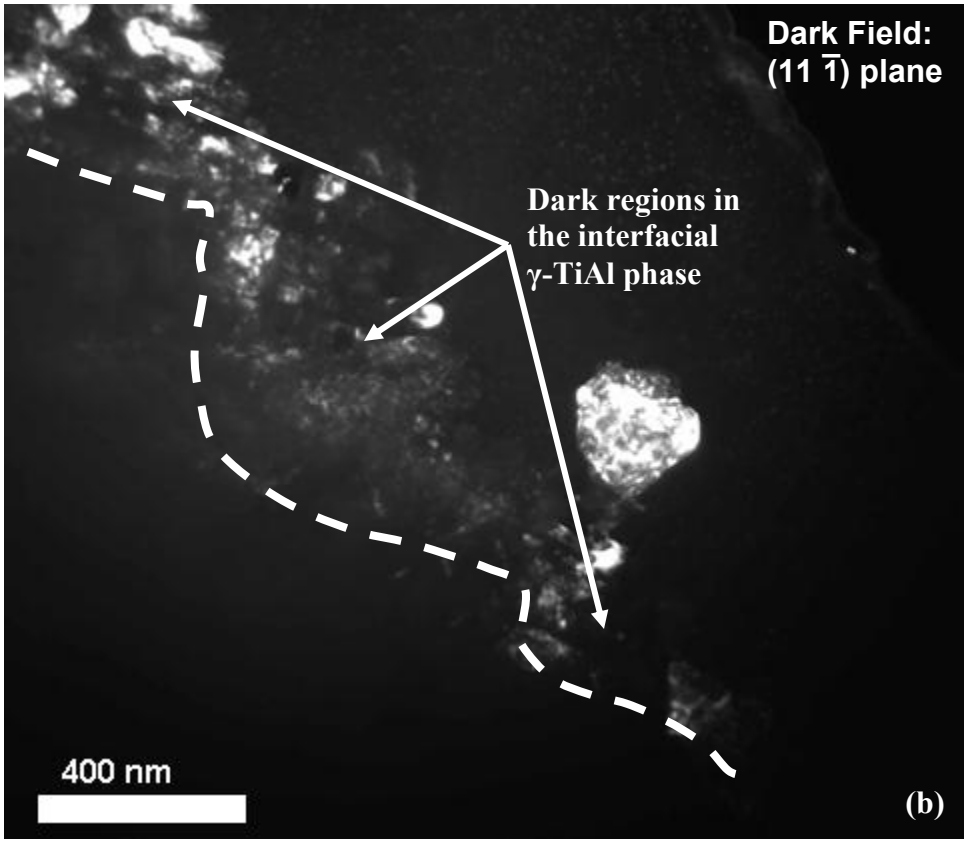

Figure 4.24: (a) Dark field TEM micrograph of the (11-1) grain that is indexed from images in Figures 4.22. (b) Low magnification dark field micrograph of the interface that highlights the interface that contains the TiAl phase.

Figure 4.25 shows the bright-field TEM micrograph of a second region along the interface between the film and the substrate of the same sample as mentioned above. The micrograph shows a grain that protruded from the interface into the Al film. An area (circular mark) on the protruded grain as shown in *Figure 4.25* was selected using the selective area aperture on the TEM for electron diffraction. The inset in *Figure 4.26* shows the 'selective area diffraction pattern' from the marked area in *Figure 4.25*. The dotted line represents the boundary between the TiO_2 substrate and the interfacial region. The solid line represents the boundary between the Al film and the interfacial region.

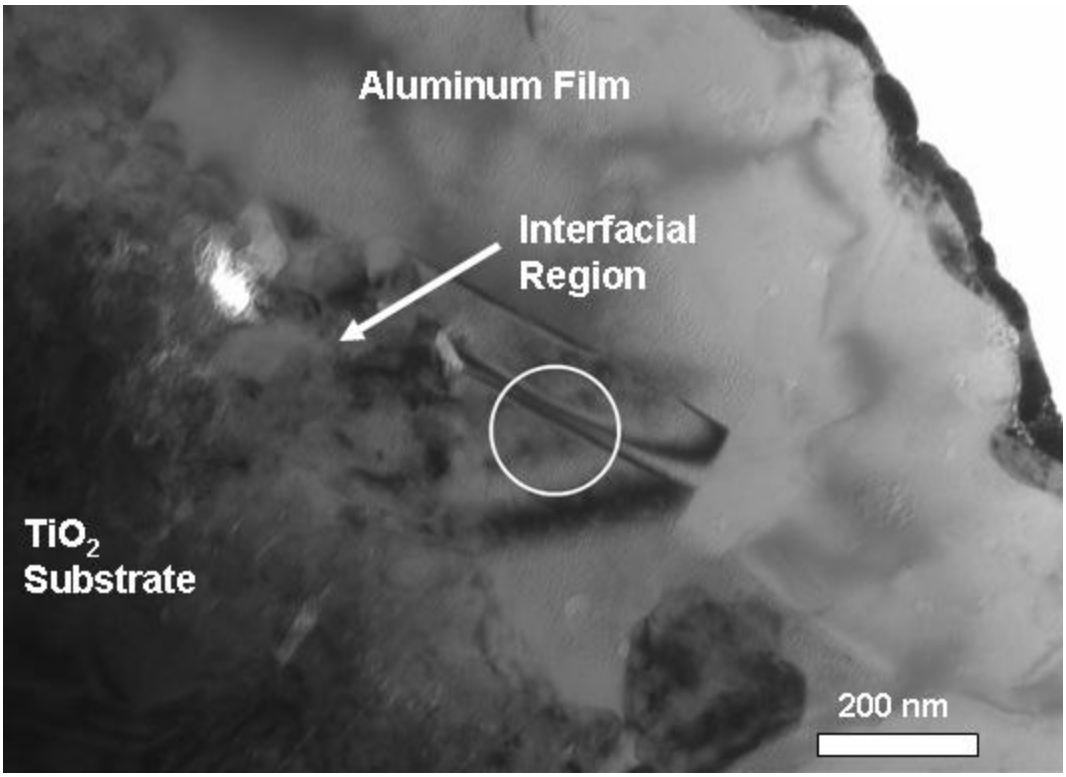

Figure 4.25: Bright field TEM micrograph of the interfacial region showing few grains protruding into the Al side. The circle marked shows the area selected for electron diffraction.

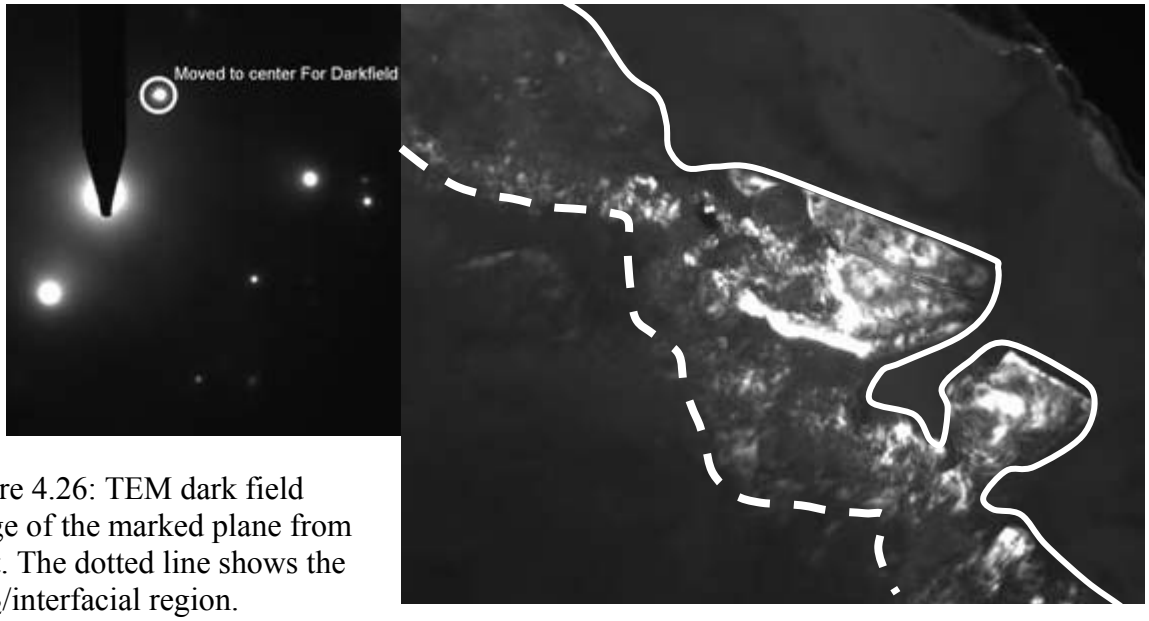

Figure 4.26: TEM dark field image of the marked plane from inset. The dotted line shows the TiO_2/interfacial region.

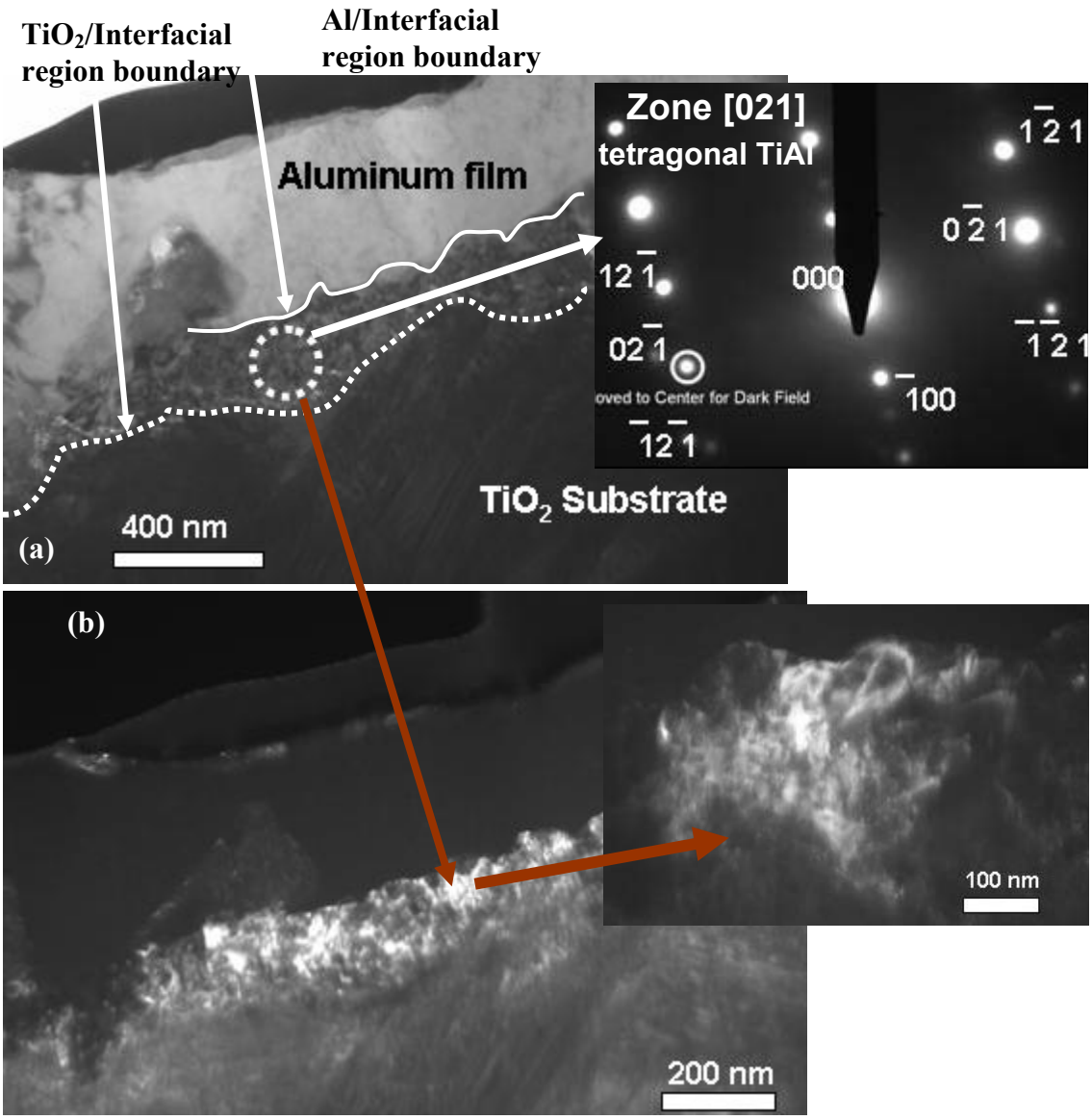

Figure 4.27: (a) TEM Bright field micrograph of interfacial region with inset showing indexed electron diffraction pattern of marked area; (b) TEM dark field micrograph with (02-1) plane lit-up at the interface.

The diffraction pattern obtained from the circled region in *Figure 4.25* did not have a low index of symmetry (simple symmetry); therefore it was not indexed. It was interesting to note that the boundaries on both sides of the interfacial region were consistent with previously explained observations. The interaction was consistent along the interface.

Another region along the interface on the same Al-TiO_2 film-substrate sample is shown by the TEM micrograph in *Figure 4.27 (a)*. The two interfaces are marked with dotted and solid lines as shown in the micrograph. The width of the interface measured from 200 to 250 nm. The interface seemed to be continuous. The inset shown in *Figure 4.27 (a)* is the indexed selective area diffraction pattern of the circular area marked (within the interfacial region) in the figure on the left side.

The diffraction pattern in the inset of *Figure 4.27 (a)* was indexed to the [021] zone of the *tetragonal* γ-TiAl phase. The McTempas® software was used to generate an electron diffraction pattern that matched within reasonable limits to the one shown in *Figure 4.27 (a)*. The parameters used to generate the pattern were obtained from JCPDS file number 00-005-0678. The lattice parameters used from the JCPDS file were: a = b = 3.976 Å, c = 4.0490 Å; α = β = γ = 90º. The calculated d-spacing of the generated planes, as shown in *Figure 4.29 (a)*, were $\boldsymbol{d}(021) = d(02\bar{1}) = 1.78$ Å, $d(12\bar{1}) = d(1\bar{2}\bar{1}) = d(1\bar{2}1) = d(\bar{1}2\bar{1}) = 1.63$ Å, $d(2\bar{1}\bar{1})$ = 1.63 Å, $d(\bar{1}00) = 3.98$ Å. The circled spot in the inset in *Figure 4.27 (a)* represents the shifting of the $(02\bar{1})$ plane (circle marked on white spot) to the center for dark field imaging.

Figure 4.27 (b) shows the dark field image of the $(02\bar{1})$ plane marked in *Figure 4.27 (a)*. The image highlights all the grains that are oriented in the (02-1) direction. Thus it was concluded that the grains shown in *Figure 4.27 (b)* are the TiAl grains having $(02\bar{1})$ orientation.

Figure 4.28 collectively showed the different regions (Regions I and III) that show the presence of TiAl at the interface. It was concluded that the interface between the Al film and TiO_2 substrate for a heated sample was not a defined boundary but a 'region' with a definite width. It was concluded from the TEM results that the interfacial region was continuous along the interface, though not uniform in thickness. It was also concluded that the interfacial region consisted of TiAl and possibly a second phase.

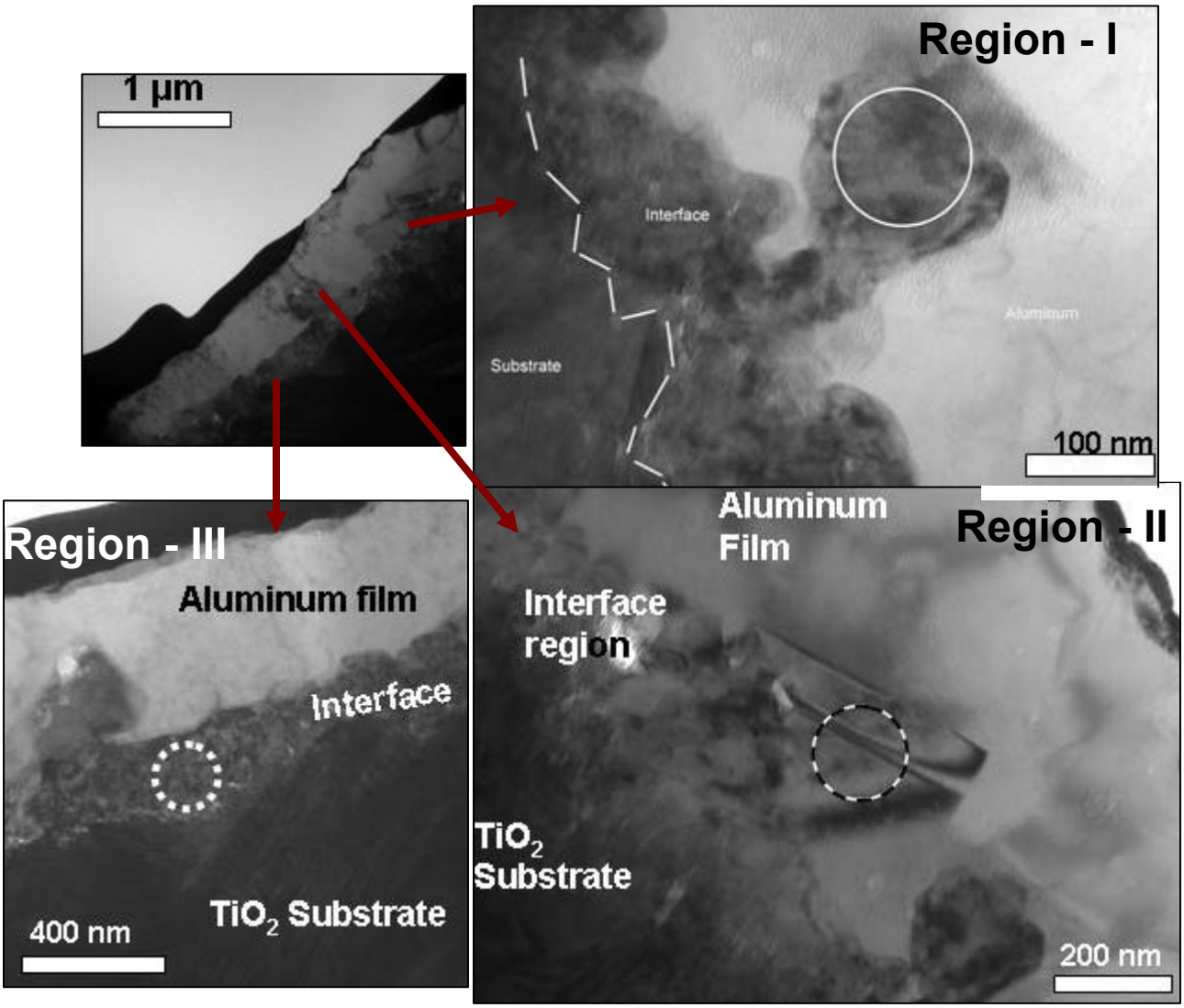

Figure 4.28: Regions I, II and III along the interface of the Al-TiO_2 film-substrate sample that was exposed for 9 hours at 700ºC.

4.5 Theoretical Determination of Possible Interfacial Compound(s)

Chapter 2 (*Section 2.5*) described the results reported for the reaction between Al and TiO_2 for various conditions of temperature, pressure and sample preparation history. Some researchers have reported the formation of a $TiAl_3$ phase while others have reported the formation of a γ-TiAl phase. The current section employs thermodynamic principles to explain the formation of a TiAl phase instead of the other competing ordered phases (Ti_3Al, $TiAl_3$ and the Al dissolved Ti phases).

4.5.1 Free Energy Calculations (assuming stoichiometry in compounds)

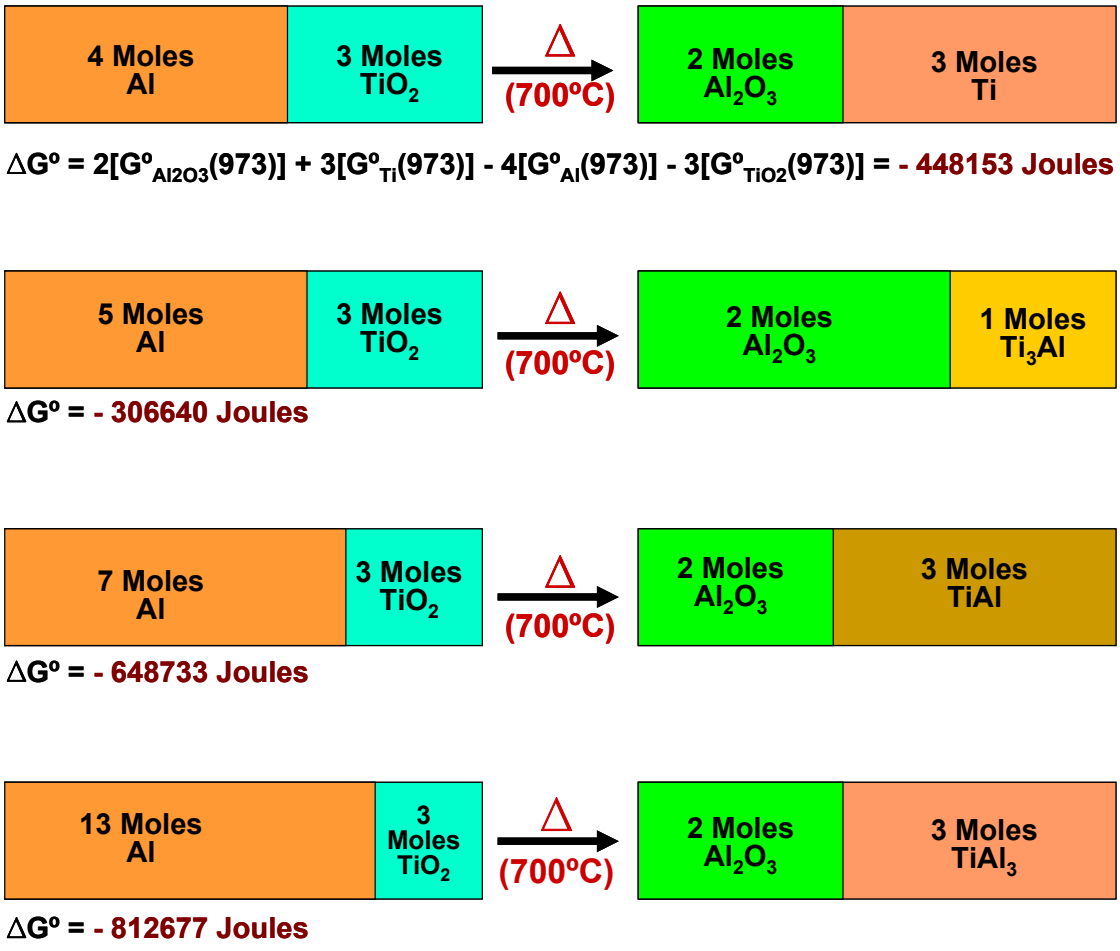

Figure 4.29: Possible reactions at the Al-TiO_2 interface.

Four possible reactions at the interface are listed below as shown in *Figure 4.29*.

$$4Al + 3TiO_2 \rightarrow 2Al_2O_3 + 3Ti \qquad 4.5.1$$

$$5Al + 3TiO_2 \rightarrow 2Al_2O_3 + Ti_3Al \qquad 4.5.2$$

$$7Al + 3TiO_2 \rightarrow 2Al_2O_3 + 3TiAl \qquad 4.5.3$$

$$13Al + 3TiO_2 \rightarrow 2Al_2O_3 + 3TiAl_3 \qquad 4.5.4$$

Equation 4.5.1 represents the complete reduction reaction of TiO_2 by Al to form Ti and Al_2O_3. *Equations 4.5.2, 4.5.3* and *4.5.4* represent the formation of Al_2O_3 and Ti_3Al, TiAl or $TiAl_3$ respectively when Al and TiO_2 react at 700ºC. The free energy calculations shown in *Figure 4.29* assumed that the compounds were stoichiometric and were perfectly ordered compounds; although in reality, that may not be the case. The phrase "compounds are stoichiometric" in the above statement means that the sublattices are precisely determined by the stoichiometry. For example, if the compound TiAl was assumed to be stoichiometric, it would be assumed that a 1:1 ratio of Ti:Al atoms was maintained in the compound. The phrase "perfectly ordered compound" for TiAl means that the Al and Ti species strictly occupy the Al and Ti sites respectively and no other sites. The above explanations suggest that deviation from "stoichiometry" and from "perfect ordering" would result in the formation of substitutional atoms in the compound structure. Free energy values for the

compounds were calculated as described in *Chapter 3*. Polynomial equations obtained from FactSage™ used for the free energy calculations were first tested by comparing the values obtained. Values of temperatures were used in the polynomials and the resulting free energy values were compared with values listed in the JANAF tables. The reference state chosen for all the free energy calculations was 298.15ºK at atmospheric pressure. Free energy calculation for the random mixing of Ti and Al on each sublattice was described by Kattner *et al.* as was shown in *Section 2.7.1.3*. Useful information for the solution of Equation 2.6.1 was found in the report by Kattner *et al.* Certain information about calculating the free energy for any composition of Al and Ti in the Ti_xAl_y system that is critical in obtaining the quantities n_{Ti}^1, $\boldsymbol{n}_{\boldsymbol{Al}}^1$, n_{Ti}^2, and n_{Al}^2 (from Equation 2.1) was not available. The above mentioned data was the only missing information that was needed to plot free energy of the ordered Ti-Al intermetallic compounds as a function of composition at any temperature.

The free energy for the reaction represented by Equation 4.5.4 seemed to be the most negative. Caution should be exercised before concluding that the $TiAl_3$ phase is thermodynamically favorable to form by the reaction represented by Equation 4.5.4. It is inappropriate to compare the free energy of reactions involving different amounts of reactants as shown in *Figure 4.29*. A fair comparison of the free energy of the above mentioned reactions was made possible by considering the free energy of a reaction per mole of the reactant consumed. The free energy of each reaction was divided by the respective number of moles of combined reactants as is listed in Table 4.1. The comparison was

legitimate since in each case, the free energy was normalized to the amount of the reactants consumed. The reaction represented by Equation 4.5.3, has the highest negative value of free energy and therefore was the most energetically favorable for formation. Results from the thermodynamic calculations are listed in Table 4.1 and are in agreement with experimental findings described in the current research as explained in section 4.4.

Table 4.1: Free energy comparison of reactions at 700ºC.

Reactions	ΔG^o per mole of combined reactant consumed
4.5.1	- 64000
4.5.2	- 38300
4.5.3	- 64800
4.5.4	- 50800

4.5.2 Formation of the Thermodynamically Favored Ti_xAl_y Compound

Li *et al.*[66] reported the calculated free energy as a function of composition at 1100°C K as shown in *Figure 2.6* in *Section 2.7.1.3*. The free energy (without the assumption of perfectly ordered Ti-Al compounds (Ti_3Al, TiAl and $TiAl_3$) could not be calculated at 700ºC due to lack of key information. The thermodynamics of the Ti-Al system is solved and reported at 1100°C by Li *et al.* An explanation for the preference of formation of the TiAl phase at 1100°C can be presented using the thermodynamic data by Li *et al.* Data was not reported at 700ºC

A free energy curve for TiO_2 (green curve) was superimposed on *Figure 2.6* shown in *Chapter 2 (see Figure 4.30)*. The lateral position of the free energy curve for TiO_2 was significant due to the small amount of Al dissolved in TiO_2 at

elevated temperatures. The vertical position of the curve is not significant for the explanation below, hence the free energy curve for TiO_2 was chosen as shown in *Figure 4.30*.

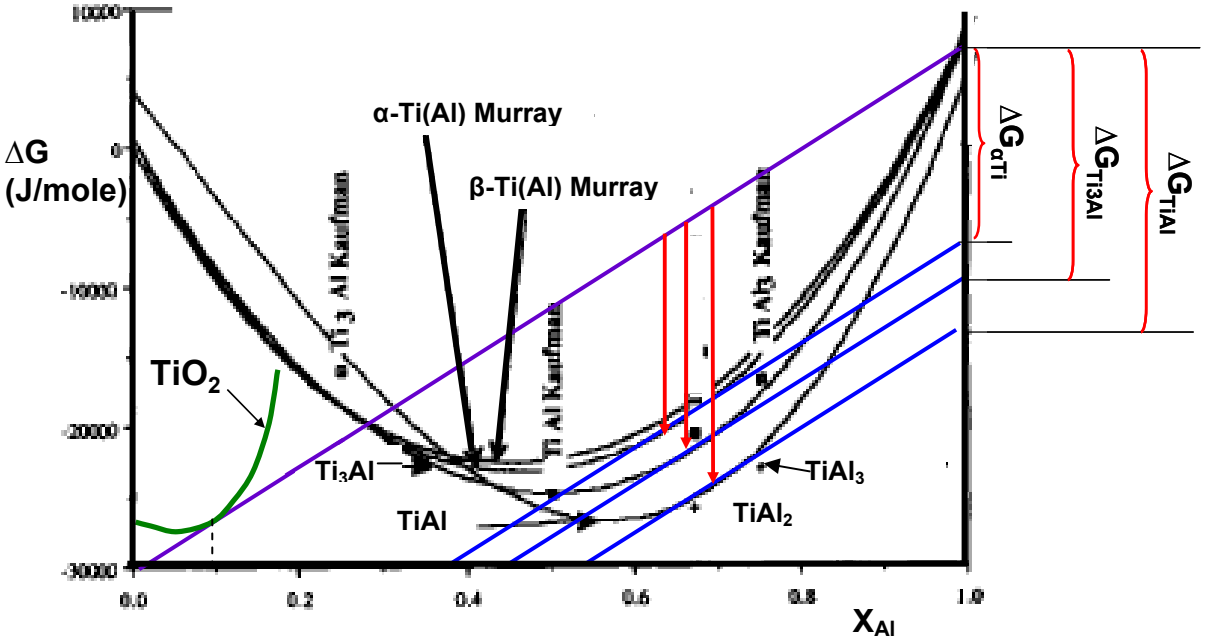

Figure 4.30: TiO_2 –free energy curve superimposed on Ti-Al Gibbs free energy diagram calculated at 1100°C by Li *et al.* for explanation of the preference of formation of TiAl compound.

The point on the free energy curve of TiO_2, through which the tangent passes, defines the amount of Al dissolved in TiO_2 (about one mole percent) as shown by the dotted line extended to the X-axis in *Figure 4.30*. Tangents on the free energy curves of Ti-Al compounds are shown by blue lines in *Figure 4.30*. Blue tangents (on free energy curves of Ti-Al compounds) are parallel to the tangent to the free energy curve for TiO_2. The red arrows represent the drop in the free energies due to the formation of the respective compounds. The magnitude in the free energy drop due to the formation of the Ti-Al compound is indicated by the red curly

bracket on the right hand side of *Figure 4.30*. The TiAl compound has the maximum drop in free energy among the other shown Ti_xAl_y compounds and hence was most energetically favorable for formation. In other words free energy change for the formation of TiAl (ΔG_{TiAl}) is greater than the free energy change for the formation of Ti_3Al (ΔG_{Ti3Al}) and α–Ti ($\Delta G\alpha Ti$) in that order. Theoretical calculations show that TiAl is most favored for formation at 1100°C. A similar proof is not furnished at 700°C in this thesis. There is no published literature that suggests transformation of a formed Ti_xAl_y compound to another compound unless a change of composition in the system is forced. Thus the result of the calculation at 1100°C, indicating the formation of TiAl, would be true at 700°C (as was observed experimentally in *Section 4.4*).

It was concluded from theoretical calculations that TiAl was the interfacial compound energetically favored for formation at elevated temperature by using thermodynamic principles and making appropriate assumptions. At elevated temperature, the formation of TiAl was favored over the formation of other Ti_xAl_y compounds and is in agreement with the experimental results.

4.6 Mechanism of Interaction at the Interface: A Proposed Model

The interaction between Al and TiO_2 yields TiAl and possibly another compound at the interface. The interfacial layer was found to be continuous; but the thickness was not uniform. The interfacial region physically separated the surfaces that were in contact with each other. Such an interfacial layer could act as a self-formed barrier against the diffusion of the reacting species towards each other; for example, the diffusion of Al towards the TiO_2 substrate, and the diffusion of Ti or O towards the

Al film. The self formation of the diffusion barrier between the reacting components would be useful in structural applications and in electronic device applications. It was necessary to understand the nucleation and growth of the interfacial compound that would be the outcome of the interaction between the two surfaces in contact at elevated temperature.

4.6.1 Nucleation and Growth Model

The current section describes a model to explain the formation and growth of TiAl at the interface under the conditions explained above. The mechanism of formation and growth of TiAl can be explained by four steps. Each step is described in detail below.

4.6.1.1 Step I

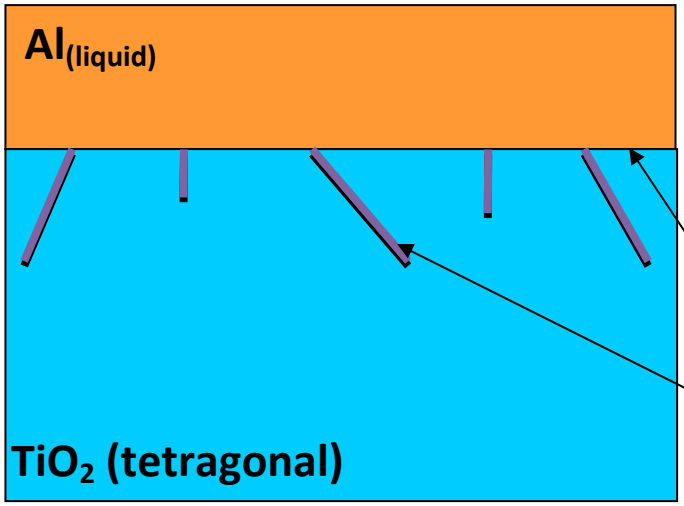

Figure 4.31: A schematic of melted Al in contact with TiO_2 substrate. Surface grain of TiO_2 has stacking faults.

The TiO_2 grains at the interface are such that part of the grain is exposed to the Al-film as shown in *Figure 4.31*. The 'purple' lines that run from the interface (surface of TiO_2 grains) into the substrate represent stacking faults in the TiO_2

grains as shown in *Figure 4.31*. The stacking faults were present at the surface and they run towards the interior of the grains and terminate within the grain (usually observed for stacking faults). *Figure 4.31* illustrates a schematic of the interface that corresponds to the TEM micrograph (*Figure 4.32*). The schematic shows a TiO_2 grain at the interface between the substrate and the film. The stacking faults are shown to initiate at the surface and terminate in the interior of the grain. Al, in contact with the substrate would have melted when the temperature of the sample reached 660ºC.

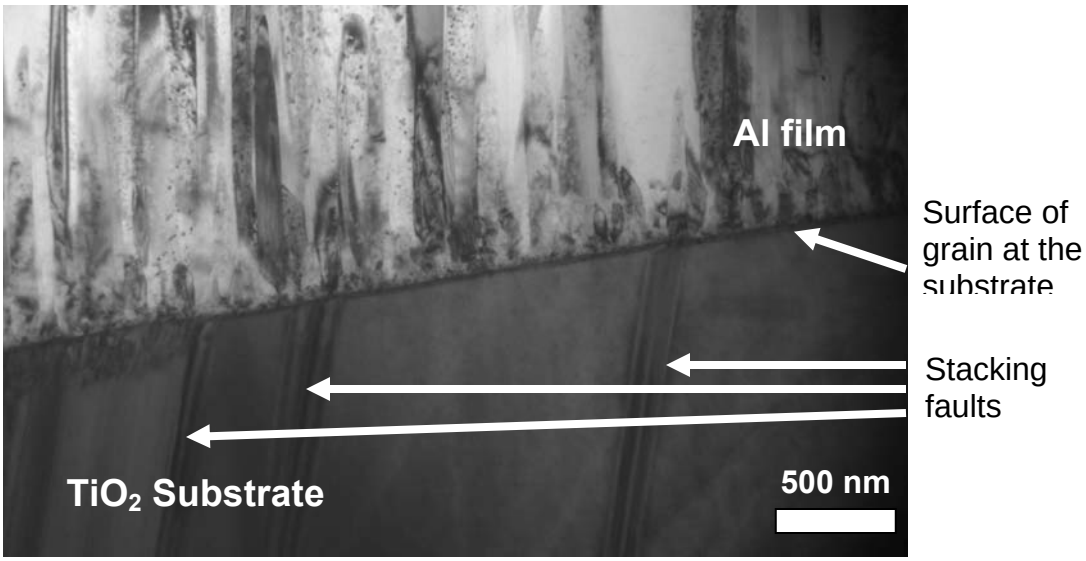

Figure 4.32: The TiO_2 grain at the surface of the substrate in contact with the Al-film. The surface grain has stacking faults that are present at the surface and run into the interior of the grain.

4.6.1.2 Step II

Liquid Al on the surface of the TiO_2 substrate diffuses towards the interface and into the TiO_2 grains. The diffusing species usually prefers high diffusivity paths because of the higher energy involved. The stacking faults are high energy

paths that are present on the surface of the TiO_2 grains. The second step involves diffusion of Al into the TiO_2 grains through the stacking faults (preferred high energy diffusivity paths) as shown in the schematic above (*Figure 4.33*).

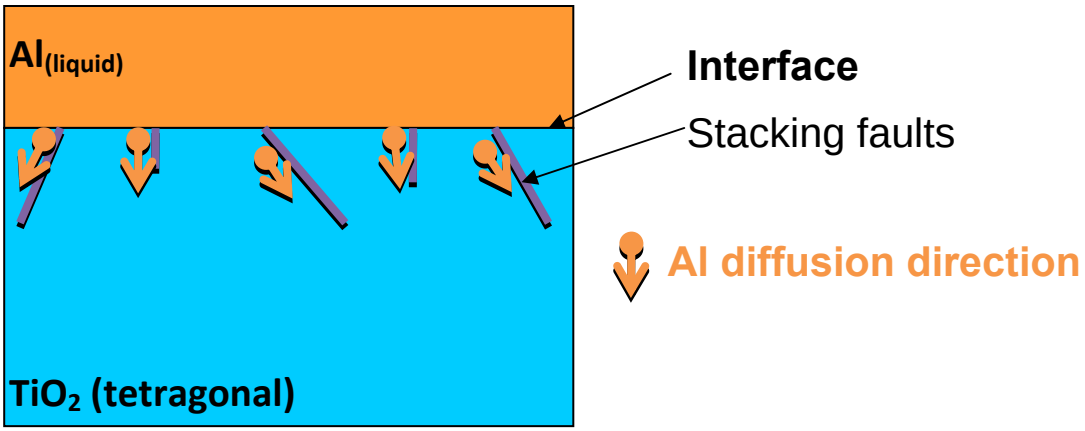

Figure 4.33: A schematic showing Al diffusing into the TiO_2 substrate through stacking faults.

Although the stacking faults seem an obvious route for Al to diffuse into TiO_2 grains, it has yet to be proven that stacking faults are indeed the path that Al would take to diffuse into TiO_2. *Figure 4.34* shows the interfacial region of the Al-TiO_2 film-substrate sample that also shows several stacking faults on the TiO_2 side of the interface. The micrograph in *Figure 4.34* was obtained through STEM mode on the FEI TITAN.

The stacking faults are marked by blue dotted lines and labeled in the micrograph in *Figure 4.35*. Some stacking faults were observed to pass through the area marked with dotted circles as shown in *Figure 4.35*. An electron energy loss spectroscopy (EDS) line scan was performed along the *red* line (shown in *Figure 4.35*) to semi-quantitatively determine the atomic composition at the

points along the line. The EDS data was superimposed on the micrograph as shown in *Figure 4.35*.

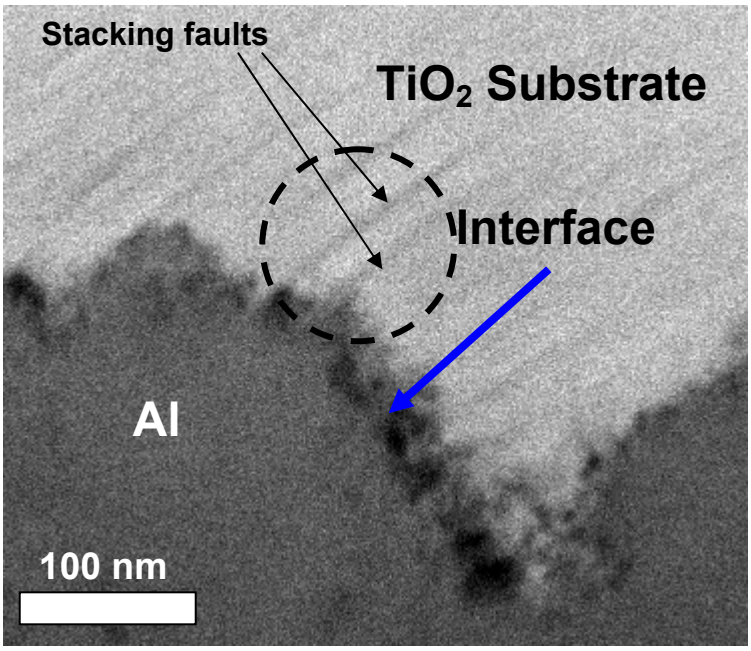

Figure 4.34: Interface of Al-TiO_2 sample exposed to 700ºC for 9 hours. Several stacking faults are observed on the TiO_2 side.

Some of the common problems encountered while using EDS data from the TEM and the steps taken here to counter those problems are described. TEM samples were prepared by milling a thin region at the interface between two surfaces using the focused ion beam. The FIB used gallium ions as the milling material. Usually some of the milled material re-deposited on the surface of the sample. Although a "cleaning cut" was employed to clean the re-deposited material, it did not always clean the surface completely. Unwanted oxygen-containing material could be left behind on the surface of the TEM sample that could render the results of the EDS scan useless if the data is not used carefully. It is common to have a slight variation in the thickness of the sample over short

distances. The differences in the thickness of the sample are usually sensitive to data counts for EDS scans even over a few nanometers. The data would show that the relative amount of a particular element would be greater in a thicker region even though the percent element concentration is uniform over the entire sample. In order to counter such problems a couple of steps were taken:

i. An EDS scan was performed at the Al-film region (where no oxygen was expected to be found) and at the oxide region. The scan did not show any trace of oxygen on the Al-film side; while it showed a significant amount of oxygen on the oxide side. This indicated that the sample surface did not have re-deposited oxide-containing material and was clean for EDS.

ii. A ratio of intensities was used that would account for the varying thicknesses from one point on the sample to the other.

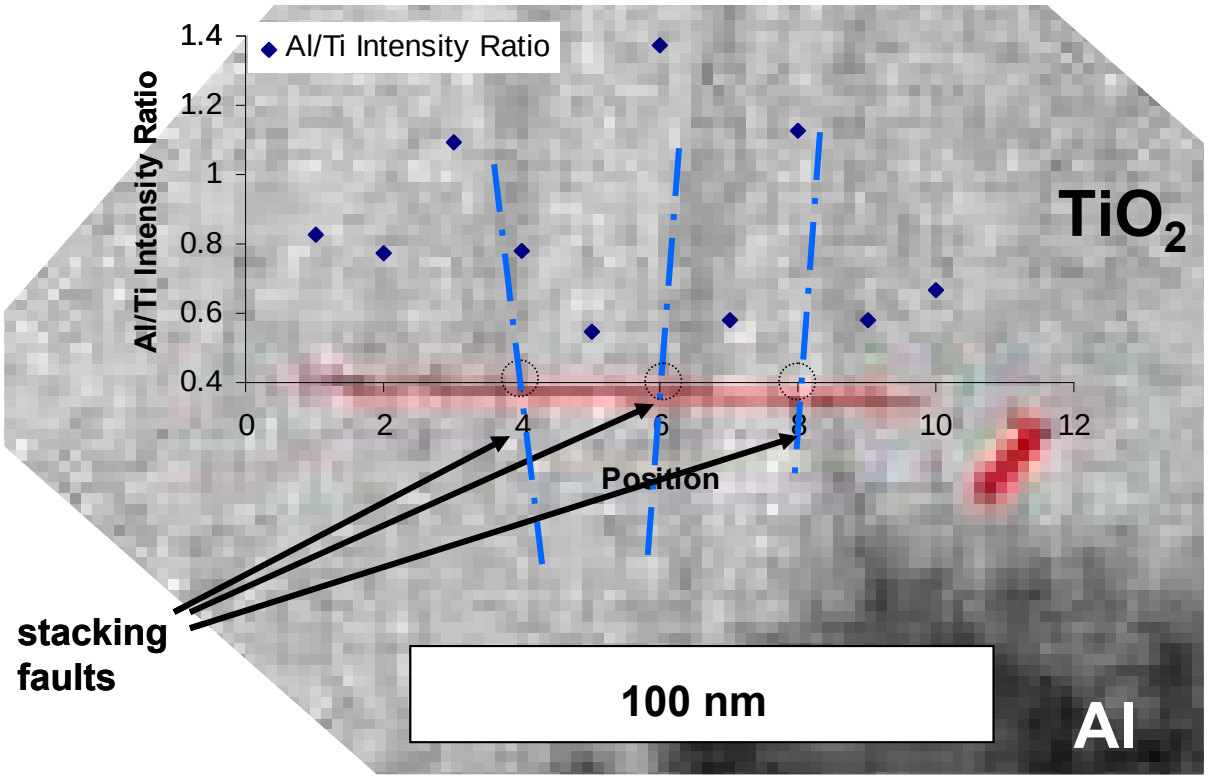

Figure 4.35: EDS line spectrum with Al/Ti intensity ratio superimposed on STEM micrograph (from marked region in Figure 4.34).

The blue dashed lines in *Figure 4.35* trace the stacking faults in TiO_2 grains. The plot superimposed on the micrograph as shown in *Figure 4.35* shows the variation of intensity ratio of Al/Ti along the distance. The data at the dotted circular marked regions showed a higher intensity of Al/Ti compared to the other regions with data points indicating a high Al concentration at the marked regions at the stacking faults. The result validates Step II of the model that explained the stacking faults as high diffusivity paths for diffusion of Al into TiO_2 grains. The stacking faults, in a similar sample that was exposed to 700ºC for 36 hours, were inspected for consistency. *Figure 4.36 (a)* shows a bright-field micrograph of the interface of the sample soaked for 36 hours at 700ºC. *Figure 4.36 (b)* represents the same location taken in STEM mode.

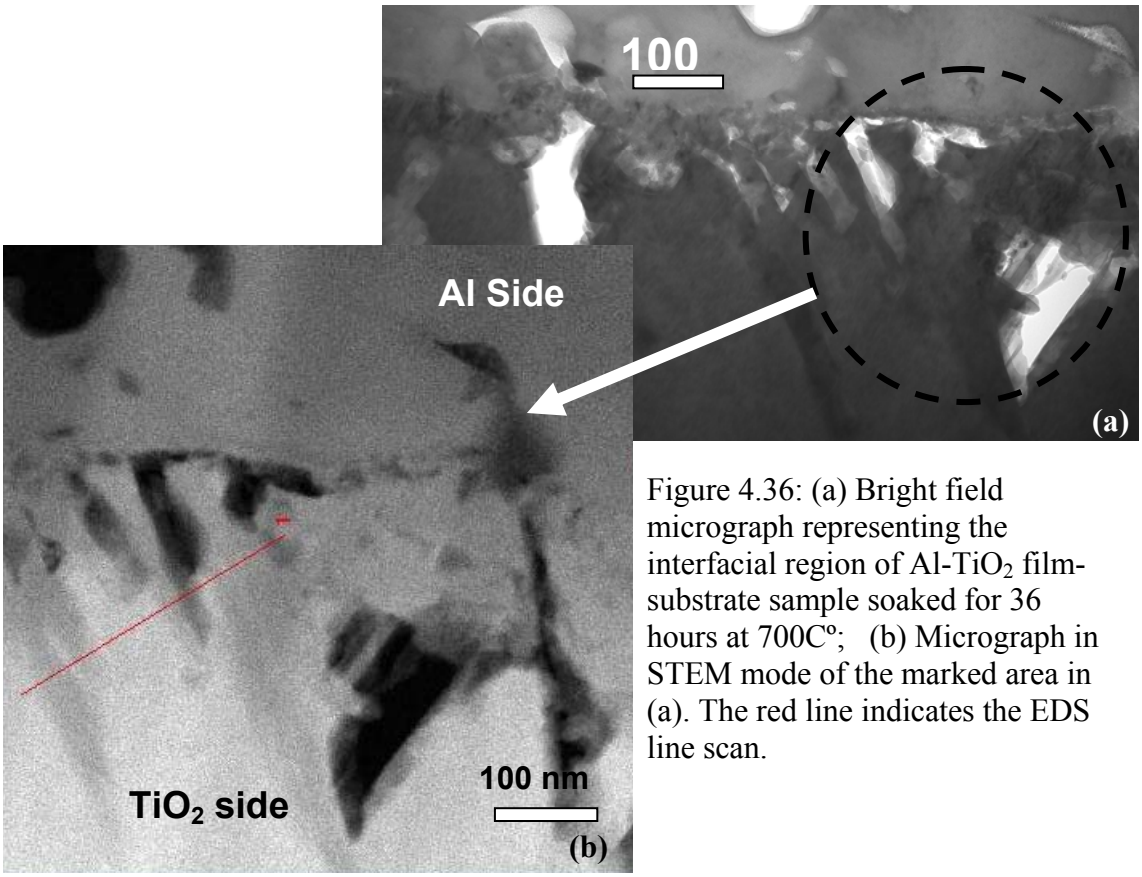

Figure 4.36: (a) Bright field micrograph representing the interfacial region of Al-TiO_2 film-substrate sample soaked for 36 hours at 700Cº; (b) Micrograph in STEM mode of the marked area in (a). The red line indicates the EDS line scan.

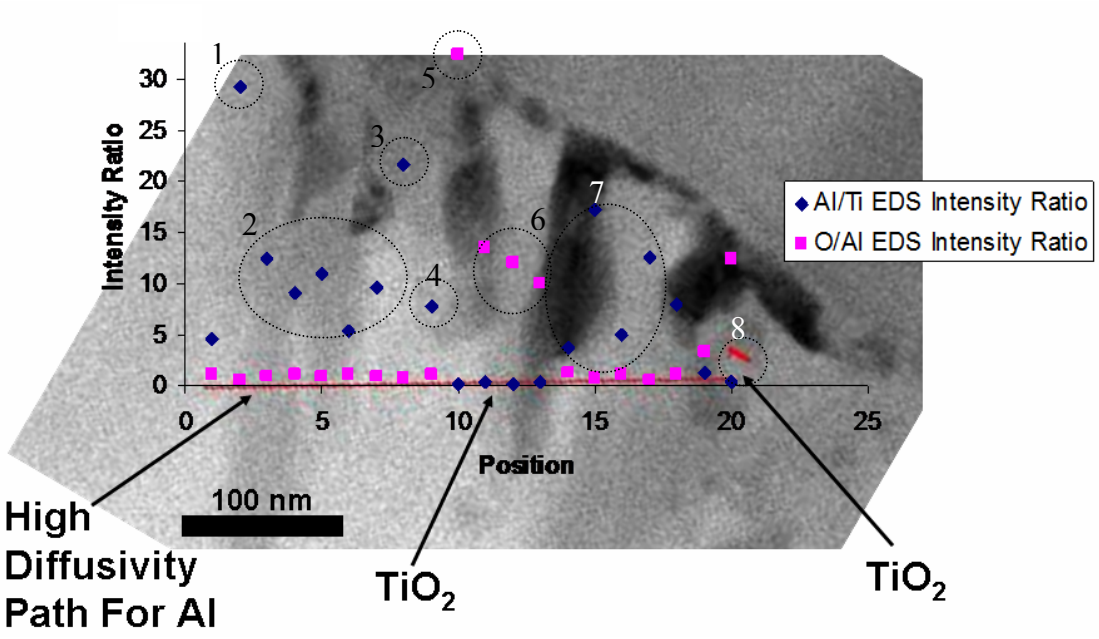

Figure 4.37: Al/Ti and O/Al intensity ratio from EDS line scan superimposed on STEM micrograph.

The EDS line scan shown in *Figure 4.37* revealed a higher concentration of Al at and near the stacking faults. The data points are marked (dotted circles) in sets (points with similar characteristics) and labeled in *Figure 4.37*. The marked *point 1* indicated a high Al/Ti ratio and very low O/Ti ratio. This showed that the marked *point 1* was a high Al-diffusion path. The marked *points 2* indicated a very low O/Al intensity ratio but a fairly high Al/Ti intensity ratio. The marked *point 2* was thus the TiAl region. The marked *points 3* and *4* represent areas in the TiAl region with a higher concentration of Al. The marked *point 5* was possibly an unreacted TiO_2 grain with a high O/Al intensity ratio and a low Al/Ti intensity ratio. The marked *point 6* represents a TiO_2 grain that possibly had transformed to the TiAl grain but contained an excess amount of oxygen from the local reduction of TiO_2. The marked *points 7* possibly indicate the TiAl region similar to the one

described as the *point 2*. The marked *point 8* represents the TiO_2 grain as explained for *point 5*. The above explained points in the Al-TiO_2 samples soaked for 9 and 36 hours verify that Al chose the stacking faults in the TiO_2 grains as preferred paths for the diffusion into the TiO_2 grains at the elevated temperature.

4.6.1.3 Step III

The Al that diffused into the TiO_2 grains through the stacking faults, as explained above in Step II, reacted with TiO_2 at the stacking fault locations as shown in *Equation 4.6.3.1* and *Equation 4.6.3.2*. The *Equations 4.6.3.1* and *4.6.3.2* represent intermediate stages during the reaction between Al and TiO_2. Step III hypothesized that the reaction sites are close to the stacking faults.

$$TiO_2 \xrightarrow{Al} Ti + 2O \quad \ldots (4.6.3.1)$$

$$\boldsymbol{Ti + Al \rightarrow TiAl} \quad \ldots (4.6.3.2)$$

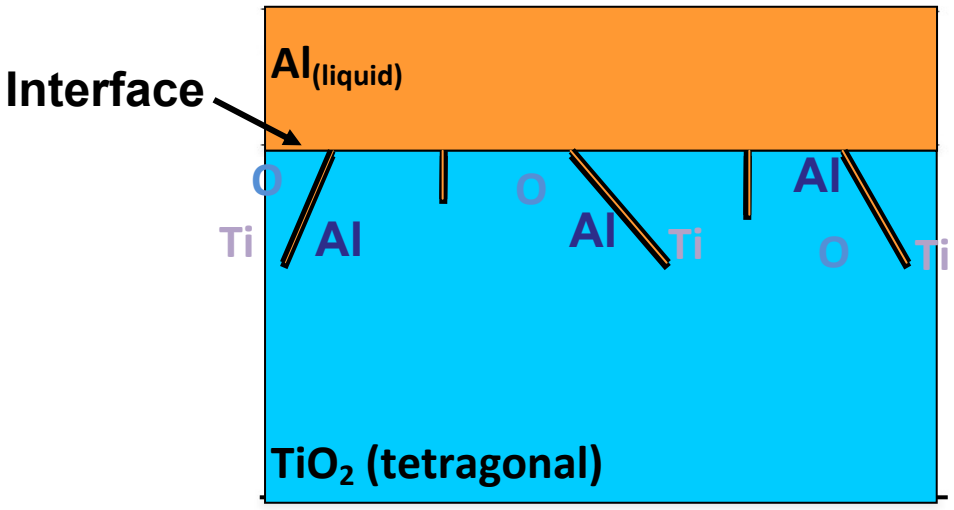

Figure 4.38: A schematic that summarizes the mechanism of formation of TiAl at regions close to the stacking faults in Step III.

Step III shows the reaction of Al with TiO_2 during the reduction of the TiO_2 to form Ti and O. The Al further reacts with the Ti, which was released by the

reduction of TiO_2, to form TiAl. The mechanism explained in *Step III* is represented in the schematic shown in *Figure 4.38*.

4.6.1.4 Step IV

Step IV represents the growth of the TiAl compound (the green area represented in *Figure 4.39*) after formation of the interfacial TiAl compound at the regions close to the stacking faults in the TiO_2 grains. The boundary between the interfacial region and the TiO_2 substrate was shown to be distinctly wavy.

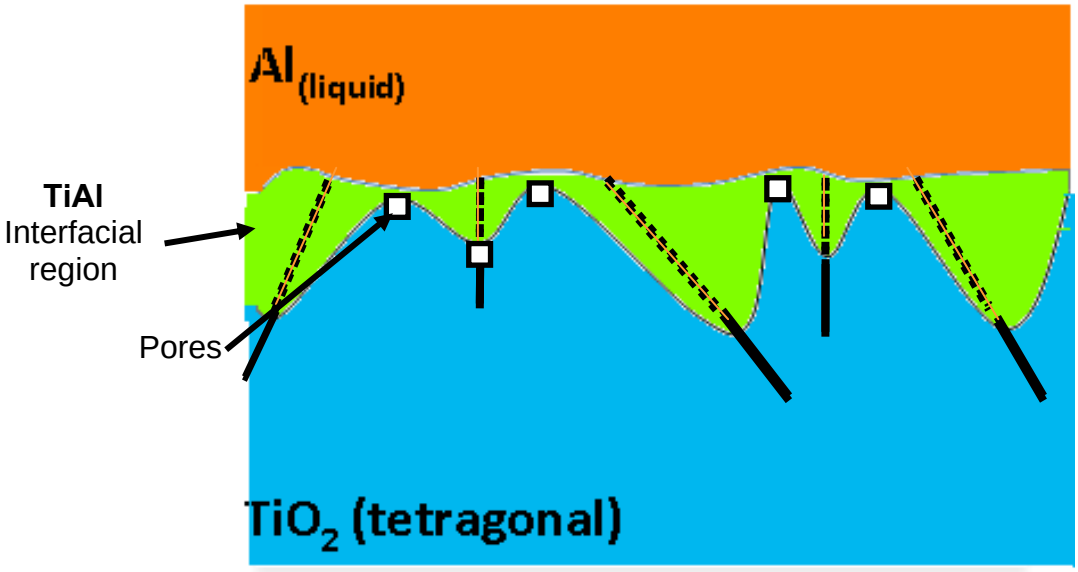

Figure 4.39: Schematic showing the growth of TiAl into the TiO_2 grains in Step IV.

The mechanism of growth of the TiAl compound at the interface into the TiO_2 substrate in Step IV is indicative of the reason for the wavy shape of the TiAl interfacial region (boundary between interfacial region and TiO_2 substrate). The region around the stacking faults in the TiO_2 grains was occupied by the TiAl compound. The TiAl compound was not expected to form at regions that were isolated from the stacking faults due to the lack of availability of Al at those

regions. *Figure 4.40 (a)* shows the interface of an unheated sample for the purpose of comparison with the interface of a similar sample that was soaked at 700ºC for 9 hours as shown in *Figure 4.40 (b)*. The microstructure shows the wavy boundary between the interfacial region and the TiO_2 substrate and hence is in agreement with the growth mechanism in *Step IV*.

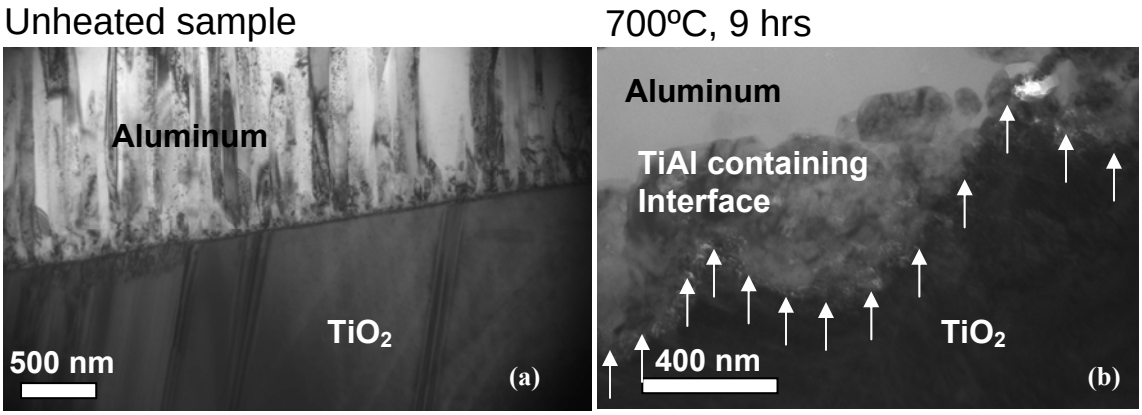

Figure 4.40: (a) A straight interface of the unheated sample; (b) a wavy interface at the TiO_2/interfacial boundary in the Al-TiO_2 sample soaked for 9 hours at 700ºC.

$$7Al + 3TiO_2 \rightarrow 2Al_2O_3 + 3TiAl \qquad 4.5.3$$

Equation 4.5.3 represents the reaction between Al and TiO_2 as explained in Section 4.5. The equation shows that three moles of TiO_2 react with seven moles of Al to form three moles of TiAl and two moles of Al_2O_3. The molar volume of TiO_2 without dissolved Al was calculated to be *18.8* cm^3. The molar volume of TiAl was calculated to be *18.7* cm^3. TiAl occupied slightly less volume (*0.01* cm^3 per mole) than TiO_2. It is possible that the difference in volume can be explained as pores at the interface.

Large pores were present at the boundary between the interfacial region and the TiO_2 substrate in the sample that was soaked at 700ºC for 36 hours as shown in *Figure 4.41(a)*. *Figure 4.41(b)* shows a different location along the interface of the same sample. The large pores that were located along the boundary between the interfacial region and the TiO_2 substrate were such that the wavy boundary demarcation was distinctly visible as a wide wavy gap (*Figure 4.41*).

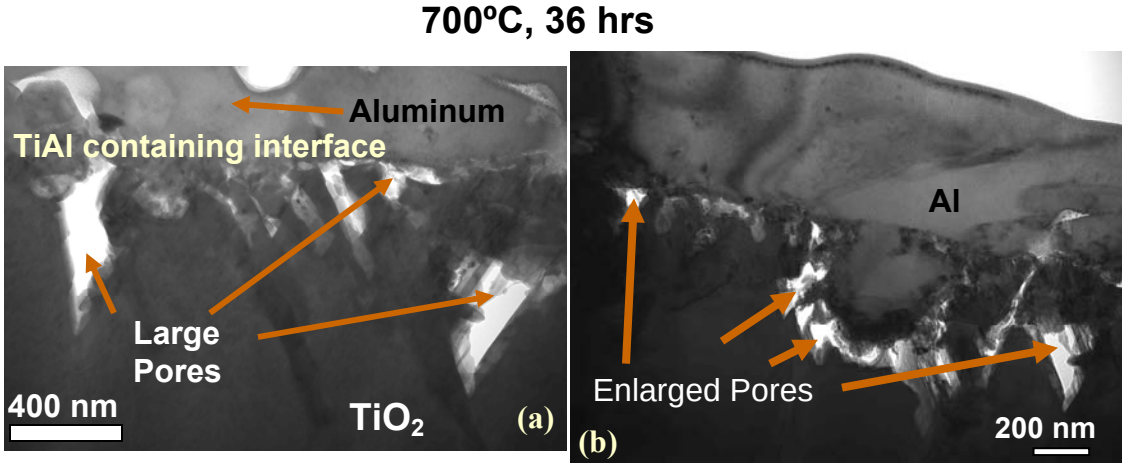

Figure 4.41: (a) Large pores at the interface for Al-TiO_2 sample soaked for 36 hrs at 700ºC; (b) Pores along the boundary between the interfacial region and TiO_2.

It was thus concluded from the analysis of the interface using the TEM that the formation of the interfacial compound (TiAl) could be described in the following way:

Step I: Melted Al was in contact with the TiO_2 substrate at elevated temperature.

Step II: Al diffused into the TiO_2 substrates more quickly through the stacking faults in the TiO_2 substrate.

Step III: At the stacking faults, TiO_2 is reduced by Al to form Ti and O. Ti reacts with Al near the stacking fault sites to form TiAl.

Step IV: The interfacial region containing TiAl grows near the stacking fault sites into the TiO_2 substrate.

4.7 An Explanation for the Oxygen Released during the Al – TiO_2 Reduction Reaction

The amount of oxygen that would have been released during the reduction of the TiO_2 would be twice as much as the amount of TiAl formed. The formation of each TiAl molecule would have been preceded by the reduction of one molecule of TiO_2 that would have released one Ti and two O atoms. The current section lists four possible ways to explain the presence of oxygen that would have been released during the reduction of TiO_2. The results thus far indicated that the following equilibrium equation was probably responsible for the interfacial reaction:

$$7Al + 3TiO_2 \rightarrow 2Al_2O_3 + 3TiAl \qquad 4.5.3$$

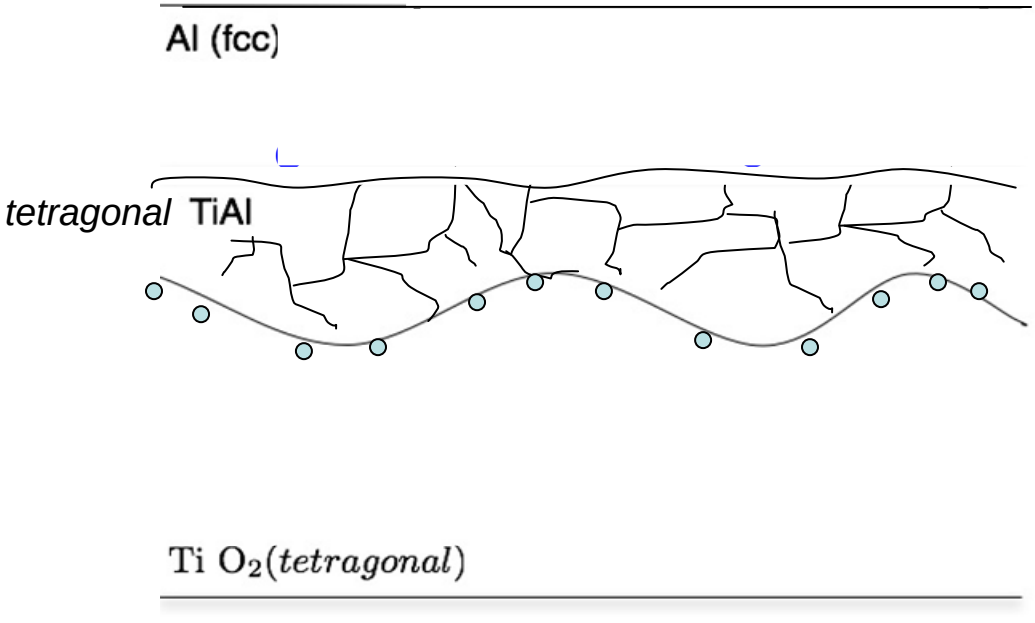

Figure 4.42: A schematic of the interface between Al and TiO_2 after the interaction between Al and TiO_2.

There were four possible ways that O released during reduction of TiO_2 at the interface as shown in *Figure 4.45* could be present:

i. The O could be dissolved in the TiAl layer.

ii. The O released at the boundary between the interfacial region and the TiO_2 below could diffuse through the interfacial region and settle as a solution in the Al.

iii. Oxygen could be present at the
   - interface between TiAl and TiO_2
   - interface between TiAl and Al
   - grain boundaries between the TiAl grains

iv. The O could combine with the Al that diffuses into the TiO_2 grains, to form Al_2O_3.

4.7.1 Possibility I (Presence of Oxygen in Layer Containing TiAl)

The possibility of the presence of O in the TiAl interfacial layer was considered, as shown in the schematic below (*Figure 4.43*). *Section 2.8* in *Chapter 2* explained that a theoretical model has been developed by Lefebvre *et al.* that indicated that there is little solubility of O in the ordered Ti_xAl_y compounds which included Ti_3Al, TiAl and $TiAl_3$. The model by Lefebvre *et al.* calculated the solubility of TiAl and the line compound $TiAl_3$ to be almost "zero".

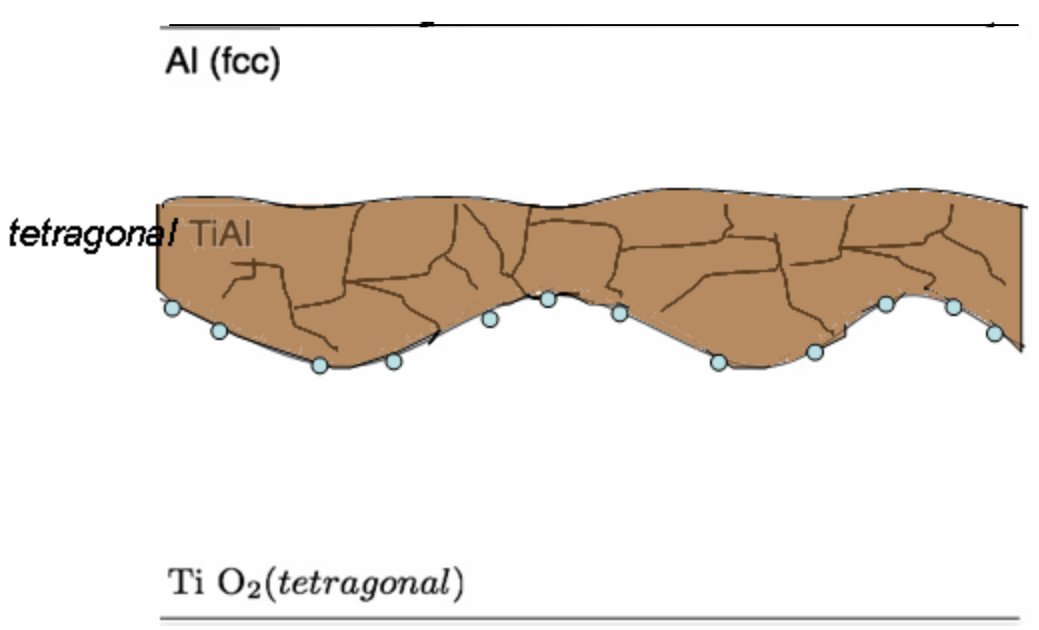

Figure 4.43: Schematic showing possibility of the presence of oxygen in the interfacial layer containing TiAl.

The current section explains the results from the analysis to detect the presence of oxygen at the interfacial region. The challenge posed by the analysis was to be able to create a sample that had a sufficient interfacial region that was created by the reaction that could be characterized suitably for the presence of O. Also, a spectroscopic technique like EDS was preferred to a diffraction technique for such an experiment. *Figure 4.44* showed a bright-field image at the interface of the Al-TiO_2 film-substrate sample that was soaked for 9 hours at 700ºC. Arrow-tips in the micrograph point to the specific points on the sample where the electron beam from the TEM collected the EDS data to semi-quantitatively determine the composition at each point. Small holes were observed at the end of most arrows that indicated the exact location where the EDS data were collected.

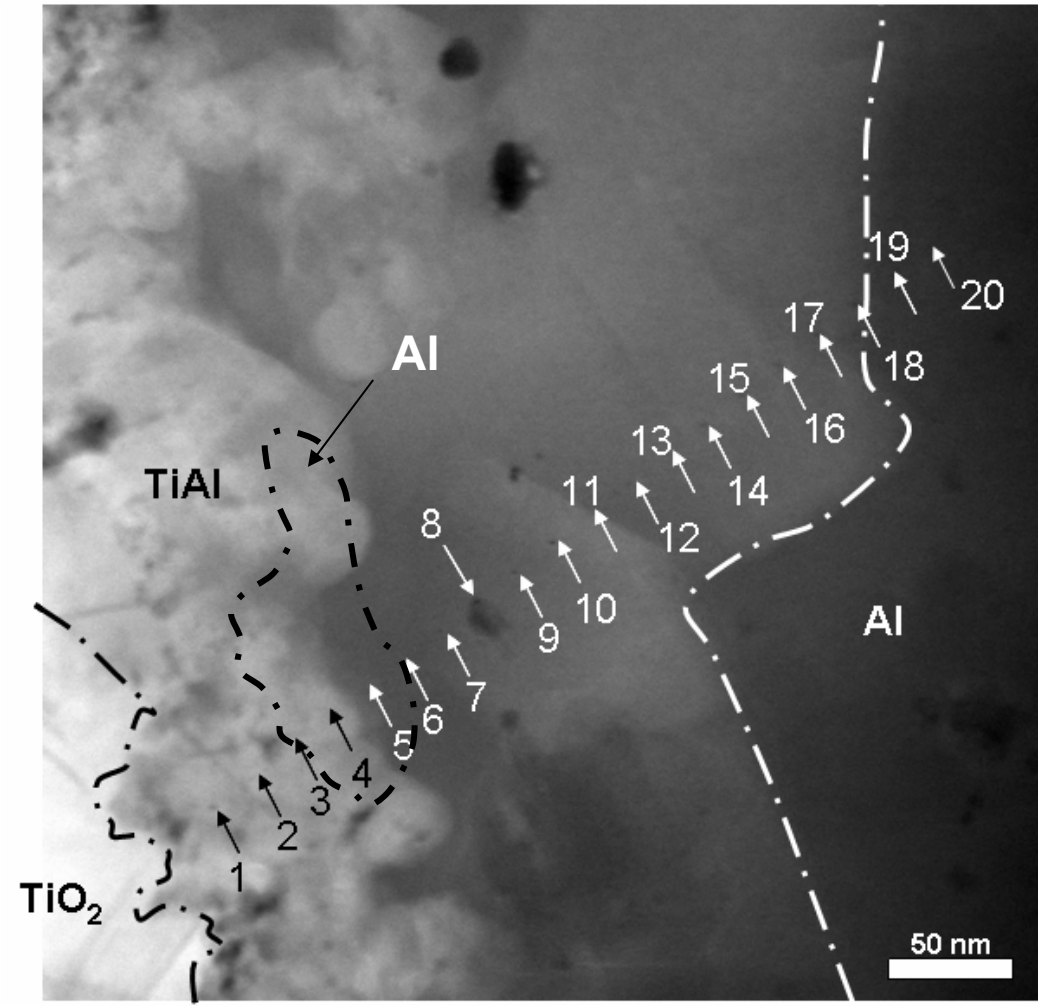

Figure 4.44: Points from the EDS line scan beginning from the TiO_2 side through TiAl interface into Al for the Al-TiO_2 sample soaked for 9 hours at 700ºC.

The EDS spectra that were collected from the interfacial region (spanning from points 1 to 18) that contained TiAl compound is shown in *Figure 4.45*.

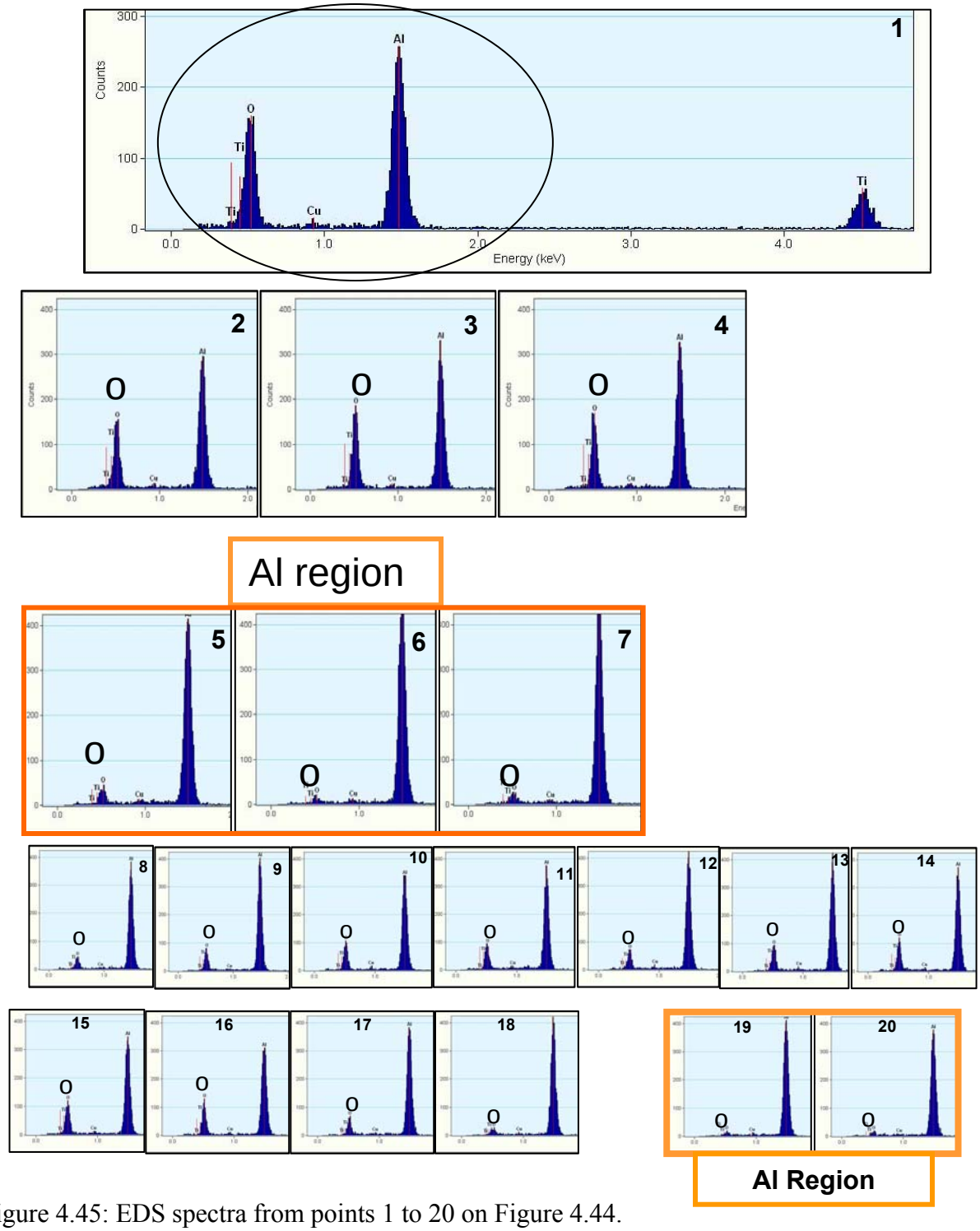

Figure 4.45: EDS spectra from points 1 to 20 on Figure 4.44.

As explained in *Section 4.6.2* in the current chapter, the ratios of the intensities from the EDS data were used to reduce errors due to non-uniform thickness of the TEM samples. *Figure 4.46* shows the EDS intensity ratios O/Al and Ti/O that were superimposed on the TEM microstructure at the interfacial region. The appropriate superimposition of the EDS data on the microstructure facilitated an easy comparison of the intensity ratios.

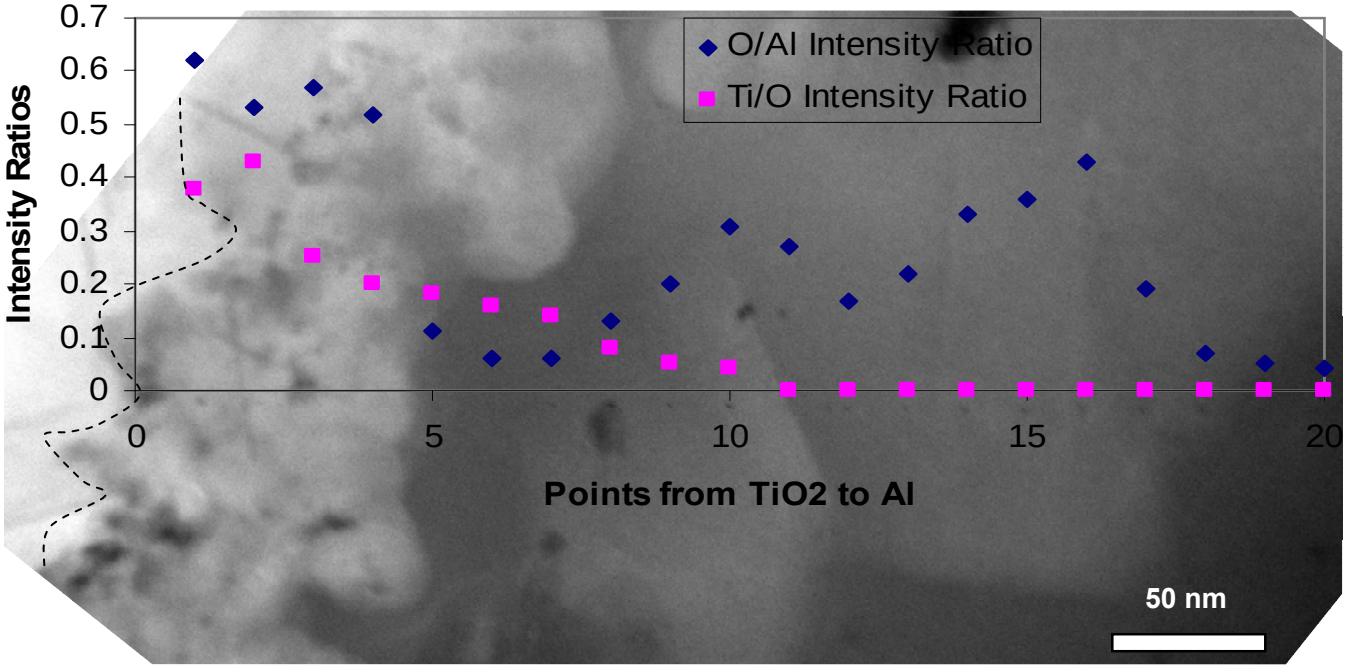

Figure 4.46: O/Al and Ti/O EDS intensity ratios superimposed on TEM microstructure at the interface of the Al-TiO_2 sample soaked for 9 hours at 700ºC.

The interfacial region-TiO_2 boundary (dotted line) is shown at the left side of the micrograph. The right side of the micrograph (dark region) was almost completely Al as is seen from the EDS intensity ratios shown in *Figure 4.46*. The interfacial layer that contained the TiAl compound clearly showed intermediate levels of the O/Al as well as the Ti/O EDS intensity ratios that indicated the presence of O in the TiAl containing interfacial layer. A very high value of the

O/Al intensity ratio at the left side of the micrograph possibly was due to the proximity to the TiO_2 side. The data points around the vicinity of the points 10 and 15 showed a very high O/Al and very low Ti/O intensity ratios. A careful examination at those regions showed a grain-like structure. The high O content at those regions could have been due to the presence of Al_2O_3 grains in the interfacial region. The determination of the presence of Al_2O_3 grains in the interfacial region will be dealt with, in detail in *Section 4.7.4*.

The current section explains the presence of O in the interfacial layer containing the TiAl compound. Although contrary to the explanation provided by Lefebvre *et al.,* it could be that O would be present in the metastable state in the TiAl compound and not in a "dissolved" state as a solid state solution of O in TiAl. The presence of O in the metastable state could possibly explain the presence of well dispersed Al_2O_3 grains (if any in the interfacial region) that could have precipitated when the sample was exposed for longer periods of time at an elevated temperature. The O could be in the metastable state thus forcing the formation of Al_2O_3.

4.7.2 Possibility II (Presence of Oxygen in Al Layer)

Figure 4.47 represents a schematic of the presence of O in the Al-layer during the interaction of Al with the TiO_2 substrate at 700ºC.

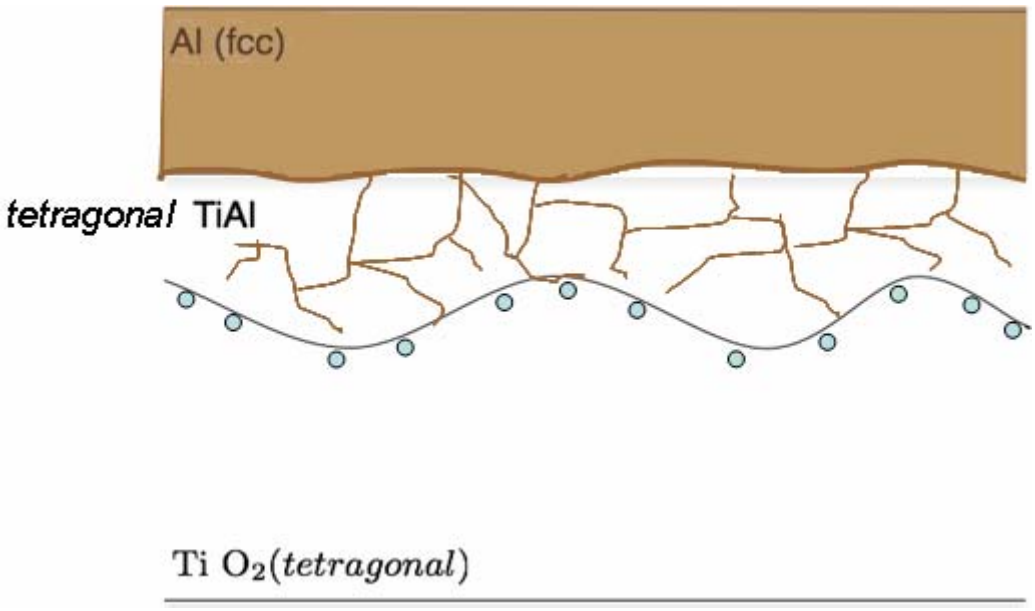

Figure 4.47: A schematic showing possibility of presence of oxygen in the Al layer on the top surface.

The presence of O in the Al-layer as a solid solution of O in Al or otherwise was not thermodynamically favorable as explained in *Section 2.7*. *Section 2.7* described the report by *Kubaschewski and Hopkins* and *Weast* about the formation of an oxide that was thermodynamically more favorable than the formation of a solid solution of O in Al. The results from the EDS characterization that was explained in *Section 4.8.1* also confirmed that O was not present in the Al layer. The points labeled 19 and 20 in *Figure 4.46* showed that very little or no oxygen was dissolved in the Al layer. Due to the above mentioned reasons it was safe to conclude that O would not exist in the Al film layer.

4.7.3 Possibility III (Oxygen at the Interface Boundaries and Grain Boundaries)

Figure 4.48 shows a schematic representation of the presence of O at the interfacial layer-TiO_2 substrate boundary, the Al layer-interfacial layer boundary, and the TiAl grain boundaries, during the interaction of Al with TiO_2 at an elevated temperature.

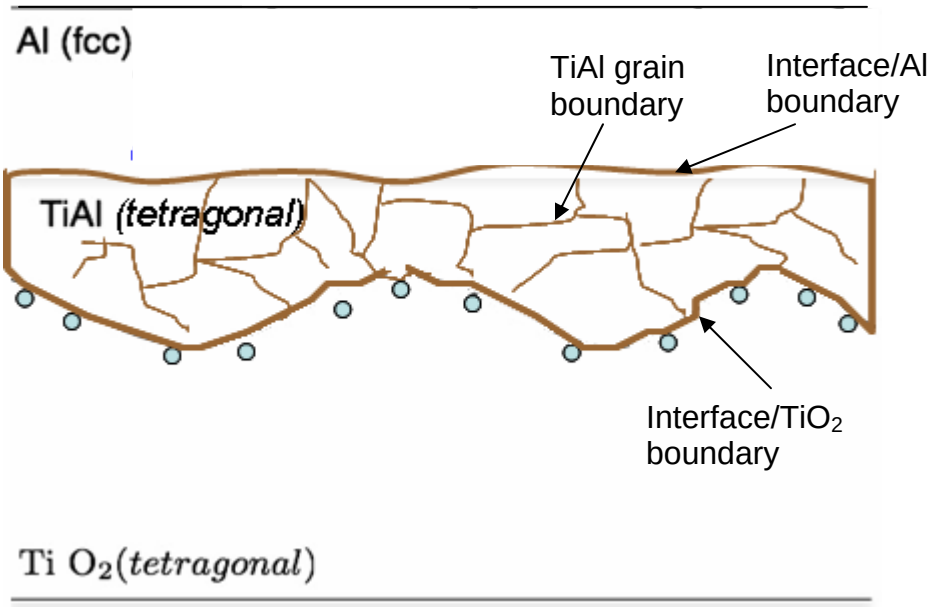

Figure 4.48: Schematic showing possibility of presence of oxygen at various interfaces and TiAl grain boundaries.

The boundary between the interfacial region, and Al and the grain boundaries between the TiO_2 grains were thin (few nanometers). It was a challenge to focus an electron probe well within the interfacial boundary, or within a TiAl grain boundary in order to characterize the grain boundary composition using the EDS. It is usually challenging to maintain the probe focus within grain boundaries since grain boundaries are not always two dimensional and also they need not

necessarily be straight but could have curves that could render the spectroscopic results invalid. The above mentioned challenges do not rule-out the possibility of the presence of O in the above mentioned regions.

4.7.4 Possibility IV (Oxygen Reacts with Al in TiAl to Form Al_2O_3)

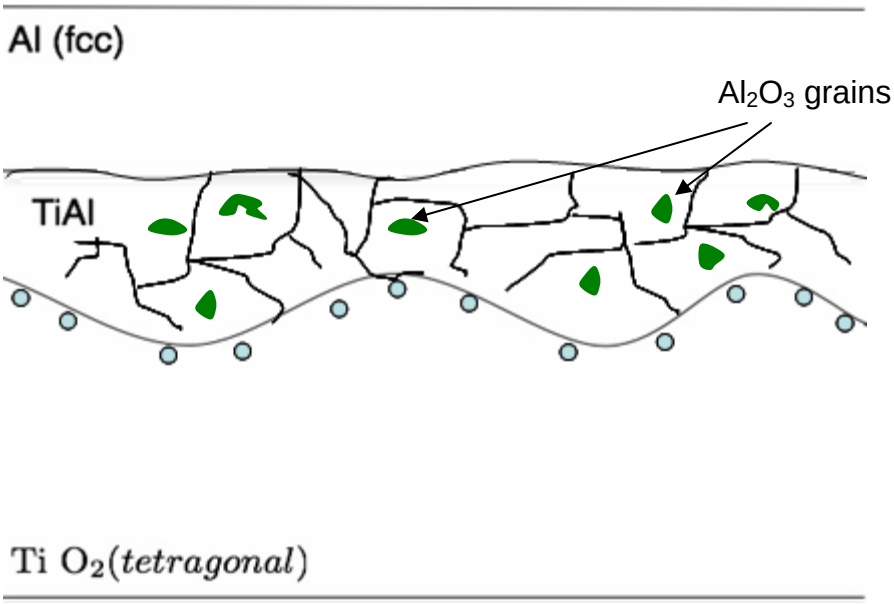

Figure 4.49: Schematic showing possibility of presence of Al_2O_3 grains in the interfacial region containing TiAl grains.

Figure 4.49 shows the presence of Al_2O_3 grains schematically in the interfacial region containing TiAl. It has been reported by Zhang *et al.* (as described in *Section 2.8*) that Al_2O_3 grains do not form instantly when Al interacts with TiO_2 to form an aluminide.

The small grain-like features observed in *Figure 4.44* were examined for the presence of Al_2O_3. *Figure 4.50* shows a region having the grain-like features (curly brackets) at the interface that contained the TiAl grains in the Al-TiO_2 sample that was soaked for 9 hours at 700ºC.

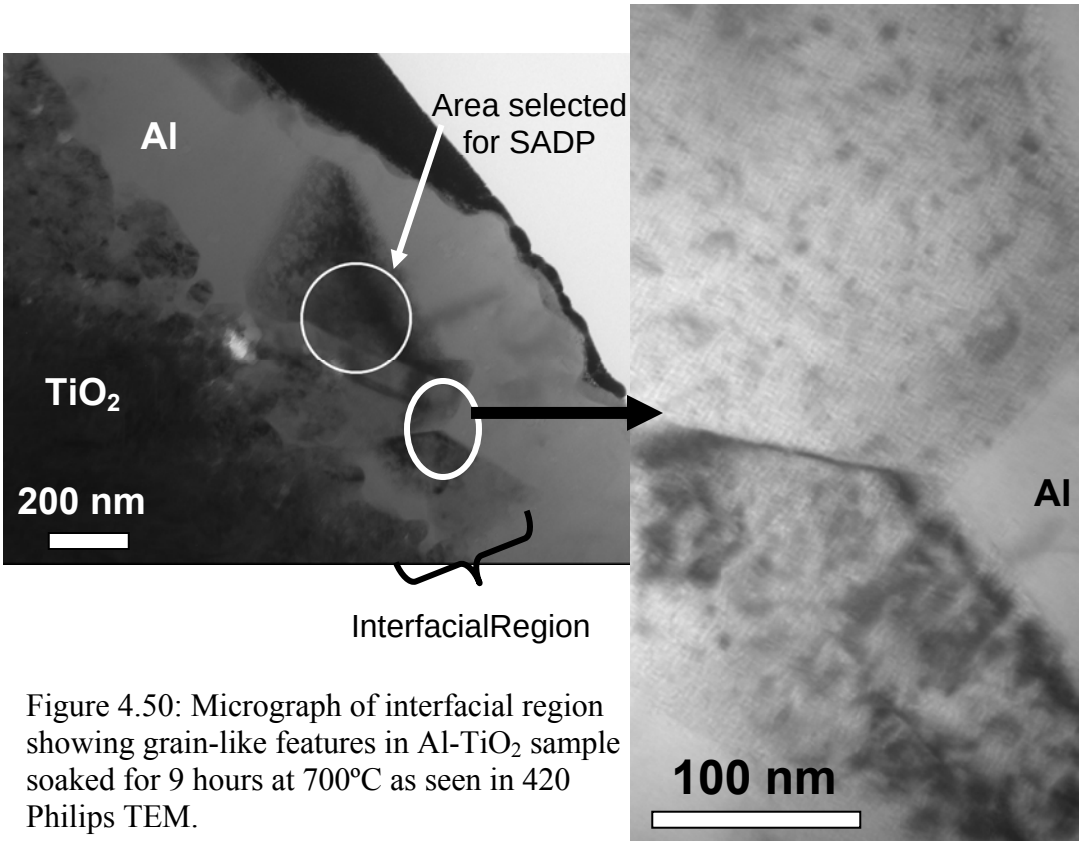

Figure 4.50: Micrograph of interfacial region showing grain-like features in Al-TiO_2 sample soaked for 9 hours at 700ºC as seen in 420 Philips TEM.

The usual route to characterize a compound or a phase with such a microscopic size (about one micron) is to select the subject with an aperture in the TEM for electron diffraction. The grains in the Al-TiO_2 sample were about an order of magnitude smaller than one micron and hence it would be difficult to select a suitable area on the grain (as in *Figure 4.50*). An indirect way was thus employed to determine the structure of the grains.

A thin TEM sample was used to examine the grain-like feature at a very high magnification in the FEI-TITAN TEM. The particles were crystalline in nature as a regular lattice arrangement was observed at a high magnification. *Figure 4.51*

shows the high magnification micrograph of the grain observed using the FEI-TITAN TEM.

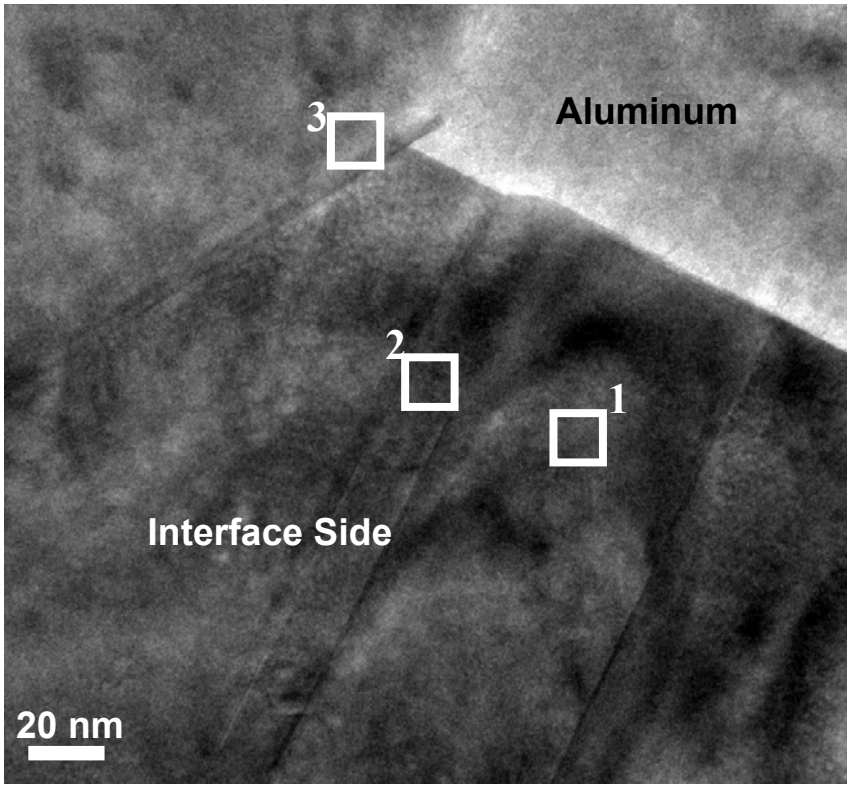

Figure 4.51: TEM micrograph of grain observed at the interfacial region containing TiAl shown in Figure 4.50.

The regions marked *1, 2* and *3* are shown in *Figures 4.52, 4.53* and *4.54* respectively at very high magnification. *Figures 4.52, 4.53* and *4.54* are high resolution TEM micrographs that reveal the lattice arrangement of atoms within the crystal structure. A software attachment with the FEI – TITAN allowed for the selection of a square region that showed the lattice image and then processed the image-data using 'Fourier Transformation'. The software converted the atomic arrangement data to a diffraction-pattern quite similar to the dot-pattern that is usually representative of an electron diffraction pattern. Insets in each of *Figures*

4.52, 4.53 and *4.54* show the 'Fourier Transformed' dot-patterns that were indexed as an ordinary electron diffraction pattern would have been indexed.

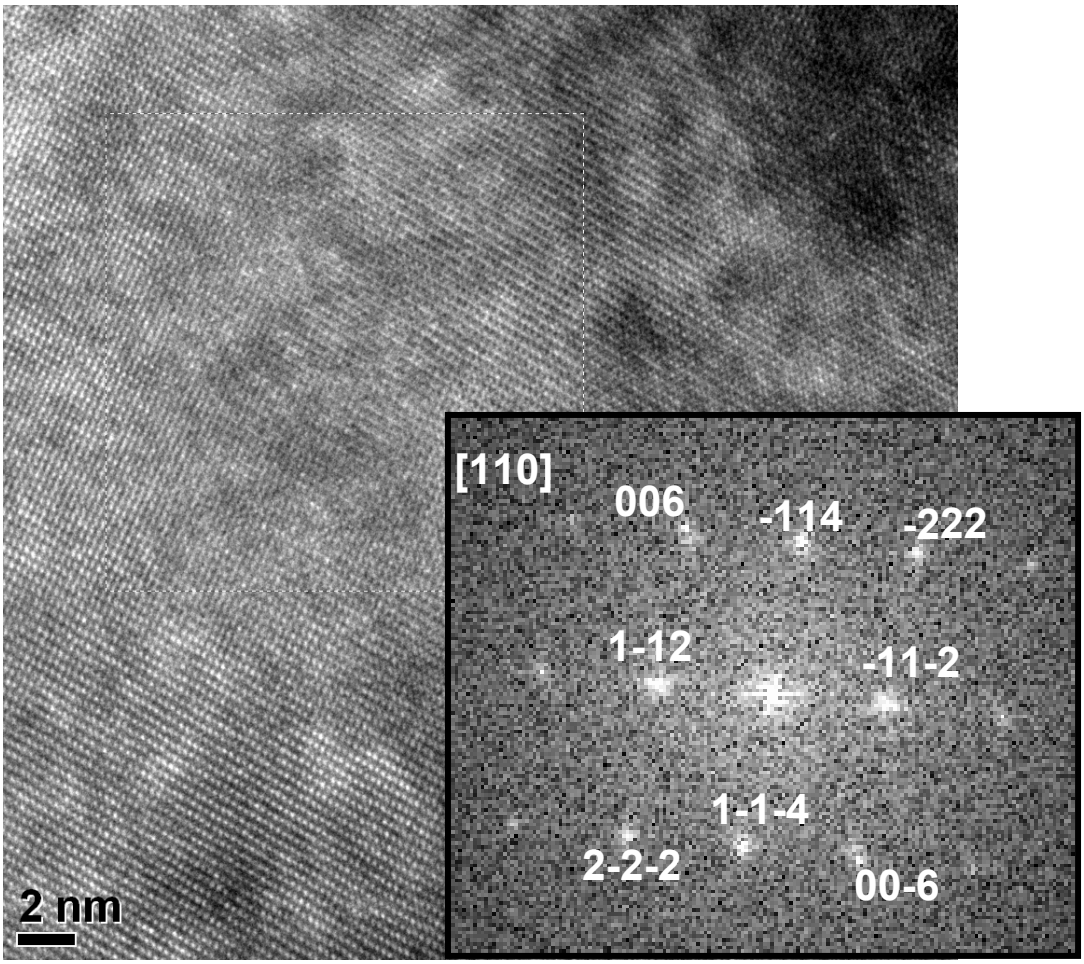

Figure 4.52: High resolution lattice image of region 1 in Figure 4.51. Inset is the indexed 'Fourier transformed' pattern.

The square shaped area that was selected was faintly visible in *Figure 4.52*. The dot-pattern generated from the selected area by performing a 'Fourier Transformation' of the selected area of the image was indexed to the [110] zone of the rhombohedral structure of Al_2O_3. The lattice parameters used for matching the rhombohedral structure of Al_2O_3 weere obtained from the JCPDS file # *00-*

001-1243. The lattice parameters were: $a = b = 4.75$ *Å*, $c = 12.97$ *Å*; $\alpha = \beta = 90^{o}$, $\gamma = 120^{o}$.

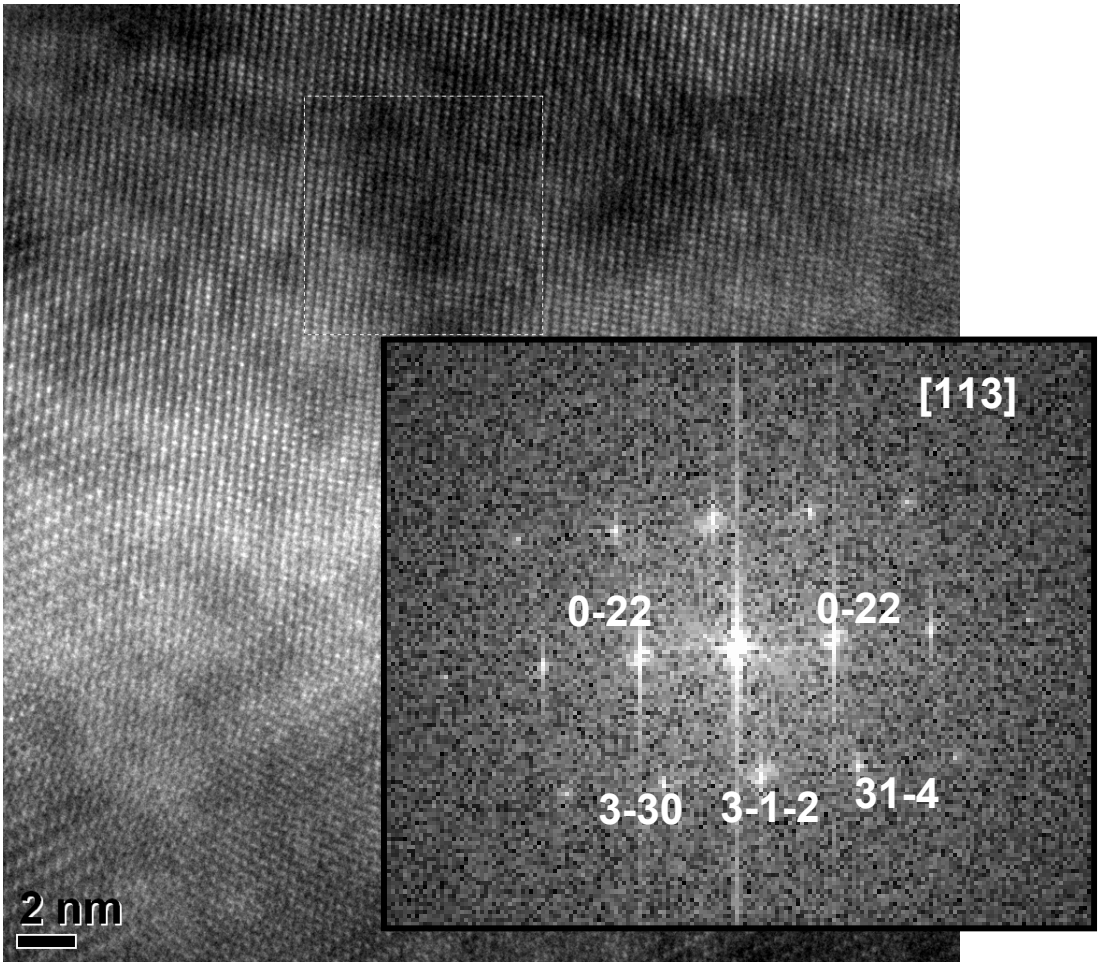

Figure 4.53: High resolution lattice image of region 2 in Figure 4.51. Inset is the indexed 'Fourier transformed' pattern.

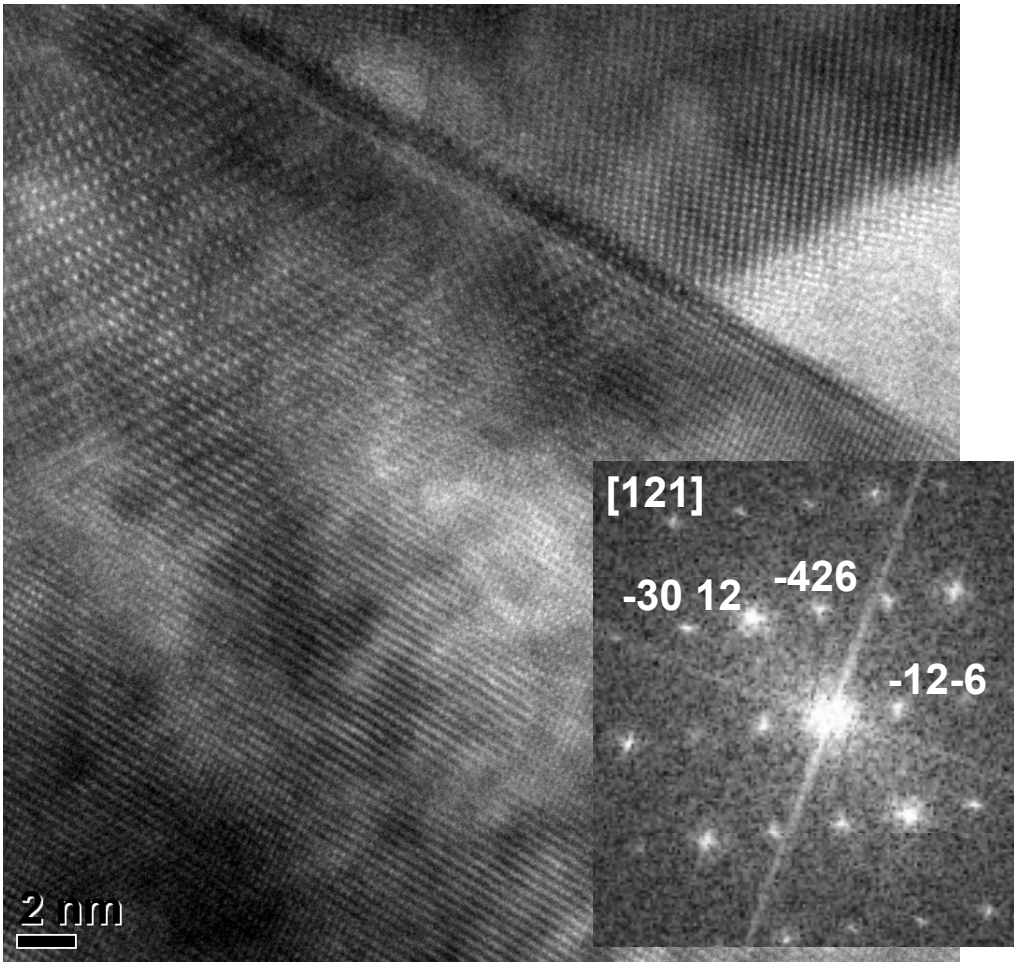

Figure 4.54: High resolution lattice image of region 3 in Figure 4.51.
Inset is the indexed 'Fourier transformed' pattern.

The insets in the above two figures are the dot-patterns that were generated by performing a 'Fourier Transformation' of the corresponding lattice images from the selected areas in the *Figures 4.53* and *4.54.* The dot-patterns were indexed to the [113] zone and the [121] zone of the rhombohedral structure of Al_2O_3 respectively. It is thus concluded that Al_2O_3 grains form when Al is in contact with TiO_2 at 700ºC and soaked at the elevated temperature for an extended period of time.

5.0 CONCLUSIONS

The current chapter presents the conclusions drawn from the results discussed in the previous chapter.

5.1 Effect of Temperature on the Al_2O_3 Shell Around Al

Al particles that are usually covered with a passivating layer of Al_2O_3 can be quickly heated to allow aluminum to be released and interact with other compounds that are present.

5.2 Morphological Understanding of the Interfaces

The interface between an Al film and TiO_2 substrate was identified for both an unheated sample and heated sample using SEM and FIB. It was concluded that the interface appeared to be a defined boundary, a 'line', at the resolution limit offered by the SEM.

5.3 High Resolution Identification of the Interfacial Phase(s) and Compound(s)

It was concluded that the interface between the Al film and the TiO_2 substrate for a heated sample was not a simple 'line', but a region with a definite width. It was concluded from the TEM results that the interfacial region was continuous along the interface, though not uniform in thickness. It was also concluded that the interfacial region consisted of TiAl and possibly a second phase. The second phase was identified to be crystalline Al_2O_3.

5.4 Theoretical Determination of Possible Interfacial Compound(s)

It was concluded from the theoretical calculations that TiAl was the interfacial compound favored for formation at elevated temperature instead of the formation of other Ti_xAl_y compounds and is in agreement with the experimental results.

5.5 Mechanism of Interaction at the Interface: A Proposed Model

It was concluded, from the analysis of the interface using the TEM, that the formation process of the interfacial compound (TiAl) could be described in the following way:

Step I: Melted Al was in contact with the TiO_2 substrate at elevated temperature.

Step II: Al diffused into the TiO_2 substrates more quickly through the stacking faults in the TiO_2 substrate.

Step III: At the stacking faults, TiO_2 is reduced by Al to form Ti and O. Ti reacts with Al near the stacking fault sites to form TiAl.

Step IV: The interfacial region containing TiAl grows near the stacking fault sites into the TiO_2 substrate.

5.6 An Explanation for the Oxygen Released during the TiO_2 – Al Reduction Reaction

Contrary to the reports in literature, it was concluded that O was dissolved in TiAl at the interfacial region. It was also concluded that fine crystalline Al_2O_3 particles were present as a second phase in the interfacial region that contained TiAl.

The current research thus describes the extent of interaction between Al and TiO_2 at an elevated temperature and standard atmospheric pressure. The resulting interface is well characterized using suitable analytical techniques in order to satisfactorily identify the interfacial compounds and explain the formation of growth of the interfacial region. Theoretical calculations for the formation of the interfacial compound are in agreement with the experimental results.

6.0 Future Work

The mechanism of formation and growth of a TiAl interfacial layer was determined and understood. It would be useful as future work to employ the self-formation of the interfacial layer in several structural and electronic device applications.

As an example for the structural application, it is suggested to expose an appropriate ratio of a mixture of Al, TiO_2 and B_2O_3 powders to 700ºC for an extended period of time before initiating the corresponding SHS reaction. A correlation between preheat time, thickness of interfacial layer, and kinetics of the SHS reaction could be drawn. The resultant SHS reaction product is expected to be significantly different in the morphology of its microstructure if the SHS reaction kinetics were inhibited by the formation and growth of an interfacial layer. Hence a correlation between the microstructure and kinetics of the SHS reaction can be drawn by an appropriate study of the formation and growth mechanisms at the interfacial layer between SHS reactants.

As an example for the electronic device application, it is suggested to expose a film - substrate sample (quite similar to a source – gate in MOSFET devices). Due to the continuing reduction in size of such electronic devices, the interfaces need to be carefully designed so that the diffusion of material from one region into another would prevent a short circuit. A self-formed interfacial layer as explained in the current thesis will help to reduce the harmful effects of diffusion.

REFERENCES

1. E. F. Bradley, 'Investment, Licensing and Strategic Partnering Opportunities, Emerging Technology, Applications and Markets for Aluminides, Iron, Nickel and Titanium,' in *Proceedings of Gorham Advanced Materials Institute Conference*, Monterey, California, November 1989.
2. I. Gil, M. A. Munoz-Morris and D. G. Morris, 'The Effect of Heat Treatments on the Microstructural Stability of the Intermetallics Ti – 46.5Al – 2 W – 0.5 Si,' *Intermetallics*, Vol. 9, pp. 373 – 385 (2001).
3. D. Hu, 'Effect of Boron Addition on Tensile Ductility in Lamellar TiAl Alloys,' *Intermetallics*, Vol. 10, pp. 851 – 858 (2002).
4. M. Wood and M. Ward-Close, 'Fiber-Reinforced Intermetallic Compounds by Physical Vapor Deposition,' *Materials Science and Engineering A*, Vol. 192 – 193, pp. 590 – 596 (1995).
5. C. M. Ward-Close, R. Minor and P. J. Doorbar, 'Intermetallic-Matrix Composites – A Review,' *Intermetallics*, Vol. 4, pp. 217 – 229 (1996).
6. D. Horvitz, I. Gotman, E. Y. Gutmanas and N. Claussen, '*In-Situ* Processing of Dense Al_2O_3 – Ti Aluminide Interpenetrating Phase Composites,' *Journal of the European Ceramic Society*, Vol. 22, pp. 947 – 954 (2002).
7. Run-hua Fan, B. Liu, Jing-de Zhang, Jian-qiang Bi and Yan-sheng Yin, 'Kinetic Evaluation of Combustion Synthesis $3TiO_2 + 7Al \rightarrow 3TiAl + 2Al_2O_3$ Using Non-isothermal DSC Method,' *Materials Chemistry and Physics*, Vol. 91, pp. 140-145 (2005).

8. M. K. Aghajanian, M. A. Rocazella, J. T. Burke and S. D. Keck, 'The Fabrication of Metal Matrix Composites by a Pressureless Infiltration Technique,' *Journal of Materials Science*, Vol. 26, pp. 447-454 (1991).

9. R. Subramanian, C. G. McKamey, J. H. Scheneibel, L. R. Buck and P. A. Menchhofer, 'Iron Aluminide – Al_2O_3 Composites by *In-Situ* Displacement Reactions: Processing and Mechanical Properties,' *Materials Science and Engineering,* Vol. A254, pp. 119 – 128 (1998).

10. K. V. Logan and J. D. Walton, 'TiB_2 Formation using Thermite Ignition,' *Ceramic Engineering and Science Proceedings*, W. J. Smothers, ed., The American Ceramic Society, Columbus, Ohio, No. 7-8, pp. 712-738 (1984).

11. K. V. Logan, Private communication.

12. Y. Shueh, J. P. Hirth and R. A. Rapp, 'Intermetallic Phase Formation and Breakdown of Mo Diffusion Barriers in Ni – O – Cu Layers,' *Metallurgical and Materials Transactions A*, Vol. 22, No. 7, pp. 1501-1510 (1991).

13. K. Ito, S. Tsukimoto, T. Kabe, K. Tada and M. Murakami, 'Effects of Substrate Materials on Self-Formation of Ti-Rich Interface Layers in Cu(Ti) Alloy Films,' *Journal of Electronic Materials*, Vol. 36, No. 5, pp. 606-613 (2007).

14. Chin-Yi Chou and Sinn-Wen Chen, 'Interfacial Reactions and Phase Equilibria in the Al – Cu/Ta Systems', *Journal of Electronic Materials*, Vol. 35, No. 1, pp. 22-27 (2006).

15. W. J. S. McLemore, 'A Thermodynamical Study of the Al – B_2O_3 System,' *Masters Thesis*, Georgia Institute of Technology (1991).

16. K. V. Logan, *U.S. Patent No. 6,090*, 321 (July 18, 2000).

17. F. F. Lange, 'Relation Between Strength, Fracture Energy, and Microstructure of Hot – Pressed Si_3N_4,' *Journal of the American Ceramic Society*, Vol 56 [10], 518-522, 1973.

18. H. Teshima, K. Hirao, M. Toriyama and S. Kanzaki, 'Fabrication and Mechanical Properties of Silicon Nitride Ceramics with Unidirectionally Oriented Rod-like Grains,' *Journal of the Ceramic Society of Japan*, Vol. 10, No. 12, pp. 1216-1220 (December 1999).

19. V. Logan and G. R. Villalobos, 'Thermodynamic Behavior of Selected SHS Reactions,' *Heat Transfer in Fire and Combustion Systems ASME*, HDT, Vol. 250, 249-257 (1993).

20. V. Sundaram, K. V. Logan and R. F. Speyer, *Journal of Materials Research*, Vol. 12 [7], 1681-1684 (1997).

21. P. A. Schweitzer, 'Fundamentals of Metallic Corrosion Atmospheric and Media Corrosion of Metals' *Corrosion Engineering Handbook - Second Edition*, CRC Press, Taylor and Francis Group.

22. K. V. Logan, J. T. Sparrow and W. J. S. McLemore, 'Experimental Modeling of Particle – Particle Interactions during SHS of $TiB_2 – Al_2O_3$,' edited by Z.A. Munir and J.B. Holt, *Combustion and Plasma Synthesis of High Temperature Materials* VCH, Weinhem, pp. 219 - 228 (1990).

23. C. Zhen, L. Li and Z. H. Wang, 'Diffusion mechanism of oxygen in orthorhombic and tetragonal c-textured epitaxial $YBa_2Cu_3O_{7-\delta}$ thin films,' *Superconductor Science and Technology*, Vol 12, No. 3, pp. 158-161, (March 1999).

24. C. H. Henager Jr., J. L. Brimhall and J. P. Hirth, 'Synthesis of a $MoSi_2$ – SiC Composite *in situ* using a Solid State Displacement Reaction,' *Materials Science and Engineering:* A, Vol. 155, Issue 1-2, pp. 109 – 114 (1992).

25. M. Yamaguchi, H. Inui and K. Ita, 'High Temperature Structural Intermetallics,' *Acta Materialia*, Vol. 48, pp. 307-322, (2000).

26. N. A. Travitsky and N. Claussen, 'Microstructure and Properties of Metal Infiltrated RBSN Composites,' *Journal of the European Ceramic Society*, Vol. 9, No. 1, pp. 61-65 (1992).

27. J. Rödel, H. Prielipp, N. Claussen, M. Sternitzke, K. B. Alexander, P. F. Becher and J. H. Schneibel, 'Ni_3Al/Al_2O_3 Composites with Interpenetrating Networks,' *Scripta Metallurgica et Materialia,* Vol. 33, no. 5, pp. 843-848 (1995).

28. M. C. Breslin, J. Ringnalda, J. Seeger, A. L. Marasco, G. S. Daehn and H. L. Frazer, 'Alumina/Aluminum Co-Continuous Ceramic Composites (C4) Materials Produced by Solid-Liquid Displacement Reactions: Processing Kinetics and Microstructures,' *Ceramic Engineering Science Proceedings*, Vol. 15, No. 4, pp. 104-112 (1994).

29. R. E. Loehman, K. Ewsak and A. P. Tomsia, 'Synthesis of Al_2O_3-Al Composites by Reactive Metal Penetration,' *Journal of the American Ceramic Society,* Vol. 79, No. 1, pp. 27 (1996).

30. M. S. Newkirk, A. W. Urquhart, H. R. Zwicker and E. Breval, 'Formation of Lanxide™ Ceramic Composite Materials,' *Journal of Materials Research*, Vol. 1, pp. 81 (1986).

31. N. Claussen and A. W. Urquhart, *Encyclopedia of Materials and Engineering*, edited by R. W. Cahn, Supplementary Vol. 2 (Pergamon Oxford).

32. I. C. Barlow, H. Jones and W. M. Rainforth, 'The Effect of Heat Treatment at 500 – 650ºC on the Microstructure and Properties of Mechanically Alloyed Al-Ti-O Based Materials,' *Materials Science nad Engineering A*, 351, 334 (2003).

33. P. C. Maity, P. N. Chakraborty and S. C. Panigrahi, 'Processing and Properties of Al-Al_2O_3 (TiO_2) in-situ Particle Composites,' *Journal of Materials Processing Technology*, 53, pp. 857, (1995).

34. C. F. Feng and L. Froyen, 'Formation of Al_3Ti and Al_2O_3 from an Al-TiO_2 system for preparing in-situ Aluminum matrix composites,' *Composites Part A*, 31, pp. 385, (2000).

35. N. Durlu, 'Titanium Carbide Based Composites For high Temperature Applications,' *Journal of the European Ceramic Society*, Vol. 19, No. 13-14, pp. 2415-2419 (1999).

36. D. L. Zang, D. Y. Ying and G. Adam, 'Reaction kinetics and Microstructure Evolution During Heating High-energy Ball Milled Al-metal Oxide Composite Powders,' *Journal of Metastable Nanocrystalline Materials*, 13, pp. 287 (2002).

37. N. Claussen, D. E. Garcia and R. Janssen, 'Reaction Sintering of Alumina-Aluminide Alloys,' *Journal of Materials Research*, 11, pp. 2884 (1996).

38. S. Schicker, D. E. Garcia, J. Bruhn, R. Janssen and N. Claussen, 'Reaction Synthesized Al_2O_3-based Intermetallic Composites,' *Acta Materialia*, 46, pp. 2485 (1998).

39. P. C. Maity, S. C. Panigrahi and P. N. Chakraborty, 'Preparation of Aluminium-Alumina in-situ Particle Composite,' *Scripta Metallurgica et. Materialia*, Vol. 28, pp. 549-552 (1993).

40. P. K. Balasubramanian, P. Srinivasa Rao, K. G. Sivadasan, K. G. Sathyanarayana, B. C. Pai and P. K. Rohatgi, 'Forging Characteristics of Al-Zn-Mg alloy containing 5wt% TiO_2 Dispersion,' *Journal of Materials Science Letters*, Vol. 8, [7] pp. 799-801, (2005).

41. H. H. Fukunaga, X. Wang and Y. Aramaki, 'Preparation of Intermetallic Compound Matrix Composites by Reaction Squeeze Casting,' Journal of Materials Science Letters, Vol. 10 [1] pp. 23-25 (1991).

42. H. X. Peng, D. Z. Wang, L. Geng, C. K. Yao, and J.F. Mao, 'Evaluation of the microstructure of *in-situ* reaction processed Al_3Ti-Al_2O_3-Al composite' *Scripta Materialia*, Vol. 37 [2] pp. 199-204 (1997).

43. Zhu Y., Zhang L., Wang L., Tan R. and Cao L., 'Interface Diffusion and Reaction Between TiO_2 film Photocatalyst and Aluminum Alloy Substrate,' *Surface and Interafce Analysis*, Vol. 32, pp. 218-223 (2001).

44. Zhang D. L., Ying D. Y. and Munroe P, 'Formation of Al_2O_3 During Heating of an Al/TiO_2 Nanocomposite Powder,' Journal of Materials Research, Vol. 20, No. 2, pp. 307-313 (2005).

45. Dake L. S. and Lad R. J., 'Electronic and Chemical Interactions at Aluminum/TiO_2(110) Interfaces,' *Surface Sciences*, Vol. 289, pp. 297 (1993).

46. Gheorghe I. and Rack H. J., 'Reactive Infiltration of 25 Vol Pct TiO_2/Al Composites,' *Metallurgical and Materials Transactions A*, Vol. 33A, pp. 2155-2162 (2002).

47. Pan J., Li J. H., Fukunaga H., Ning X. G., Ye H. Q., Yao Z. K. and Yang D. M., 'Microstructural Study of the Interface Reaction Between Titania Whiskers and Aluminum,' *Composites Science and Technology*, Vol. 57, pp. 319-325 (1997).

48. T. B. Massalski, ed., *Binary Alloy Phase Diagrams*, 2nd Ed., Vol. 1-3 (Materials Park, OH: ASM) 1990.

49. K. Wefers and C. Misra, 'Oxides and hydroxides of Aluminum,' *Alcoa Technical Paper,* No. 19, Alcoa Laboratories, Pittsburgh, PA (1987).

50. I. Levin and D. Brandon, 'Metastable Alumina Polymorphs: Crystal Structures and Transition Sequences,' *Journal of the American Ceramic Society*, Vol. 81, No. 8, pp. 1995-2012 (1998).

51. F. Wagner, D. E. Garcia, A. Krupp and N. Claussen, 'Interpenetrating Al2O3-$TiAl_3$ Alloys Produced by Reactive Infiltration,' *Journal of the European Ceramic Society*, Vol. 19, No. 13-14, pp. 2449-2453 (1999).

52. I. Tsuchitori and H. Fukunaga, 'Reactivity of Potassium Titanate Whiskers with Al Alloys,' *Journal of the Japan Institute of Metals*, Vol. 56, No. 3, pp. 333-341 (1992).

53. P. Beyer, R. Janssen and N. Claussen, 'Synthesis of Aluminide – Alumina Composites by Reactive Squeeze Casting,' Advan*ced Engineering Materials*, Vol. 2, No. 11, pp. 734-737 (2000).

54. I. Gheorghe, and H. J. Rack, 'Influence of TiO_2:Al Ratio on Reaction Path During Reactive Infiltration of TiO_2 by Molten Al,' *Materials Science and Technology*, Vol. 18, No. 10, pp. 1079-1084 (2002).

55. I. C. Barlow, H. Jones and W. M. Rainforth, 'Evolution of Microstructure and Hardening, And the Role of Al_3Ti Coarsening, During Extended Thermal Treatment in Mechanically Alloyed Al-Ti-O Based Materials,' *Acta Materialia*, Vol 49, pp. 1209-1224 (2001).

56. R. H. Doremus, 'Oxidtion of Alloys Containing Aluminum and Diffusion in Al_2O_3,' *Journal of Applied Physics*, Vol. 95, No. 6, pp. 3217-3222 (2004).

57. R. H. Doremus, 'Reply to "Comment on "Oxidation of Alloys Containing Aluminum and Diffusion in Al_2O_3" [J. Appl. Phys. 97, 116111 (2005)],' *Journal of Applied Physics*, Vol. 97, pp. 116112-1 (2005).

58. B. A. Pint and R. M. Deacon, 'Comment on "Oxidation of Alloys Containing Aluminum and Diffusion in Al_2O_3" [J. Appl. Phys. 95, 3217 (2004)],' *Journal of Applied Physics*, Vol. 97, pp. 116111-1 to 116111-3 (2005).

59. J. A. Nychka and D. R. Clarke, 'Quantification of aluminum outward diffusion during oxidation of FeCrAl alloys,' *Oxidation of Metals*, Vol. 63, No. 5-6, pp. 325-352 (June 2005).

60. P. Waldner and G. Erikson, 'Thermodynamic Modeling of the System Titanium-Oxygen,' *CALPHAD*, Vol. 23, No. 2, pp. 189-218 (1999).

61. K. Das, P. Choudhary and S. Das, 'The Al-O-Ti (Aluminum-Oxygen-Titanium) System,' *Journal of Phase Equilibria and Diffusion*, Vol. 23, No. 6, pp. 525-536 (2002).

62. U. R. Kattner, J. C. Lin and Y. A. Chang, 'Thermodynamic Assessment and Calculation of the Ti-Al System,' *Metallurgical Transactions A*, Vol. 23A, pp. 2081-2090 (1992).

63. J.C. Schuster and H. Ipser, 'Phases and Phase Equilibria in the Partial System $TiAl_3$-TiAl,' *Z. Metallkd.*, Vol. *81*, pp. 383–86 (1990).

64. L. Kaufman and H. Nesor, Titanium Science and Technology, Vol. 2, Proc. Int. Conf., R. I. Jaffe and H. M. Burte, eds., Plenum Press, New York, NY, pp. 773-800 (1973).

65. L. Kaufman and H. Nesor, 'Coupled Phase Diagrams and Thermochemical Data Transition Metal Binary Systems – V*,' *CALPHAD*, Vol. 2, No. 4, pp. 325-348 (1978).

66. D. Dew-Hughes and L. Kaufman, 'Ternary Phase Diagrams of the Manganese-Titanium-Iron and the Aluminum-Titanium-Iron Systems: A comparison of the Computer Calculations with Experiment,' *CALPHAD*, Vol. 3, pp. 175-203 (1979).

67. J. L. Murray, 'Calculation of the Titanium-Aluminum Phase Diagram,' *Metallurgical and Materials Transactions A*, Vol. 19, No. 2, pp. 243-247 (1988).

68. X. L. Li, R. Hillel, F. Teyssandier, S. K. Choi and F. F. Van Loo, 'Reactions and Phase Relations in the Ti-Al-O System,' *Acta Materialia*, Vol. 40, No. 11, pp. 3149-3157 (1992).

69. J. L. Murray, *Phase Diagrams of Binary Titanium Alloys, ASM INTERNATIONAL*, Metals Park, OH, 1987.

70. J. C. Mishurda and J. H. Perepezko, 'Microstructure/Property Relationships in Titanium Aluminides and Alloys,' *TMS Conference Proceedings*, ed. by U.-W. Kim and R. R. Boyer, Warrendale, PA, pp. 3-30 (1991).

71. S. T. Norberg, S. Hoffman, M. Yoshimura and N. Ishizawa, '$Al_6Ti_2O_{13}$, a New Phase in the Al_2O_3-TiO_2 System,' *Acta Crytsallographica Section C*, Vol. C61, pp. i-35-i38 (2005).

72. A. Kussmaul, H-J. Seifert, J. A. Golczewski, H. L. Lukas and F. Aldinger, 'Thermodynamic Calculation of Diffusion Paths Applied to the Oxidation of γ-TiAl,' *Materials Research and Advanced Techniques*, Vol. 89, No. 10, pp. 683-686 (1998).

73. N. Zheng, W. Fischer, H. Grubmeier, V. Shemet and W. J. Quadakkers, 'The Significance of Sub-Surface Depletion Layer Composition for the Oxidation Behavior of γ-Titanium Aluminides,' *Scripta Materialia,* Vol. 33, pp. 47-53 (1995).

74. R. Beye, M. Verwerft, J. T. M. De Hosson and R. Gronsky, 'Oxidation Subscale of γ-Titanium Aluminides,' *Acta Materialia,* Vol. 44, pp. 4225-4231 (1996).

75. F. Dettenwanger, E. Schumann, J. Rakowski, G. H. Meier and M. Ruhle, 'Development and Microstructure of the Al-Depleted Layer of Oxidized TiAl,' *Materials and Corrosion*, Vol. 48, pp. 23-27 (1996).

76. H. J. Seifert and F. Aldinger, 'Applied Phase Studies,' *Zeitschrift für Metallkunde*, Vol. 87, No. 11, pp. 841-853 (1996).

77. B-J. Lee and N. Saunders, 'Thermodynamic Evaluation of the Ti-Al-O Ternary System,' *Zeitschrift für Metallkunde*, Vol. 88, pp. 152-161 (1997).

78. K. L. Luthra, 'Stability of Protective Oxide Films on Ti-Based Alloys,' *Oxidation of Metals*, Vol. 36, pp. 475-490 (1991).

79. R. E. Tressler, T. L. Moore and R. L. Crane, 'Reactivity and Interface Characteristics of Titanium-Alumina Composites,' *Journal of Materials Science*, Vol. 8, pp. 151-161 (1973).

80. K. Choi, F. J. J. van Loo and R. Metselaar, 'Reactions and Phase Relations in the Ti-Al-O System,' *Mat Tech'90 – The Proceedings of the First European East-West Symposium on Materials and Processes*, University of Technology, Helsinki, Finland, pp. 1-12 (1990).

81. M. X. Zhang, K. C. Hsieh, J. DeKock and Y. A. Chang, 'Phase Diagram of Ti-Al-O at 1100ºC,' *Scripta Metallurgica et Materialia*, Vol. 27, pp. 1361-1366 (1992).

82. A. Rahmel and P. J. Spencer, 'Thermodynamic Aspects of TiAl and $TiSi_2$ Oxidation: The Al-Ti-O and Si-Ti-O Phase Diagrams,' *Oxidation of Metals*, Vol. 35, pp. 53-68 (1991).

83. G. P. Kelkar and A. H. Carim, 'Phase Equilibria in the Ti-Al-O system at 945ºC and Analysis of Ti/Al_2O_3 Reactions,' *Journal of the American Ceramic Society*, Vol. 78, No. 3, pp. 572-576 (1995).

84. J. L. Murray and H. A. Wriedt, 'The O-Ti (Oxygen –Titanium) System,' Phase Diagrams of Binary Titanium Alloys, J. L. Murray, ed., *American Society for Metals*, Metals Park, OH, pp. 221-229 (1987).

85. H. A. Wriedt, 'The Al-O (Aluminum - Oxygen) System,' *Bulletin of Alloy Phase Diagrams*, Vol. 6, pp. 548-553 (1985).

86. W. Lefebvre, A. Loiseau, M. Thomas and A. Menand, 'Influence of Oxygen on the α→γ massive Transformation in a Ti - 48at.% Al Alloy,' *Philisophical Magazine A*, Vol. 82, No 11, pp. 2341-2355 (2002).

87. Levis G and Kaplan W. D., *Acta Materialia*, Vol. 50, pp. 75-88, (2002).

88. O. Kubaschewski and B. E. Hopkins, *Oxidation of Metals and Alloys*, London, Butterworths (1962).

89. R. C. Weast, editor, *CRC Handbook of Chemistry and Physics*, D-45, 60th edition, Boca Raton: CRC Press, Inc; (1980).

90. S. Yoo, A. Sheikh and S. Kenneth, 'Nanocarving of Bulk Titania Cyrtsals into Oriented arrays of Single – Crystal Nanofibers via. Reaction with Hydrogen – Bearing Gas,' *Advanced Materials*, Vol. 16 [3], pp. 260-264 (2004).

91. C. R. A. Catlow, *Nonstoichiometric Oxides* (Ed. O. Sorensen), Academic Press, New York (1981).

92. JANAF-Thermochemical Tables, D. R. Schull and H. Prophet, US Department of Commerce, Washington, 1985.

93. NIST-JANAF Thermochemical Tables Edition 4, Malcolm W. Chase Jr., American Chemical Society; Woodbury, N.Y.: American Institute of Physics for the National Institute of Standards and Technology, 1998.

Appendix I

Validation of the Thermodynamic Parameters from FACTSage™ with the Corresponding Values from JANAF Tables

FactSage™ (obtained from JANAF-Thermochemical Tables[92]), a thermochemical software, has documented the free energy of several metallic and ceramic compounds, and the corresponding temperature range at which the equations are valid. Thermodynamic parameters like the *Cp(T)*s (specific heats), *H(T)* (enthalpy), *G(T)* (Gibb's Free Energy) and *S(T)* (entropy) are listed in *FactSage™*. Thermodynamic parameters are presented as equations for different temperature ranges. For example, the Gibb's Free Energy *G(T)* of a compound at a specific temperature range is given by an equation which is a function of temperature.

The calculation for *ΔH(T)* in Joules per mole for Al using the equation listed in the JANAF-Thermochemical Table[92] for temperature range of 298 – 1200ºK is:

$$H(T) = 5025.23805 + 45.9248180 * T + 5.232429015 * 10 - 6 * T^3 - 2850.41894 * \ln(T) - 0.514611719 * (T^{1.5}) + 2972635.17 * (T^{-2})$$

Change in enthalpy for Al is calculated at 300K with 298.15K as the reference temperature.

$$\Delta H(300) = H(300) - H(298.15)$$

$$\Delta H(300) = 45.924818[300 - 298.15] + 5.232329015 * 10^{-6}[300 - 298.15] - 2850.41894[\ln 300 - \ln 298.15] - 0.514611719[300^{1.5} - 298.15^{1.5}] + 2972735.17[300^{-2} - 298.15^{-2}]$$

$$= 48.44969253 \text{ Joules per mole.}$$

The value reported in JANAF-Thermochemical Tables[93] is 45 Joules per mole at 300K. The error is only 7.6% of the value reported in the JANAF-Thermochemical Tables[2] and is used in the calculations shown in *Chapter 3*.

Calculation of *ΔH(T)* in Joules per mole for aluminum using the equation listed in the JANAF-Thermochemical Table[92] for temperature range of 298 – 1200ºK.

$$H(T) = 5025.23805 + 45.9248180 * T + 5.232429015 * 10 - 6 * T^{3} - 2850.41894 * \ln(T) - 0.514611719 * (T^{1.5}) + 2972635.17 * (T^{-2})$$

Change in enthalpy for Al is calculated for 1000K with 298.15K as the reference temperature.

$$\Delta H(1000) = H(1000) - H(298.15)$$

$$\Delta H(1000) = 45.924818[1000 - 298.15] + 5.232329015 * 10^{-6}[1000 - 298.15] - 2850.41894[\ln 1000 - \ln 298.15] - 0.514611719[1000^{1.5} - 298.15^{1.5}] + 2972735.17[1000^{-2} - 298.15^{-2}]$$

= 20.22 kJoules per mole.

The value of enthalpy for Al reported in the JANAF-Thermochemical Tables[93] is 30.806 kJoules per mole at 1000ºK. The error is 34.36% of the value reported in the JANAF-Thermochemical Tables[93] and is used in the calculations shown in *Chapter 3*.

The values obtained using the equations provided by FACTSage are comparable with the values reported in the widely accepted JANAF-Thermochemical Tables[92] and hence can be used for calculations shown in *Chapter 3.*